

**ABANT İZZET BAYSAL UNIVERSITY
THE GRADUATE SCHOOL OF NATURAL AND APPLIED
SCIENCES**



**FABRICATION AND INVESTIGATION OF Fe/MgB₂
SUPERCONDUCTING WIRES AND RACETRACK COILS**

DOCTOR OF PHILOSOPHY

FIRAT KARABOĞA

BOLU, NOVEMBER 2016

ABANT İZZET BAYSAL UNIVERSITY
THE GRADUATE SCHOOL OF NATURAL AND APPLIED
SCIENCES
DEPARTMENT OF PHYSICS



FABRICATION AND INVESTIGATION OF Fe/MgB₂
SUPERCONDUCTING WIRES AND RACETRACK COILS

DOCTOR OF PHILOSOPHY

FIRAT KARABOĞA

BOLU, NOVEMBER 2016

APPROVAL OF THE THESIS

FABRICATION AND INVESTIGATION OF Fe/MgB₂ SUPER-CONDUCTING WIRES AND RACETRACK COILS submitted by FIRAT KARABOĞA in partial fulfillment of the requirements for the degree of Doctor of Philosophy in Department of Physics, Abant İzzet Baysal University by,

Examining Committee Members

Signature

Supervisor
Prof. Dr. İbrahim BELENLİ
Abant İzzet Baysal University


.....

Member
Prof. Dr. Ekrem YANMAZ
İstanbul Gelişim University


.....

Member
Prof. Dr. Erdal BEKİROĞLU
Abant İzzet Baysal University


.....

Member
Assoc. Prof. Dr. Mustafa AKDOĞAN
Abant İzzet Baysal University


.....

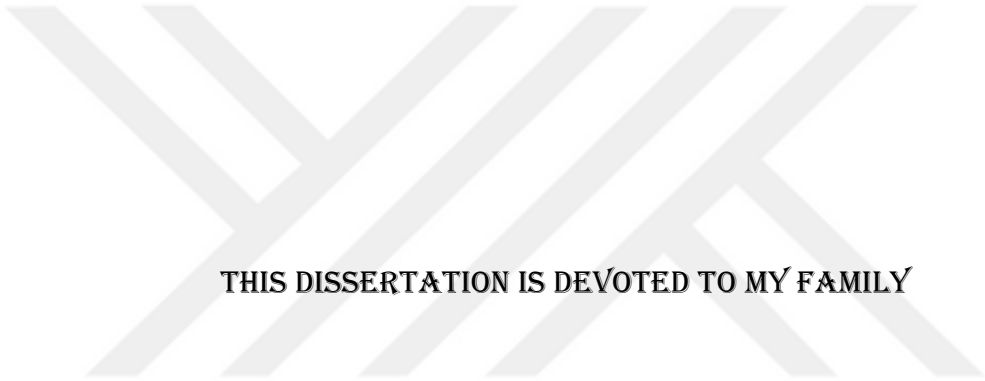
Member
Assist. Prof. Dr. Mehmet Akif ŞENOL
İstanbul Gelişim University


.....

November 03, 2016

Prof. Dr. Duran KARAKAŞ

Director, Graduate School of Natural and Applied Sciences



THIS DISSERTATION IS DEVOTED TO MY FAMILY

DECLARATION

I hereby declare that all information in this document has been obtained and presented in accordance with academic rules and ethical conduct. I also declare that, as required by these rules and conduct, I have fully cited and referenced all material and results that are not original to this work.



FIRAT KARABOĞA

ABSTRACT

**FABRICATION AND INVESTIGATION OF Fe/MgB₂
SUPERCONDUCTING WIRES AND RACETRACK COILS
PHD THESIS
FIRAT KARABOĞA
ABANT IZZET BAYSAL UNIVERSITY GRADUATE SCHOOL OF
NATURAL AND APPLIED SCIENCES
DEPARTMENT OF PHYSICS
(SUPERVISOR: PROF. DR. İBRAHİM BELENLİ)**

BOLU, NOVEMBER 2016

In this dissertation, we struggled to solve some problems of a drawing for the fabrication of various MgB₂/Fe wires and improved the drawing process by employing available techniques. We produced monocoire and MF (6+1 and 18+1) superconducting MgB₂/Fe wires and tapes by using PIT or PLIT techniques with original initial filling process following the ex-situ or in-situ reaction routes. Then, we studied the effect of sintering temperatures, times and initial filling density on T_c , I_c , J_c , morphological/geometrical structure, densification, ρ , critical field, temperature dependence of upper critical field $B_{c2}(T)$ of MgB₂/Fe monocoire and MF wires in various diameter produced with IA. The obtained in-situ monocoire Fe/MgB₂ wires with 1.90 mm and 1.00 mm diameter were sintered under argon pressure (5-10 bar) in a three-zone tube furnace at temperatures in the range of 800-900°C for 1 hour to achieve superconducting property. Optimum sintering conditions to achieve better superconducting properties in terms of J_c under external magnetic field are related with monocoire wire diameter. The most suitable sintering temperature for 1.90 mm wires is 900 °C while it is 850 °C for 1.00 mm wire, duration of sintering is 1 hour for both cases. Also, we studied the effect of excessive mechanical deformation by pressing under 1GPa and BP , AP and PA on the microstructure and transport properties of monocoire sintered (800-1000 °C for 1 hour) Fe/MgB₂ 1.00 mm wires (cross sectional area 0.00785 cm²). The subsequent heat treatment on the Fe/MgB₂ tapes (cross sectional area 0.00667 cm²) improved the microstructure and the grain connectivity. Moreover, the fabricated MgB₂/Fe (18+1) MF wires with an outer diameter of 1.00 mm were

sintered at temperature in the range of 700-850 °C for 1 hour and 2 hours under 5-10 bar argon pressure. The most convenient sintering temperature and time were found to be 700 °C and 1 hour in terms of achieving highest critical current value under magnetic field since the in-field J_c is one of the most important properties for superconducting materials in applications. Bending angle was examined for the monocoire and MF wires in small diameters as comparison with strength wires in Bend&React process. The superconducting wires produced within this thesis were characterized using XRD, SEM, EDS, transport J_c and magnetoresistivity measurements. The results of the produced of in-situ monocoire Fe/MgB₂ wires as a function of the initial tube filling density indicates that increment of the initial filling density with PLIT (Filling 2) method improved the critical current of the Fe/MgB₂ wires, and a high I_c (4.2 K) = 140 A at $B = 5$ T is achieved. The pressure of 1.1 GPa applied via HIP method increases T_c quite significantly in high magnetic field range of 6-12 T, improves the B_{irr} and B_{c2} and increases the J_c at 4.2 K and 20 K about three times. Moreover, initial filling with mixture of the amorphous boron and amorphous nano boron powders at equal amounts improved the transport engineering J_c ($I_c > 150$ A under 3 T) values of the wires in magnetic fields (< 6 T). The excessive mechanical deformation by pressing and consecutive heat treatment improved the microstructure, the grain connectivity and transport properties of monocoire sintered in-situ Fe/MgB₂ wires. Finally, the in-situ MF wires were obtained by using the monocoire MgB₂/Fe wires which already have high J_c values under applied magnetic field and we observed that the MgB₂/Fe (18+1) wires have high critical current values under low external magnetic field (< 6 T). Bending diameter size did not affect superconducting properties of the monocoire and MF MgB₂/Fe small diameter wires significantly in Bend&React process. Optimum sintering temperature depends on diameter of the wires. Four racetrack coils were made by winding the pieces of monocoire and MF MgB₂/Fe wires with about 25 meters length. The transport current of them and the produced magnetic field at the center of a racetrack coil was measured at 4.2 K.

KEYWORDS: MgB₂/Fe wires and tapes, PIT method, Transport critical current density, Racetrack coil.

ÖZET

**Fe/MgB₂ SÜPERİLETKEN TELLER VE PARKUR TİPİ BOBİNLERİN
ÜRETİLMESİ VE İNCELENMESİ
DOKTORA TEZİ
FIRAT KARABOĞA
ABANT İZZET BAYSAL ÜNİVERSİTESİ FEN BİLİMLERİ ENSTİTÜSÜ
FİZİK ANABİLİM DALI
(TEZ DANIŞMANI: PROF. DR. İBRAHİM BELENLİ)**

BOLU, KASIM - 2016

Bu tezde, çeşitli MgB₂/Fe tellerin üretimi ilgili çekme işleminin bazı problemlerini çözmek için uğraştık ve uygun tekniklerle çekme işlemini geliştirdik. Tek – çok damarlı süperiletken MgB₂/Fe telleri ve şeritleri ex-situ veya in-situ reaksiyon eşliğinde orjinal doldurma yöntemleriyle tüp içine toz metodu kullanılarak ürettik. Daha sonra ısıtma işlem sıcaklığı, süresi ve başlangıç doldurma yoğunluğu ara ısıtma işlem ile üretilmiş çeşitli çaplardaki tek – çok damarlı MgB₂/Fe tellerin MgB₂ fazının oluşumu, kritik geçiş sıcaklığı, kritik akım yada kritik akım yoğunluğu, iç ve geometrik yapısı, yoğunluğu, öz direnci, kritik alan ve sıcaklığa bağlı üst manyetik alan üzerindeki etkisini çalıştık. Elde edilmiş olan tek gözenekli Fe/MgB₂ 1.90 ve 1.00 mm çapındaki tellerimiz süperiletken özelliğini kazandırmak için 3 bölmeli boru fırınımızda 800-900 °C aralığında 1 saat süreyle 5-10 bar argon basıncı altında ısıtma işlemi yapıldı. Manyetik alan altındaki kritik akım yoğunluğu açısından daha iyi super iletken özellikleri elde etmek için en uygun ısıtma işlem sıcaklığı tek damarlı telin çapıyla ilişkilidir. Aynı ısıtma işlem süresine ait tellerde en uygun sıcaklık 1.00 mm tel için 850 derece iken 1.90 mm tel için 900 derecedir. Ayrıca elde edilmiş tekdamarlı 1.00 mm tellerimizde mekanik deformasyonun, presleme öncesi ve sonrasında yapılan ısıtma işleminin (800-1000 °C / 1 saat), mikroyapıda ve taneciklerin bir araya tutunmasındaki etkisini çalıştık. Presleme sonrası ısıtma işlem mikroyapı ve parçacıklar arası kuvveti arttırdı. Bundan başka, üretilmiş olan çok damar (18+1) MgB₂/Fe 1.00 mm çaplı tellerimiz 700-850 °C 1 saat ve 2 saat ısıtma işlem süresiyle aynı şartlar altında tavlendiğinde, uygulamalarda süperiletkenler için en önemli özelliklerden biri olan uygulanan manyetik alan altında kritik akım değeri açısından çok damarlı

telimiz için en uygun sıcaklık 700 °C ve süre 1 saat bulundu. Bük ve reaksiyonu gerçekleştirilmesi prosesiyle küçük çaplı tek ve çok damarlı tellerin bükme açısını düz tel ile karşılaştırarak inceledik. Bu tezde üretilmiş olan süperiletken teller XRD, SEM, EDS, taşıma J_c ve manyetik öz direnç ölçümleriyle karakterize edildi. Başlangıç boru doldurma yoğunluğunun bir fonksiyonu olarak demir (Fe) kılıflı in-situ MgB_2 tekdamarlı tellerin üretimi boru içine pellet metoduyla başlangıç doldurma yoğunluğunun artması Fe/MgB_2 tellerin kritik akımını geliştirildiği ve $I_c(4.2\text{ K}) = 140\text{ A}$, $B = 5\text{ T}$ manyetik alan altında başarıldığını gösteriyor. Daha sonra, sıcak izostatik presleme ile 1.1 GPa basınç yüksek alandaki (6-12 T) T_c belirgin olarak arttırıyor, tersinmez ve üst kritik alanı geliştiriyor ve 4.2 K ve 20 K deki J_c yaklaşık 3 kat arttırıyor. Bundan başka eşit miktarda amorf ve amorf nano bor'un karışımı tellerin kritik akımını 3 T manyetik alanda $I_c > 150\text{ A}$ değerine ulaştırdı. Sırasıyla presleme ve ardışık ısı işlem ile aşırı mekanik deformasyon tek damarlı ısı işlem görmüş MgB_2/Fe telin mikro yapı, tanecik bağlılığını ve transport özelliklerini geliştirdi. Sonuç olarak, manyetik alan altındaki kritik akım değeri yüksek olan tek damarlı tellerimizi kullanarak in-situ çok damarlı (18+1) teller elde edildi and bu çok damarlı MgB_2/Fe tellerimizin düşük alanlarda yüksek kritik akım sahip olduğunu gözlemledik. Bük ve reaksiyonu gerçekleştirilmesi prosesinde bükme çapı, küçük çaplı tek ve çaplı çok damarlı süperiletken tellerin özelliklerini belirgin şekilde etkilemedi. Uygun ısı işlem sıcaklığı tellerin çapına bağlıdır. Yaklaşık 25 m uzunluğundaki tek ve çok damarlı MgB_2/Fe tellerin parçaları sararak dört parkur tipi bobin yapıldı. Bobinlerin taşıma akımı ve bir tanesinin merkezinde üretilen manyetik alan 4.2 K (sıvı helyum) sıcaklığında test edildi.

ANAHTAR KELİMELER: MgB_2/Fe tel ve şeritler, PIT method, Transport kritik akım yoğunluğu, Parkur bobin

TABLE OF CONTENTS

	<u>Page</u>
ABSTRACT	v
ÖZET.....	vii
TABLE OF CONTENTS.....	ix
LIST OF FIGURES	xi
LIST OF ABBREVIATIONS AND SYMBOLS	xvii
1. INTRODUCTION	1
2. MgB₂ SUPERCONDUCTORS.....	2
2.1 The Discovery and Importance of MgB ₂	2
2.2 Crystal and Electronic Structure of MgB ₂	2
2.3 Superconductivity Mechanism in MgB ₂	3
2.3.1 Isotope Effect (α)	5
2.3.2 Anisotropy (γ)	5
2.3.3 Absence of Weak Links	7
2.3.4 Critical Temperature (T_c)	8
2.3.5 Critical Current (I_c)	9
2.3.6 Critical Magnetic Field (B_c) and Meissner Effect.....	10
2.3.7 Penetration Depth (λ)	11
2.3.8 Coherence Length (ξ).....	12
3. MgB₂ SUPERCONDUCTING WIRES.....	14
3.1 Fabrication Methods for Superconducting MgB ₂ Wires and Tapes... 14	
3.1.1 Powder-In-Tube (PIT) Method	14
3.1.2 Continuous Tube Forming and Filling (CTFF) Method.....	15
3.1.3 Metal Matrix Composite (MMC) Method	16
3.2 Procedures for Production of MgB ₂ Superconducting Wires	16
3.2.1 Initial Filling Techniques.....	16
3.2.1.1 In-situ Reaction Technique	16
3.2.1.2 Ex-situ Reaction Technique	17
3.2.1.3 Reactive Liquid Mg Infiltration and External Mg Diffusion Technique	17
3.2.2 Sheath Materials for MgB ₂ Wires.....	18
3.2.3 Chemical Doping or Addition.....	19
3.2.4 The Annealing Temperature	22
3.2.5 Grain Connectivity.....	24
3.3 MgB ₂ Coils and Properties	25
3.4 Importance of MgB ₂ Applications	26
4. AIM AND SCOPE OF THE STUDY	28
5. EXPERIMENTAL TECHNIQUES.....	29
5.1 Preparation of Initial MgB ₂ Powders	29
5.2 Fabrication of MgB ₂ Wires and Tapes	30

5.2.1	Production of Ex-situ MgB ₂ Monocore Wires	32
5.2.2	Production of Ex-situ MgB ₂ Multifilamentary Wires.....	34
5.2.3	Production of In-situ MgB ₂ Monocore Wires.....	35
5.2.3.1	Preparation of Fe/MgB ₂ Monocore Wire With Pelletized In-situ Powder	35
5.2.3.2	Preparation of In-situ Fe/MgB ₂ Monocore Wires With Mixture of Different Two Borons	36
5.2.4	Production of In-situ MgB ₂ Monocore Tapes.....	36
5.2.5	Preliminary Coil Production of In-situ Fe/MgB ₂ Monocore wire	37
5.2.6	Production of In-situ MgB ₂ Multifilamentary Wires.....	38
5.2.7	Bending Process of In-situ Fe/MgB ₂ Multifilamentary Wires.....	39
5.2.8	S-Glass Insulation Process of Long MgB ₂ Wires	40
5.2.9	Fabrication of Racetrack Coils	43
5.2.10	Sintering Processes	44
5.3	Characterization Techniques	44
5.3.1	X-Ray Diffraction (XRD) Technique	44
5.3.2	Scanning Electron Microscopy (SEM)	45
5.3.3	Resistivity-Temperature (<i>R-T</i>) and Current-Voltage (<i>I-V</i>) Measurements	45
5.3.4	Magnetization (<i>M-H</i>) Measurements	46
5.3.5	Mechanical Tests	47
5.3.6	Metallographic Process.....	47
6.	RESULTS AND DISCUSSIONS	49
6.1	Investigation of Ex-situ MgB ₂ Monocore Wires.....	49
6.2	Examination of Ex-situ MgB ₂ Multifilamentary Wires	54
6.3	Investigation of In-situ MgB ₂ Monocore Wires.....	57
6.4	Examination of In-situ MgB ₂ Monocore Tapes	74
6.5	Investigation of In-situ MgB ₂ Multifilamentary (18+1) Wires	83
6.6	Examination of Preliminary Coil Wound with In-situ Fe/MgB ₂ Monocore Wire.....	86
6.7	Bending test of In-situ Fe/MgB ₂ Multifilamentary(18+1) wires	89
6.8	Test of The Fabricated Racetrack Coils	94
7.	CONCLUSIONS.....	96
8.	REFERENCES	98
	CURRICULUM VITAE.....	116

LIST OF FIGURES

	<u>Page</u>
Figure 2.1 Crystal structure of MgB ₂ (Buzea and Yamashita, 2001)	3
Figure 2.2 H_{c2} values of various MgB ₂ samples at low temperatures (Buzea and Yamashita, 2001).....	6
Figure 2.3 The absence of weak links in MgB ₂ (Buzea and Yamashita, 2001)..	7
Figure 2.4 The presence of weak links in BSCCO (Han et al., 1993; Giri et al, 2007).....	8
Figure 2.5 The temperature dependence of the resistivity of polycrystalline MgB ₂ under zero magnetic field (Kambara et al, 2001).	9
Figure 2.6 The magnetic lines of force (flux lines) in and around a superconductor (a) in the normal state above the critical temperature (T_c) (b) in superconducting state below T_c (Ford and Saunders, 2005).....	11
Figure 2.7 Penetration of the magnetic field into a superconducting sample λ is the penetration depth (Mourachkine, 2004).	12
Figure 3.1 In-situ or Ex-situ powder in tube (PIT) and pellet-in-tube (PLIT) scheme	15
Figure 3.2 The schematic representation of the CTFF method (HyperTech, 2008).....	15
Figure 3.3 Annealing temperature versus T_c values for commercial MgB ₂ /SUS316 tapes (Matsumoto et al, 2002).	23
Figure 3.4 Annealing temperature versus transport J_c values for commercial MgB ₂ /SUS316 and MgB ₂ /Fe tapes for 1h (Matsumoto et al, 2002; Fujii et al, 2002)	23
Figure 3.5 Comparison of H-T curves for MgB ₂ and LTS wires (Vinod and Upendran, 2010).....	27
Figure 5.1 Image of ball milling machine	30
Figure 5.2 Filling processes for ex-situ and in-situ MgB ₂	30
Figure 5.3 Photograph of the dies used in drawing process.....	31
Figure 5.4 Wire drawing machine.....	33
Figure 5.5 Wire pointing machine	33
Figure 5.6 Programmable tube furnace	33
Figure 5.7 Photograph of (a) preparation of ex-situ MgB ₂ /Fe 7 filamentary wire, (b) ex-situ MF MgB ₂ /Fe wire and (c) ex-situ MF MgB ₂ /Fe wires	34
Figure 5.8 Presentation of voltage and current contacts (a), image of the preliminary solenoid coil covered by G-vanish before measurement (b).....	38
Figure 5.9 Image of the MgB ₂ /Fe (18+1) wires bent to different diameters.....	39
Figure 5.10 Schematic illustrations of wire pieces taken for measurement from different sections of the bent MgB ₂ /Fe (18+1) wires	39
Figure 5.11 Images of the fabricated long MgB ₂ /Fe wires before (a) and after (b) S-Glass braiding.	40
Figure 5.12 Terz M. Expo Braiding Machine	40
Figure 5.13 Image of the produced wire 1.10 mm in diameter after braiding with S-glass fiber.....	41

Figure 5.14 Image of the solenoid coil wound on a steel former and coated with EX-THEMP glue before heat treatment.....	41
Figure 5.15 Photograph of the solenoid coil after sintering under argon flow .	42
Figure 5.16 Images of the isolated wires after sintering under different conditions.	42
Figure 5.17 Winding process of racetrack coils.	43
Figure 5.18 The manufactured racetrack coils before (a) and after (b) sintering.	43
Figure 5.19 Three Zone Programmable Furnace.	44
Figure 5.20 a) Mounting Machine, b) Polishing Machine.	48
Figure 5.21 Optical Microscope OLYMPLUS GX41.	48
Figure 6.1 Microhardness values of ex-situ monocoire MgB_2/Fe wires of different diameters (crossection includes Al material in core).....	50
Figure 6.2 Microhardness values of ex-situ monocoire MgB_2/Fe wires (Filling 1) of different diameters (crossection includes MgB_2 powder in core).....	50
Figure 6.3 XRD patterns of ex-situ monocoire MgB_2/Fe (2.00mm ϕ) wires and iron sheath sintered at 850°C for 1 hour.	51
Figure 6.4 Resistance vs Temperature graph of Ex-situ monocoire MgB_2/Fe wire 2.00 mm ϕ	52
Figure 6.5 SEM image ;Ex-situ monocoire MgB_2/Fe wire (2.00mm ϕ -850-1h) longitudinal region (Filling 2).....	52
Figure 6.6 SEM image; Ex-situ monocoire MgB_2/Fe wire (2.00mm ϕ -850-1h) longitudinal region (Filling 1).....	53
Figure 6.7 Current vs Voltage curves of Ex-situ monocoire MgB_2/Fe wires measured at temperatures below T_c . These wires were produced by PIT and PLIT filling methods with 2 mm diameter and sintered at 850 °C for 1 hour	53
Figure 6.8 Resistivity vs Temperature graphics of MgB_2/Fe (6+1) and MgB_2/Fe (18+1) filamentary wires sintered at different temperatures.	54
Figure 6.9 SEM Images taken from the cross sections of the MgB_2/Fe wires sintered at 900 °C for 1 hour with a) (6+1) and b) (18+1) filaments.	55
Figure 6.10 Graphics of dependence of resistive transition upon (a) applied current for different values of constant magnetic fields the MgB_2/Fe (6+1) and (b) applied magnetic field for different values of constant transport currents (18+1) wires.	56
Figure 6.11 XRD graph of in-situ monocoire MgB_2/Fe wire 1.90 mm Φ sintered at various temperatures and the used paste to hold samples in the inserted graph.	57
Figure 6.12 ρ vs T graph and Resistivity normalized (ρ_n) vs T inserted of in-situ monocoire MgB_2/Fe wire at 1.90 mm Φ sintered at different temperatures.	58
Figure 6.13 In-situ monocoire MgB_2/Fe wire 1.90 mm Φ sintered at 900 °C for 1h (Filling 1).....	59
Figure 6.14 In-situ monocoire MgB_2/Fe wire 1.90 mm Φ sintered at 900 °C for 1h (Filling 2).....	59
Figure 6.15 In-situ monocoire MgB_2/Fe wire 1.90 mm Φ sintered at 800 °C for 1h (Filling 2).....	60

Figure 6.16 Magnetic field dependence of the critical currents of the in-situ Fe/MgB ₂ wire samples at 4.2 K.	61
Figure 6.17 The line scan of SEM-EDX analysis of the (a) Filling 2 – 800 °C, (b) Filling 2 – 900 °C samples, (c) Filling 1 – 900 °C for 1 hour samples.	62
Figure 6.18 Polished cross-sectional SEM images of the in-situ Fe/MgB ₂ wires. Columns belong to Filling 2-900, Filling 2-800 and Filling 1-900°C from left to right.	63
Figure 6.19 The EDS analysis of samples cross-section for (a) and (b) sample A (0.1 MPa) and (c) sample B (1 GPa).	64
Figure 6.20 Transport R - T curves for samples A and B, (a) in low magnetic fields, (b) in high magnetic fields and (c) Transport R_N - B curves for samples A.	65
Figure 6.21 Transport J_c - B curves for samples A and B (a) at 4.2 K, (b) at 20 K and (c) Transport F_p - B curves for samples A and B.	66
Figure 6.22 The SEM images of samples' cross-sections in the mode of secondary electron (SE), (a) and (b) show sample A, (c) and (d) indicate sample B.	67
Figure 6.23 The SEM analysis of samples cross-section in the BSE mode for sample A(a) and sample B(c). Sample A(b) and sample B(d) in the SE mode.	68
Figure 6.24 Transport measurements of the F5E850 and F5E900 in-situ monocoresh MgB ₂ /Fe wire samples.	69
Figure 6.25 Magneto-resistivity measurements of the F5E900 and the F5E850 in-situ monocoresh MgB ₂ /Fe wire samples.	69
Figure 6.26 Transport I_c measurements of the F5E850 and F5E900 in-situ MgB ₂ /Fe monocoresh wire samples at 4.2 K under different magnetic field strengths up to 9 T.	70
Figure 6.27 Transport engineering J_c measurements of F5E850 and F5E900 in-situ MgB ₂ /Fe wire samples at 4.2 K with different magnetic field strengths up to 9 T.	71
Figure 6.28 Transport I_c measurements of F5E900 (a) and F5E850 (b) in-situ MgB ₂ /Fe wire samples at constant temperatures just below T_c in self-field.	72
Figure 6.29 X-Ray Diffraction analyses of the wire samples after the Fe sheath material was extracted mechanically.	73
Figure 6.30 SEM images as cross sectional of F5E900 wire core (on left) and F5E850 wire core (on right).	74
Figure 6.31 SEM images of a-b) F5E900 and c-d) F5E850 wire samples at 10 μ m and 5 μ m scales.	74
Figure 6.32 The ρ - T curves of the Fe/MgB ₂ wire sample sintered at 950°C and the insert graph for the Fe/MgB ₂ wire sintered at 800°C for PA of both samples was performed at 850 oC for 1 hour each experimental step.	75
Figure 6.33 Variation of $T_{c,onset}$ (a) $T_{c,offset}$ (b) ΔT (c) of the five sintered Fe/MgB ₂ samples in the BP, AP, and PA steps.	77
Figure 6.34 XRD patterns of (black) the Fe/MgB ₂ samples initially sintered at 950°C, (red) after pressing and (blue) after post annealing at 850 °C.	78

Figure 6.35 I - V curves of (a) the Fe/MgB ₂ wire sample initially sintered at 950 °C (b) the sample after pressing and (c) the sample after post-annealing at 850 °C.	79
Figure 6.36 T vs J_{cc} curves of a) BP , b) AP , and c) PA at 850 °C for the samples initially sintered at different temperatures from 800 °C to 1000 °C.....	80
Figure 6.37 SEM images taken from fracture cross sections of Fe/MgB ₂ samples initially sintered at 950 °C after steps of (a) BP , (b) AP and (c) PA at 850 °C.....	82
Figure 6.38 Microstructural SEM images of Fe/MgB ₂ samples initially sintered at 950 °C after a) BP , b) AP and c) PA at 850 °C.	83
Figure 6.39 Resistivity vs temperature curves of MgB ₂ /Fe 18+1 in-situ filamentary wire sample for the first set sintered at different temperatures.	84
Figure 6.40 Resistivity vs temperature curves of MgB ₂ /Fe 18+1 in-situ filamentary wire samples for the second set sintered at different temperatures for 1 and 2 hours heat treatment durations.	84
Figure 6.41 Current vs voltage curves of second set in-situ MgB ₂ /Fe 18+1 filamentary wires at a constant temperature slightly below their $T_{c,offset}$	85
Figure 6.42 (a) Polished surface of MF5E at 700 °C/1h, (b) fcs of MF5E at 750°C/1h, (c) fcs MF5E 700 °C/1h and (d) MF5E 750 °C/1h in 5 μm scale.....	86
Figure 6.43 R vs T graph for various potential links on preliminary solenoid coil.	87
Figure 6.44 Current vs voltage graph for the solenoid coil with FL (a) and MD (b) voltage contacts under various applied magnetic fields....	87
Figure 6.45 Transport I_c of the preliminary solenoid coil at different temperatures.	88
Figure 6.46 SEM images of the produced MgB ₂ /Fe monocoil wire for the solenoid preliminary coil before and after bending.	88
Figure 6.47 XRD taken from MgB ₂ /Fe monocoil wire for the solenoid preliminary coil.	89
Figure 6.48 R vs T graph of straight (black) and 70 mm bent (red) F5 multifilamentary 1.00 mm in diameter annealed at 700 °C for 1 hour.....	90
Figure 6.49 I_c values of F5 (18+1) filamentary straight (black) and 70 mm bent (red) wire with 1.00 mm diameter at 22 K under 6 T.	91
Figure 6.50 SEM images of the polished (a) three filaments of MgB ₂ /Fe (18+1) straight wire, (b) two upper filaments of 7 cm bent wire 1.00 mm in diameter.....	91
Figure 6.51 R - T graph of 0.56 mm (OD) MgB ₂ /Fe MF straight and bent to 70 mm wires	92
Figure 6.52 R - T graph of 0.56 mm (OD) MgB ₂ /Fe MF straight and bent to 50 mm wire.....	92
Figure 6.53 I - V graphs of 0.56 mm (OD) MgB ₂ /Fe MF straight, bent wires at 22 K under external magnetic field.	93
Figure 6.54 SEM images of polished and etched cross section of 0.56 mm (OD) MgB ₂ /Fe MF wire at two different magnifications.	93

Figure 6.55 *I-V* curves at room temperature of the racetrack coil before
(black) and after (red) sintering.....94
Figure 6.56 The measured magnetic field at the center of F5B racetrack coil..95



LIST OF TABLES

	<u>Page</u>
Table 2.1 Important superconducting parameters of MgB ₂ sample (Pachla et al, 2005).....	4
Table 2.2 The coherence lengths values reported for MgB ₂ superconductor (Buzea and Yamashita, 2001).	13
Table 3.1 List of the studied MgB ₂ samples with type of dopants	22
Table 3.2 Magnetic field values of various coils for applications (MIT, 2003)	26
Table 3.3 Properties of technological superconducting materials at 4.2 K (Vinod and Upendran, 2010).....	27
Table 5.1 Drawing process of ex-situ MgB ₂ /Fe sample	31
Table 5.2 The HIP process of parameters for unreacted MgB ₂ wires.	36



LIST OF ABBREVIATIONS AND SYMBOLS

MRI	: Magnetic Resonance Imaging
NMR	: Nuclear Magnetic Resonance
T_c	: Critical Transition Temperature
T_s	: Sintering Temperature
MgB₂	: Magnesium Diboride
BCS	: Bardeen–Cooper–Schrieffer Theory
d	: Density
ρ	: Resistivity
B_{c2}	: Upper Critical Field
B_{c1}	: Lower Critical Field
B_{irr}	: Irreversibility Field
α	: Isotope Effect Coefficient
γ	: Anisotropy Factor
PIT(Filling 1)	: Powder-In-Tube
PLIT(Filling 2)	: Pellet-In-Tube
DC	: Direct Current
AC	: Alternative Current
J_c	: Critical Current Density
I_c	: Critical Current
V	: Voltage
K	: Kelvin
A	: Amps
cm	: Centimeter
IMD	: Internal Magnesium Diffusion
T	: Tesla
λ	: Penetration Depth
ξ	: Coherence Length
E_F	: Fermi Energy
p	: Momentum
v	: Velocity
r_b	: Bending Radius

θ	: Bragg Angle
MMC	: Metal Matrix Composite
CTFF	: Continuous Tube Forming and Filling
MNPs	: Magnetic Nano Particles
<i>a, b, c</i>	: Lattice Parameters
Mg	: Magnesium
B	: Boron
nB	: Nano Boron
Fe	: Iron
SS	: Stainless Steel
h	: Hour
°C	: Celsius
Ni	: Nickel
C	: Carbon
HIP	: Hot Isostatic Pressing
SMES	: Superconducting Magnetic Energy Storage
LTS	: Low Temperature Superconductors
HTS	: High Temperature Superconductors
LH2	: Liquid Hydrogen
LH	: Liquid Helium
BSCCO	: Bismuth Strontium Calcium Copper Oxide
YBCO	: Yttrium Barium Copper Oxide
μ	: Micro
Ω	: Ohm
nm	: nanometer
ϕ	: Diameter
 	: Parallel
Ψ	: Wave function
<i>H</i>	: Applied Magnetic Field
<i>T</i>	: Temperature
rpm	: revolutions per minute
mm	: millimeter
IA	: Intermediate Annealing
g	: gram

OD	: Outer Diameter
ID	: Inner Diameter
MPa	: Mega Pascal
GPa	: Giga Pascal
AP	: After Pressed
BP	: Before Pressed
PA	: Post Annealed
Ar	: Argon
XRD	: X-Ray of X-Ray Diffraction
SEM	: Scanning Electron Microscopy
PPMS	: Physical Properties Measurement System



ACKNOWLEDGEMENTS

I would like to thank my advisor, Prof. Dr. İbrahim BELENLİ for his guidance, support throughout this dissertation and also with my professional development. In particular, it is great fun studying with him on several important projects.

I would like to thank my thesis committee members for their guidance and assistance through this process. Of course, their discussion, comments, ideas and especially feedback have certainly been invaluable to interpret and improve the results obtained.

Assoc. Prof. Dr. Hakan YETİŞ in our project is willing to help me throughout this dissertation and my all studies. I learnt many things about superconductivity from his lengthy and useful conversations.

The technical assistance of R.A. Dr. A.Tolga ÜLGEN and Mrs. Emine DEMİRTÜRK are gratefully acknowledged. I would like to thank my best friends being especially Uğur SOYKAN, Mehmet AVCI, Şenol KAYA, Fatih GÜRLER and others.

I am very grateful to my amazing parents: Mom, Dad, Sisters and Brother for their love, moral support, constant encouragement, and prayers throughout this process. I would like also thank my darling, Seda TANYILDIZI being here for me with their love, continued support and prayers.

This study was supported by the The Scientific and Technological Research Council of Turkey, Grant No: 113F080

1. INTRODUCTION

Onnes who observed that electrical resistance of mercury suddenly dropped to zero below 4.2 K discovered initially superconductivity in 1911 (Onnes, 1911). Since that time, physicists continued to search for other materials having superconducting properties. Until today, a lot of superconductors with important physical and superconducting properties were discovered and produced for practical applications. The explored superconductors have been used in different areas such as MRI, NMR, energy storages, loss-free electrical transmission cable, motors, generators and levitation trains (Hull, 2003). Among them, one of most studied superconductor MgB_2 which is a binary compound has been discovered in 2001 (Nagamatsu et al., 2001). MgB_2 superconductors have superior properties such as high critical current density, binary chemical composition, simple crystal structure, low mass density (2.55 g/cm^3), low anisotropy, and high upper critical field (Zhou et al., 2009b). Critical transition temperature (T_c) of MgB_2 is highest among inter-metallic superconductors (Ford and Saunders, 2005) and it does not have a serious weak link problem at grain boundaries. MgB_2 samples are produced in various formations as single crystals, bulk samples, wires, tapes and thin films (Buzea and Yamashita, 2001). MgB_2 wires which may operate in liquid hydrogen are good candidate to replace NbTi and Nb_3Sn wires which have to operate in liquid Helium. In-situ MgB_2 wires and tapes exhibit better performance in high magnetic fields, however, production of the in-situ MgB_2 wires and tapes (Flukiger et al, 2011) has volume shrinkage problem due to reaction between Mg and B powders (Pan et al, 2003; Zhou et al., 2002; Shimada et al, 2011; Ye et al., 2014; Sobrero et al, 2015) constituting a real obstacle before real applications.

2. MgB₂ SUPERCONDUCTORS

2.1 The Discovery and Importance of MgB₂

MgB₂ was a well-known material before discovery of superconductivity in this material by Akimatsu (2001). Since 2001, a large number of researchers have carried out studies on MgB₂ materials as bulk samples, single crystals, thin films, tapes and wires (Buzea and Yamashita, 2001). Their mechanical, physical and superconducting properties have been improved by heat treatment procedure (Yang et al, 2015), dopants (Qin et al, 2015; Wang et al, 2015b), additives (Da Silva et al, 2015) and diffusion process (Yilmazlar et al, 2014) etc. MgB₂ superconducting materials, especially tapes and wires, have a good potential of usage in transformers, motors, MRI magnets, accelerator magnets, wind turbines and generators. MgB₂ becomes more advantageous when used at around 20 K in liquid hydrogen and superconducting coils, especially rotors (racetrack), can be produced with MgB₂ materials in a much lighter manner compared to other superconductors. MgB₂ superconducting materials will be more beneficial for medical practices as compared to other type II superconductors having high potential in industrial applications and marketing.

2.2 Crystal and Electronic Structure of MgB₂

Magnesium diboride (MgB₂) is an intermetallic compound and it has a simple hexagonal AlB₂ type crystal structure which is common among borides. Hexagonal structure of metallic compounds including borides belongs to space group P6/mmm. It contains graphite type boron layers separated by hexagonal layers of magnesium (Nagamatsu et al, 2001; Qin et al, 2015).

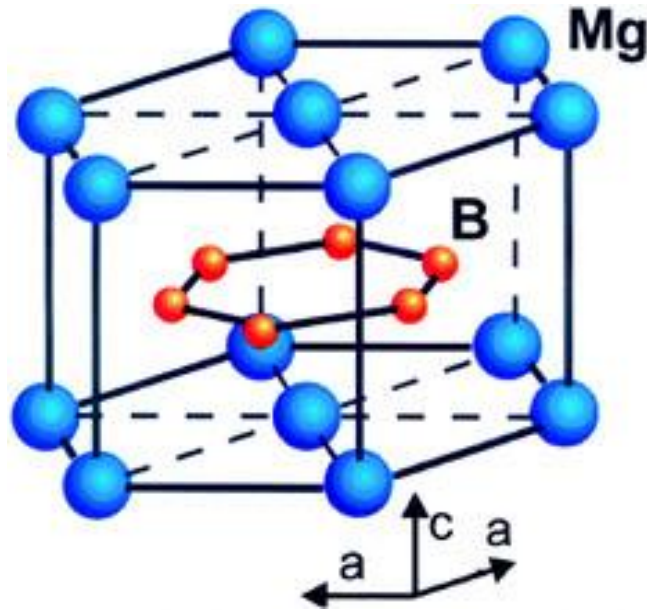


Figure 2.1. Crystal structure of MgB₂ (Buzea and Yamashita, 2001)

The lattice constants are reported as $a=b= 3.0834 \text{ \AA}$ and $c= 3.5213 \text{ \AA}$ with 0.0003 and 0.0006 \AA deviations, respectively (Jones and Marsh, 1954). As seen in Figure 2.1. Magnesium atoms are located at the centers of the boron hexagons. Each Mg atom donates their electrons to the boron planes. MgB₂ shows a strong anisotropy in the B-B lengths. Also, the structure of MgB₂ similar to graphite and the distance between the boron planes is longer than the intra-planar B-B bonds in the planes. The metallic B layers play an important role in the superconductivity of MgB₂ (Kortus et al, 2001). The band structure of MgB₂ depicts the substantial ionization of magnesium by completely transferring the electrons in 3s orbital to 2 dimensional boron planes (Buzea and Yamashita, 2001; Kortus et al, 2001). Therefore, covalent B-B bonds and ionic Mg-B bonds forms the hexagonal structure of MgB₂. 2p boron states have metallic character and determine the density of states at the Fermi energy (An and Pickett, 2001).

2.3 Superconductivity Mechanism in MgB₂

After the exploration of superconductivity in MgB₂, many scientists were curious whether superconductivity of MgB₂ can be explained with BCS theory. Several experimental and theoretical studies have been done to explain superconductivity of MgB₂ and its superconducting properties. The results of some studies have been

listed in Table 2.1. It has been agreed upon that superconductivity mechanism in MgB₂ can be explained with BCS theory. According to this theory, high frequency phonons in the low atomic mass compounds may produce a higher T_c . Also, MgB₂ seems to be a conventional BCS type superconductor according to band structure studies (Xi, 2008). BCS theory assumes that the superconductivity occurs via pairing of electrons with attractive interaction between electrons sufficiently near to the Fermi surface and this interaction is mediated by phonons (Bardeen et al, 1957). According to some findings, it is said that there are several effects such as isotope effect, anisotropy and energy gap for explanation of superconducting mechanism in MgB₂.

Table 2.1. Important superconducting parameters of MgB₂ sample (Pachla et al, 2005)

PARAMETERS	VALUES
Critical Temperature	$T_c=39$ or 40 K
Hexagonal Lattice Parameters	$a=b=3.086$ Å, $c=3.524$ Å
Theoretical Density	$d=2.57$ g/cm ³
Pressure Coefficient	$dT_c/dP=-1.1-2$ K (Gpa) ⁻¹
Carrier Density	$n_s=1.7-2.8 \times 10^{23}$ holes cm ⁻³
Isotope Effect	$\alpha_T = \alpha_B + \alpha_{Mg} = 0.30 + 0.02$
Resistivity Near Tc	ρ (40 K)= $0.4-16$ $\mu\Omega$ cm
Resistivity Ratio	$RRR = \rho$ (40 K)/ ρ (300 K)= $1-27$
Upper Critical Field	$H_{c2} // ab(0)=14-39$ T $H_{c2} // c(0)=2-24$ T
Lower Critical Field	$H_{c1}(0)=27-48$ mT
Irreversible Field	$H_{irr}(0)=6-35$ T
BCS Coherence Lengths	$\xi_{ab}(0)=3.7-12$ nm $\xi_c(0)=1.6-3.6$ nm
Penetration Depths	$\lambda(0)=85-180$ nm
Energy Gap	$\Delta(0)=1.8-7.5$ meV
Debye Temperature	$\Theta_D=750-880$ K
Critical Current Densities	$J_c(4.2$ K, 0 T) $>10^7$ Acm ⁻² $J_c(4.2$ K, 4 T) $=10^6$ Acm ⁻² $J_c(4.2$ K, 10 T) $>10^5$ Acm ⁻² $J_c(25$ K, 0 T) $>10^6$ Acm ⁻² $J_c(25$ K, 2 T) $>10^5$ Acm ⁻²

2.3.1 Isotope Effect (α)

The isotope effect of boron in MgB₂ superconductor is observed by Budko et al, (2001a). Budko and his co-workers studied with ¹⁰B and ¹¹B. The critical temperature varies from 40.2 K to 39.2 K as the average atomic mass of boron varies from 10 to 11 in MgB₂. They have reported the isotope effect coefficient is $\alpha=0.28$ for boron. The dependence of T_c on the isotopic mass reveals that electron lattice interactions have a great importance on superconductivity mechanism. The isotope effect was measured for Mg and B and they found as $\alpha= 0.02$ for Mg, $\alpha= 0.30$ for B respectively. Also, they reported that B atoms contribute more to the pairing mechanism in superconductivity of MgB₂ than Mg atoms do (Hinks et al, 2001; Canfield et al, 2003). The total measured isotope effect coefficient of MgB₂ (α_t) is 0.32 and this value is smaller than the value predicted by BCS theory. This value revealed that MgB₂ is a special material among all superconducting materials and it is a BCS type superconductor. The smaller isotope effect coefficient in MgB₂ is explained with strong coulomb repulsion (Lorenz et al, 2001) and large anharmonicity of Boron vibrations (Bordet et al, 2001).

2.3.2 Anisotropy (γ)

Differences of magnitudes in crystal structure lattice parameters a , b and c of any superconducting phase leads to anisotropy level. The anisotropy of MgB₂ superconductor can be tested by resistivity measurements in magnetic field applied parallel and perpendicular to Mg and B planes of MgB₂ single crystals. Electrons move easily in some directions and with difficulty in others because of the layered structure of some high temperature superconductors (HTS). This gives rise to the property known as anisotropy (Sheahen, 2002). In single crystals, the critical current density in the ab plane is much higher than that of c plane. Coherence length ξ of these compounds is small and grain boundaries in high temperature superconductors act as weak links due to the difference the region of crystallographic disturbance in the boundary between two grains (Dew-Hughes, 2001). Some superconducting parameters are different along different crystal directions within the crystal structure. Anisotropy of MgB₂ is important not only for basic understanding of this material

but also practical applications (MRI, NMR, etc..), strongly affecting the pinning, thus the critical currents. There are the detailed investigations for various MgB₂ form such as bulk, single crystal, thin film and wire in literature. For instance, the anisotropy of one material can be estimated on epitaxial films (Collings et al, 2008), wire ($\gamma \approx 5$) (Bud'ko et al, 2002), aligned powders (Handstein et al, 2001) and single crystals (Xu et al, 2001; Pradhan et al, 2001). Many groups have been measured anisotropy of MgB₂ by different methods (Vinod et al, 2006; Kortus et al, 2007). The anisotropy factor γ can be written as in equation 2.1;

$$\gamma = H_{c2}^{\parallel ab} / H_{c2}^{\parallel c} \quad (2.1)$$

The question about the anisotropy level of MgB₂ has unresolved, yet. Reported values of anisotropy level range from 1.1 to 9 (Handstein et al, 2001; Shinde et al, 2001). That is, this anisotropy is smaller than oxide superconductors. We can say that MgB₂ samples have H_{c2} values at magnetic measurements parallel to ab directions or perpendicular to c axis. For instance, as seen in Figure 2.3., H_{c2} value at 0 K is 32 T for films being T_c at 39K (Jung et al, 2001), ~ 40 T for films having critical transition temperatures lower than 39K (Patnaik et al, 2001), 25 T for single crystals (Xu et al, 2001), 19 T for bulk (Takano et al, 2001; Fuchs et al, 2001) and 16 T for wires (Bud'ko et al, 2001b).

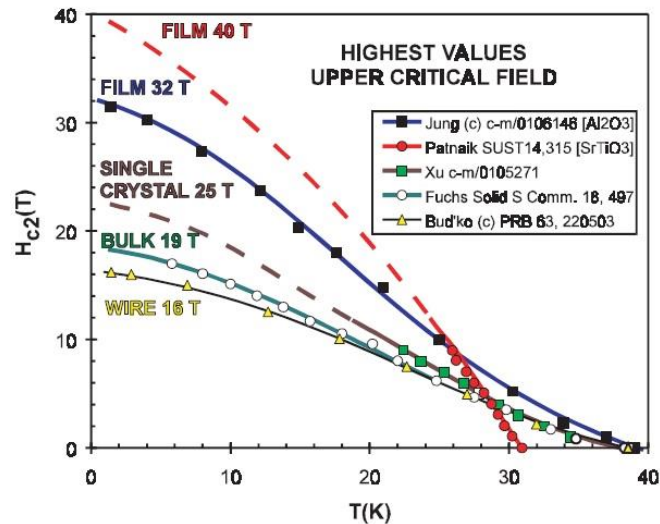


Figure 2.2. H_{c2} values of various MgB₂ samples at low temperatures (Buzea and Yamashita, 2001)

2.3.3 Absence of Weak Links

MgB₂ does not exhibit weak link behaviour at grain boundaries (Larbalestier et al, 2001) or fast flux creep (Thompson et al, 2001) which limits the performance of high T_c superconducting cuprates. Dhalle et al, (2001) and Kim et al, (2001) reported that the transport measurements of dense bulk samples in high magnetic fields yield very similar J_c values as the magnetization critical current measurements. This means that the inductive current flows coherently throughout the sample, unaffected by grain boundaries and the flux motion will determine dependence of J_c at magnetic field and temperature (Buzea and Yamashita, 2001). The absence of weak links in MgB₂ is illustrated in Figure 2.3. On the other hand, Figure 2.4 shows the J_c dependence applied magnetic field at 77 K and temperature dependence of J_c as evidence of weak link on grain boundaries in BSCCO samples. The critical current was suddenly decreased to very low values even below 1 T (Han et al, 1993).

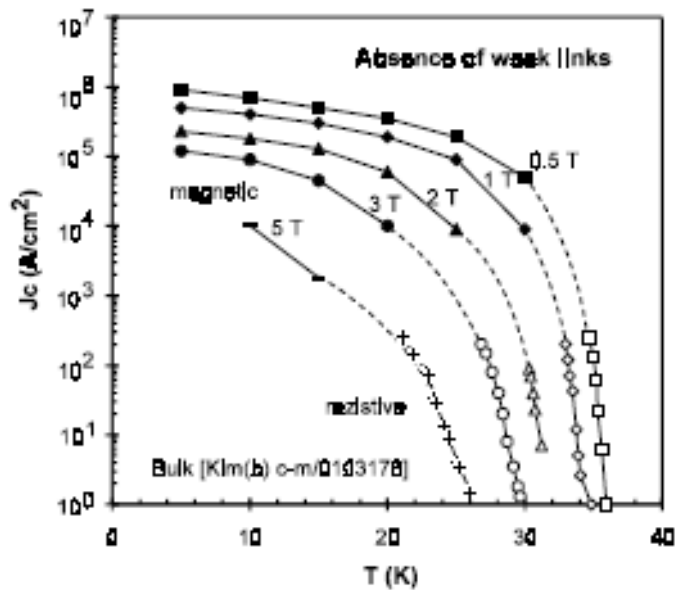


Figure 2.3. The absence of weak links in MgB₂ (Buzea and Yamashita, 2001).

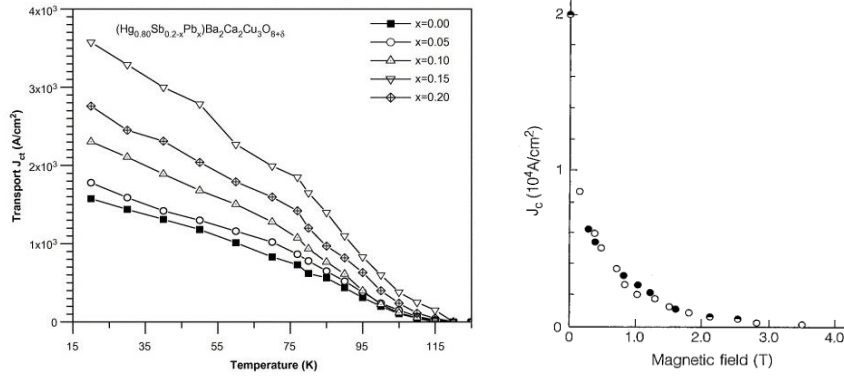


Figure 2.4. The presence of weak links in BSCCO (Han et al, 1993; Giri et al, 2007).

High critical current densities have been obtained in bulk samples regardless of the degree of grain alignment (Kim et al, 2001; Suo et al, 2001). This is an advantage for making wires or tapes without much degradation of J_c due to the lack of grain alignment, in contrast to grain boundary induced degradation in cuprate high temperature superconductors. Jin et al, (2001) has reported that some materials used as tubes or sheaths in the PIT method dramatically reduce the critical current of MgB₂. Although magnesium diboride (MgB₂) itself does not show the weak-link effect, contamination from the sheath materials may result in weak-link-like behaviour, most probably due to contamination from the sheath materials through the grain boundaries. One of the best ways is observation of the effect of magnetic field modulation on the DC resistance of superconductors. The phase detected response to the magnetic field modulation indicates a peak at T_c . Observation of a second peak at low temperature in the dc resistance vs temperature curve below T_c means the presence of weak links in the superconducting sample (Bohandy et al, 1990).

2.3.4 Critical Temperature (T_c)

A superconducting material loses its electrical resistivity below a certain temperature. This temperature is called the critical transition temperature (T_c). MgB₂ superconductor has the highest T_c (39 K) (Nagamatsu et al, 2001) in intermetallic compounds and narrow transition width of about 1 K as shown in Figure 2.5. T_c of other intermetallic compounds NbTi and Nb₃Sn are 9.8 K and 18.1 K, respectively (Bray, 2009). The T_c of MgB₂ sample doesn't change significantly with use of different production methods as PIT and IMD. For instance, The onset temperature

of the pure MgB₂ wire annealed at 700 °C for 1 h is ~38 K, which is comparable to that of PIT-processed samples annealed at the same temperature (Hur et al, 2008). Addition of 5 mol% SiC decreases T_c of MgB₂ to ~36 K as similar to those for PIT processed wires (Kumakura et al, 2005). On the other hand, some studies show that preparing different powders with additions, dopings and substitutions may increase with small difference (Varghese et al, 2011), decrease (Fischer et al, 2003; Shcherbakova et al, 2007; Eisterer et al, 2007) or do not significantly affect (Jiang et al, 2007; Li et al, 2012) when compared to T_c of pure MgB₂ among the studied samples. Also, T_c of MgB₂ prepared by in-situ powder is lower than that of the MgB₂ samples obtained with ex-situ powder (Kovac et al, 2006). Decrement of T_c for in-situ MgB₂ may be accompanied by an increased J_c in various annealing processes such as hot isostatic pressure (Wang et al, 2012) and spark plasma sintering (Sandu et al, 2011).

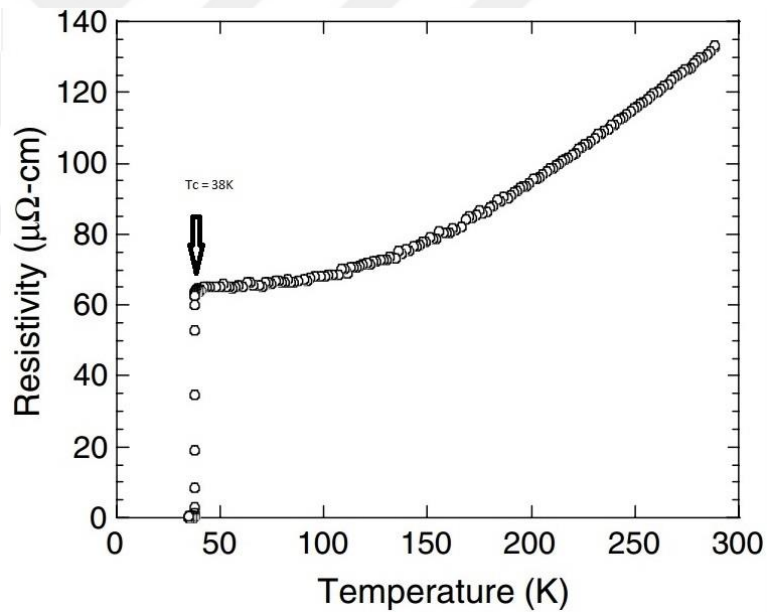


Figure 2.5. The temperature dependence of the resistivity of polycrystalline MgB₂ under zero magnetic field (Kambara et al, 2001).

2.3.5 Critical Current (I_c)

A superconducting material can carry a certain current without exhibiting resistivity at any temperature below T_c . There is a threshold value for the current value even though the material may be below its T_c . This threshold value is called as the critical

current (I_c) and Critical current density (J_c) is obtained from I_c by deviding by cross sectional area of the measured samples. The J_c value is the most important parameter in terms of many industrial applications. J_c can be obtained by transport measurements (Jun et al, 2015) or magnetization measurements (Barua et al, 2015), usually in liquid helium. MgB₂ samples obtained with various forms as thin films, bulks and wires etc. have different J_c . According to most literature, maximum magnetic J_c value for MgB₂ thin film can be 2.3×10^8 A/cm² at 5 K under self-field (Chen et al, 2016) calculated using bean model formula as in equation 2.2 (Bean, 1962). a and b refer to cross sectional parameters of the studied samples as width and thickness.

$$J_c = 20\Delta M / [a(1 - a/3b)] \quad (2.2)$$

Transport critical current density values for MgB₂ wires produced by IMD process have reached 1.1×10^5 A/cm² at 4.2 K under 10 T (Kumakura, 2011) and MgB₂ tape obtained by PIT method has highest J_c value 2.5×10^4 A/cm² at 4.2 K under 10 T (Yamada et al, 2004). Also, magnetic J_c value of pure MgB₂ bulk sample is approximately 5×10^4 A/cm² at zero field (Da Silva et al, 2016), here it should be noted that bulk samples contain large amount of voids.

2.3.6 Critical Magnetic Field (B_c) and Meissner Effect

Meissner effect is an important magnetic property of superconducting materials. If a superconductor specimen is cooled below T_c under external magnetic field, it expels the magnetic field from its interior. The metal becomes superconducting and the magnetic field is completely expelled from the superconductor; hence the flux density B is zero inside the sample, as seen Figure 2.6 (Ford and Saunders, 2005). This phenomenon is called the Meissner Effect. In the normal state above the T_c or when the applied magnetic field is greater than the critical field (B_c). The magnetic lines of force (flux lines) in and around a superconductor behave like in Figure 2.6 and it can be used to make magnetically levitated high speed magnetically levitated trains.

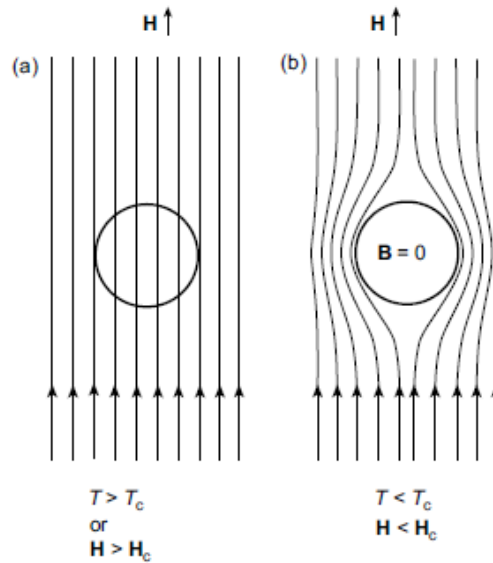


Figure 2.6. The magnetic lines of force (flux lines) in and around a superconductor (a) in the normal state above the critical temperature (T_c) (b) in superconducting state below T_c (Ford and Saunders, 2005).

2.3.7 Penetration Depth (λ)

When a superconducting sample exposes to an applied external magnetic field, the screening currents which circulate to cancel the flux inside must flow within a surface layer. So, the flux density does not fall abruptly to zero at the boundary of the metal but dies away within the region where the screening currents are flowing. For this reason the depth within which the currents flow is called the penetration depth (Rose-Innes and Rhoerick, 1978). It is given the symbol λ as shown in Figure 2.7.

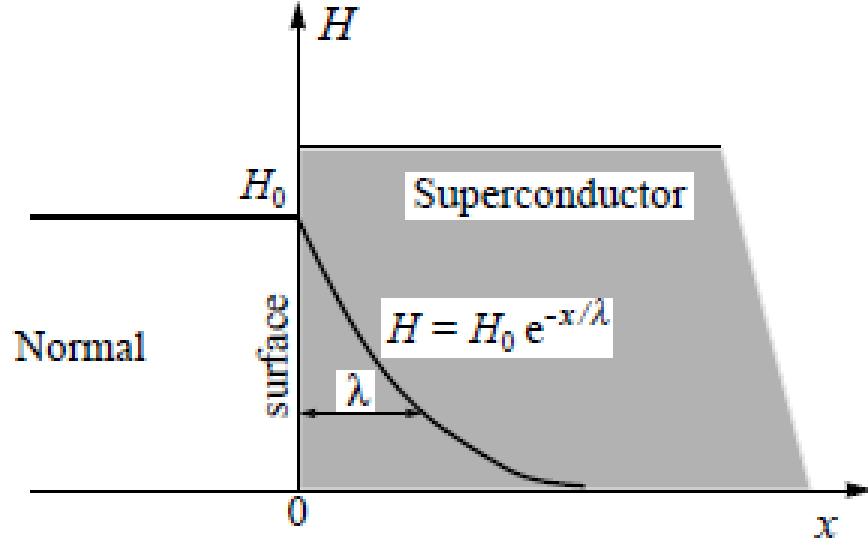


Figure 2.7. Penetration of the magnetic field into a superconducting sample λ is the penetration depth (Mourachkine, 2004).

2.3.8 Coherence Length (ξ)

When a superconducting material is cooled below its transition temperature additional order establishes between conduction electrons. There are two types conduction electrons, the first type electrons behave as superelectrons which can pass through the material without resistance, the second type electrons behave as normal electrons which are scattered by the lattice. The superelectrons form pairs which is called Cooper pairs. Whilst the cooper pair size is related to the wavefunction of a cooper pair, $\Psi(r)$, the coherence length ξ is determined by variation of the order parameter $\Psi(r)$. The coherence length depends on temperature, while the cooper pair size is independent. Since the order parameter in conventional superconductors is a “magnified” version of cooper pair wavefunctions, the value of coherence length and cooper pair size coincide $T=0$: $\xi(0) = \xi_0$ (Mourachkine, 2004).

$$\Delta k \sim k_F \cdot 2\Delta_0 / E_F \quad (2.3)$$

Where E_F in equation 2.3 equals to $\hbar^2 k_F^2 / 2m$ is the Fermi energy. Then in real space, large variations of the order parameter of the ground state can be expected within the interval Δx defined by the uncertainty relation.

$$\Delta x \Delta k \sim 1 \quad (2.4)$$

When it is continued,

$$\Delta x \sim E_F / 2\Delta_0 \cdot k_F = (1/2\Delta_0 \cdot k_F) \cdot (\hbar^2 k_F^2 / 2m) = \hbar \cdot p_F / 4m \Delta_0 = \hbar \cdot v_F / 4\Delta_0 \quad (2.5)$$

In equation 2.5, p_F is the electron momentum and v_F is electron velocity at the Fermi surface. By definition, Δx is the coherence length at $T=0$ K, thus the intrinsic coherence length $\xi_0 \equiv \Delta x$.

Table 2.2. The coherence lengths values reported for MgB₂ superconductor (Buzea and Yamashita, 2001).

Form	$\xi_{ab}(0)$ [nm]	$\xi_c(0)$ [nm]
Textured Bulk	5.5	5.0
Aligned Crystallites	6.5-7.0	4.0-4.1
Films	3.7-5.0	2.0-3.0
Single Crystals	6.1-6.5	2.5-3.7
Powders	11.4-12.8	1.6-1.7

The coherence lengths values along the ab -plane range between $\xi_{ab}(0) = 3.7 - 12.8$ nm and along c -axis between $\xi_c(0) = 1.6 - 5.0$ nm (Buzea and Yamashita, 2001). The coherence lengths values are showed in Table 2.2 for different forms of MgB₂ superconductors.

3. MgB₂ SUPERCONDUCTING WIRES

3.1 Fabrication Methods for Superconducting MgB₂ Wires and Tapes

Importance of superconducting materials for industrial applications such as power lines, motors, generators and superconducting cables increases progressively (Zhou et al, 2002). MgB₂ material in the form of the flexible wires or tapes with satisfactory performances must be developed for these applications. As a result of recent developments in the transport J_c , most investigators are further interested in MgB₂ wires and tapes for future applications due to low running costs (without liquid helium) in magnetic fields of a few tesla and temperatures up to 20 K (Wang et al, 2010). Several techniques such as the Metal Matrix Composite (MMC) (Scheuerlein et al, 2007), Continuous Tube Forming and Filling (CTFF) (Suo et al, 2007) and Powder-In-Tube (PIT) have been used to fabricate MgB₂-based and other superconducting wires (Dou et al, 2003a). Among them, PIT is the most crucial and common method for the fabrication of low-cost and practically MgB₂-based wires and tapes.

3.1.1 Powder-In-Tube (PIT) Method

PIT method is the most popular process for fabrication of good quality wires or tapes (Braccini et al, 2007; Kumakura et al, 2001; Flukiger et al, 2003; Fujii et al, 2002). MgB₂ wires and tapes have been fabricated successfully by using the PIT method as indicated in Figure 3.1. The ex-situ PIT method is very attractive for large scale practical applications since the fabrication process has intermediate annealing steps depending on distance between initial and final diameter of the sample, low production cost (Kumakura et al, 2007; Glowacki et al, 2001; Malagoli et al, 2002; Nakane et al, 2006; Tanaka et al, 2002; Vinod et al, 2006) and easy formation. In this method, superconducting powder is filled into a ductile metal tube and then rolled drawn or swaged into small diameters for various applications.

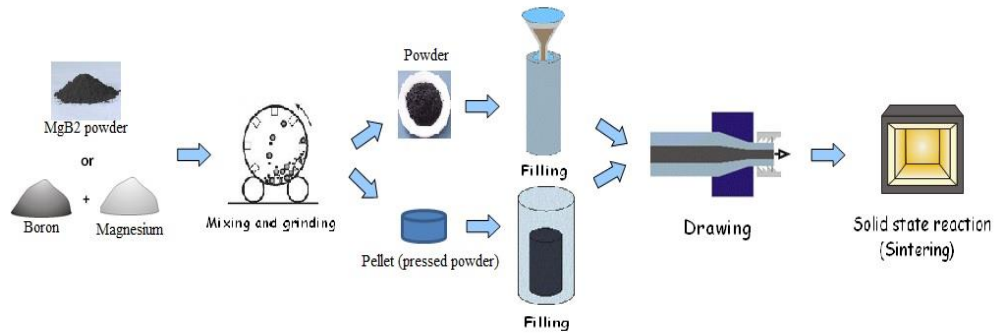


Figure 3.1. In-situ or Ex-situ powder in tube (PIT) and pellet-in-tube (PLIT) scheme

3.1.2 Continuous Tube Forming and Filling (CTFF) Method

Hyper Tech Research developed a modified PIT process which is called the Continuous Tube Forming and Filling (CTFF) for low cost continuous production of MgB_2 wires (Tomsic et al, 2007). They claim that in the method, precursor MgB_2 powder is dispensed onto a strip of metal as it is being continuously formed into a tube. This process results in an overlap closed tube filled with powder in continuous lengths. CTFF is an alternative process for MgB_2 wires fabrication. CTFF is essentially an in situ PIT method without the long mechanical or thermo mechanical processes (HyperTech, 2008). In this method, homogeneity along the wire is better than PIT method and there is no limit on the length of wire produced. There are still several studies about fabrication of superconducting wires and tapes which have high J_c values using the CTFF process.

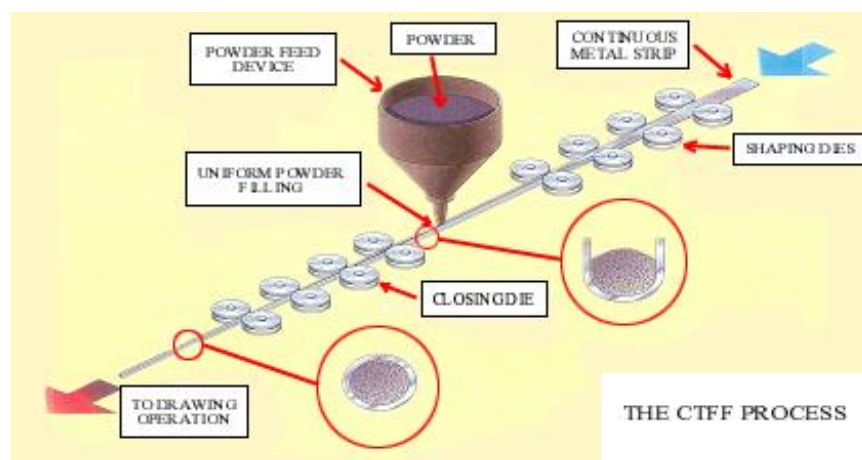


Figure 3.2. The schematic representation of the CTFF method (HyperTech, 2008)

3.1.3 Metal Matrix Composite (MMC) Method

Metal matrix composites, consist of at least two components, one of which is the metal matrix, and the other component is a ceramic or an intermetallic compound in forms of powder, whisker or short fibres. The metal matrix maintains the shape and the form of the composite, acts as a reinforcement medium, improves ductility and provides fracture toughness while the particulate constituent enhances the properties such as the electrical conductivity, wear resistance, hardness and elastic modulus values (Egilmez, 2006). Fabrication of MgB_2 superconductors via this method includes a hybrid method combining internal Mg diffusion and PIT processes (Ye et al, 2014), magnesium diffusion method, liquid infiltration (Giunchi et al, 2003; Dunanda, 2001) and CTFE techniques.

3.2 Procedures for Production of MgB_2 Superconducting Wires

3.2.1 Initial Filling Techniques

In preparation of initial powder for fabrication of MgB_2 wires or tapes, there are two methods as ex-situ (with commercial powder) and in-situ (with green Mg + B mixture) processes. Both techniques have been employed to fabricate MgB_2 wires, and tapes. There are advantages and disadvantages of both methods.

3.2.1.1 In-situ Reaction Technique

In this method, after a stoichiometric mixture of Mg and B is prepared, it is filled into a metal tube and this composite is drawn to the needed diameter for obtaining wire or tape with different processes (Kovac et al, 2011). There are several advantages like high J_c values, controlling particle size and difficulties such as Mg oxidation, existence of voids, higher reactivity with some sheaths and difficulty in obtaining homogeneity in this technique (Eisterer et al, 2002). Despite these difficulties, the most commonly investigated technique is the in-situ technique, since,

relatively high J_c values are obtained owing to its reasonably strong intergrain coupling (De-Silva et al, 2011; Yamamoto et al, 2004; Ma et al, 2009). The J_c values reported for ex-situ MgB_2 are still lower than J_c values of in-situ MgB_2 . Inter-grain coupling is insufficient and grain connectivity is low in ex-situ MgB_2 compared to in-situ MgB_2 (Wu et al, 2014).

3.2.1.2 Ex-situ Reaction Technique

Ex-situ reaction method means that the fully or almost fully reacted commercial MgB_2 powder is filled into appropriate metal tubes. Then, the obtained sample is drawn to suitable diameter and annealed for obtaining superconducting properties. The grain connectivity of reasonably high J_c ex-situ MgB_2 tapes is obtained to be less 10% than (Malagoli et al, 2008; Nakane and Kumakura, 2009) that of the typical grain connectivity of in-situ MgB_2 (Jiang et al, 2006; Ma et al, 2010; Matsumoto et al, 2006). That is, the J_c values of the samples prepared by the ex-situ method are not so good as J_c values of the in-situ samples in especially magnetic field (Romano et al, 2009). This shows that interfaces between ex-situ MgB_2 grains/agglomerates are weakly coupled in comparison with the chemically formed strong coupling in the in-situ MgB_2 . Higher density of the MgB_2 core in comparison with in-situ processed MgB_2 wires and tapes is a big advantage for ex-situ processing. The ex-situ method can be preferred to attain higher bulk density of 75% (the close-packing of rigid spheres) (Wu et al, 2014).

3.2.1.3 Reactive Liquid Mg Infiltration and External Mg Diffusion Technique

When MgB_2 wires or tapes are prepared with the mixture of B and Mg powders, the resultant MgB_2 tapes consist of a large amount of pores due to the volume shrinkage during chemical reaction of Mg and B to form MgB_2 phase (Matsumoto et al, 2003; Hata et al, 2006). As solution to the low J_c problem which arises from existence of pores, Mg vapor diffusion process (Canfield et al, 2001) and a liquid Mg diffusion process (Giunchi et al, 2003; Giunchi, 2003) have been used to produce MgB_2 . MgB_2

phase with higher mass density and much smaller amounts of pores has been obtained through these methods. Internal-Mg-diffusion (IMD) process being also one of Mg diffusion processes to fabricate MgB₂ wires with high density and superior J_c properties was first announced by Togano et al, (2007) and was improved by Giunchi et al, (2003); Xu et al, (2016); Rosova et al, (2015); Ye et al, (2012). In addition to this process, a process called hybrid between the IMD and PIT processes has been developed recently and this causes a reduction in the amount of unreacted B particles (or B-rich regions) and can also yield high J_e values as compared with IMD process (Ye et al, 20014). These Mg diffusion techniques produce MgB₂ material with much less pore, but generally a big hole remains where the Mg was placed at the beginning of the process.

3.2.2 Sheath Materials for MgB₂ Wires

The reactivity between powder and sheath materials is important in the production of a superconducting MgB₂ wires and tapes. Some researchers have investigated the effect of different sheath materials such as Cu, Ag (Soltanian et al, 2002), SS (Kumakura et al, 2007; Glowacki et al, 2001), Ni (Tanaka et al, 2002), Ta, Fe (Kumar et al, 2007; Akdoğan, 2015; Collings et al, 2003) and Glidcop sheaths (Kovac et al, 2014) on superconducting properties of MgB₂ wires/tapes. Iron sheath is widely used in fabrication of MgB₂ wire for being ductile and economical. It is reactive with MgB₂ above 900 °C (Wang et al, 2001; Grovenor et al, 2004) and with boron above 600 °C with very thin interaction layer (Kovac, 2015; Grivel et al, 2006). The Fe/MgB₂ annealed at 900 °C has still high critical current density 1.43×10^5 A/cm² at 4.2 K and it is one of the best sheath materials (Feng et al, 2003) in terms of sintering process at high temperatures among the used cladding materials in literature. On the other hand, since copper tubes can easily be deformed and are not very expensive, some researchers have used Cu tubes for cladding, but reactivity of Cu with Mg in MgB₂ at high sintering temperatures is a serious obstacle (Xiang et al, 2003). Moreover, Nb and Ta tubes were used either as cladding material or as a barrier to prevent the reaction with superconducting core and diffusion of magnesium and/or boron into sheath material (Goldacker et al, 2001; Fu et al, 2003; Kovac et al, 2006).

3.2.3 Chemical Doping or Addition

Many researchers struggle to improve grain connectivity, create pinning centers and increase J_c under self, low and high magnetic fields by using chemical addition or doping into MgB₂ powder. The used dopants affect superconducting properties in a negative or positive manner depending on fabrication parameters such as pressure, temperature and duration of heat treatment process. In literature, MgB₂ samples with 2 wt.% urea doping have best critical current density under magnetic field greater than 2.5 T as comparison with MgB₂ pure and samples doped with different amount of urea (Quin et al, 2015). MgB₂ thin films doped carbon (Gurevich et al, 2003) and nanoparticle (Collings et al, 2008) using single crystal can be improved its B_{c2} above 50 T at 4.2 K (Braccini et al, 2005). When MgB₂ in Fe-clad wire is doped with various magnetic nanoparticles (MNPs), T_c is generally suppressed and excessive MNPs doping affects superconducting properties of MgB₂ wires negatively. However, doping less than 2.5 wt. % with MNPs improves flux pinning and consequently increases in field J_c (Novosel et al, 2015). In addition, some studies obtained with doping of various elements (Feng et al, 2002; Goto et al, 2003; Slusky et al, 2001; Parisiades et al, 2009) have indicated the decrement of T_c and the increment of J_c with low substitution levels. At low field, while MgB₂ samples doped with TaB₂ have high critical current density (J_c) MgB₂ samples co-doped SiC and TaB₂ have even higher J_c (Da-Silva et al, 2015). On the other hand, Os doping leads to improved J_c and stronger flux pinning at magnetic field above 0.5 T (Grivel et al, 2014). Addition of Sb₂O₃ to MgB₂ samples causes the enhancement of J_c and H_{irr} through a mechanism which may be explained with the formation of nanometric MgB₄ and the indirect effect of oxygen or oxygen and Sb (Burdusel et al, 2012). Also, production of MgB₂ by using MgB₄ and Mg is an effective way of reducing amount of impurity phases and increasing J_c (Nardelli et al, 2013). Effects of SiC (Dou et al, 2002; Dou et al, 2007) and carbohydrate (Kim et al, 2006) dopings to MgB₂ for J_c improvement are comparable and nano-sized SiC dopant is more effective. Excess-Mg(15%) and SiC addition for formation of MgB₂ in wire cause to J_c of 10^4 A/cm² at 4 K under 11.5 T (Collings et al, 2008) and J_c for the nano-SiC 10% doped bulk sample is 2.4×10^5 A/cm² at 20K under 2 T (Dou et al, 2002). 2wt% glucose deteriorates superconducting properties of in-situ MgB₂ (Shahabuddin et al, 2011), Ti and Zr addition improves J_c of MgB₂ at low magnetic fields (Zhao et al,

2002; Feng et al, 2002) and Ti doping to MgB₂/Fe wires increase J_c about 3 times for $x=0.1$ and J_c value is approximately 10^6 A/cm² at 20 K without external magnetic field (Zhou et al, 200). SiC is most effective dopant to increase grain connectivity related to critical current density at high magnetic fields but at low magnetic fields, Ti is preferred instead of SiC at low magnetic fields (Pan et al, 2011). Doping of rare-earth oxides (Y₂O₃, Dy₂O₃, Ho₂O₃) (Wang et al, 2002; Chen et al, 2006; Cheng et al, 2006) and compounds consisting of carbon (nano-SiC, nano-diamond, CNTs, hydrocarbon, nano-C, diamond, amorphous C, B₄C, Mo₂C-TiC) (Matsumoto et al, 2006; Dou et al, 2002; Kim et al, 2006; Cheng et al, 2003; Serquis et al, 2007; Viljamaa et al, 2001; Dou et al, 2003b; Soltanian et al, 2003; Zhao et al, 2003; Yeoh et al, 2006; Mickelson et al, 2002; Yamamoto et al, 2005; Yamamoto et al, 2006) as graphene (Tang et al, 2014; De-Silva et al, 2011), C₆₀ (Zhang et al, 2008a) and activated carbon (Zhang et al, 2008b) to MgB₂ samples leads to improved J_c , higher H_{irr} and stronger flux pinning. A powder including two types of Mg, three types of amorphous B and C (carbon black; SigmaAldrich Japan) is named as homemade MBC, the refined MBC powder with acid solutions has been suggested for ex-situ MgB₂/Fe tapes and its critical current density reached to 6×10^3 A/cm² under 10 T at 4.2 K (Fujii et al, 2014). Doping of graphite as C source (MgB_{1.985}C_{0.015}) causes an improvement of J_c reaching 5.8×10^5 A/cm² at 10 K under self-field, while J_c values of MgB_{1.945}C_{0.055} samples are 1×10^4 A/cm² at 5 K under 7 T and at 10 K under 6 T. J_c value of MgB_{1.945}C_{0.055} sample are two times higher than that of the pure MgB₂ samples and all results indicates that graphite doping which causes grain growth and increases grain boundary flux pinning is very effective for improving of J_c at high field (Pan et al, 2008). On the other hand, some researchers found that low cost carbon dopant may not affect J_c and H_{c2} values positively due to different synthesis conditions (Ban et al, 2005; Agatsuma et al, 2006). Increment of J_c in high magnetic fields has been obtained by 10% melanin doping to MgB₂ bulk sample (Shah et al, 2014). The effect of silicone oil doping on J_c and n-factor for MgB₂ PIT wires is positive and this method is cheap, useful and a good candidate for applications (Hossain et al, 2012). The J_c of MgB₂ wire with polyacrylonitrile (PAN, –[C₃H₃N]–) doping (1.46×10^3 - 3.82×10^3 A/cm²) is higher than pure sample (1.1×10^2 A/cm²) at 5 K under 6.6 T (Hwang et al, 2010). Over-doped value is 10% for Maleic anhydride (C₄H₂O₃) and the optimally doped MgB₂/Fe wire reaches 1.08×10^4 at 12 T, 5.42×10^3 at 14 T, and 2.18×10^3 A/cm² at 16 T (Gao et al, 2007c). Also, the J_c of Ni doped

MgB₂/Fe wires (3.3×10^3 A/cm² at 5 K under 10 T) is 2.5 times larger than the J_c of undoped wire (Novosel et al, 2012). J_c of 10% yttrium acetate (Y(C₂H₃O₂)₃) doped MgB₂ tapes is best and about 10^4 Acm⁻² at 4.2 K under 12 T at 800 °C and over doping ratio is 20% for yttrium acetate in MgB₂ samples (Wang et al, 2011). Moreover, as comparison with pure samples, the effect of Nd₂O₃ doping on MgB₂ tapes is beneficial for J_c in magnetic fields as 2.46×10^3 Acm⁻² at 10 T and 5.27×10^2 Acm⁻² at 12 T, but these dopings cause some declines in T_c (Yao et al, 2011). Acetone doping for MgB₂/Fe tapes causes the anisotropy ratios to decrease and increases J_c at high field to increase. Lowering of anisotropy may cause MgB₂ texture to decrease and produces MgB₂ grains with smaller sizes, and also induces disorder by carbon substitution (Wang et al, 2010). MgB₂ wires doped with Lauric acid (LA) have a lower T_c , but better J_c in high magnetic field. The highest critical current density (J_c) has been reported as 5.32×10^3 A/cm² for 5wt.% among LA doped samples (Lee et al, 2010). Ethyltoluene (C₉H₁₂) and SiC powders added MgB₂ tapes fabricated with and without pre-heat treatment exhibits J_c of 3.3×10^4 A/cm² at 4.2 K under 10 T (Yamada et al, 2009). MgB₂ tapes doped with Co₃O₄ (0.5wt.%) and sintered at 700 °C for 1 hour can tolerate a maximum J_c approximately 10^8 A/m² at 4.2 K under 7 mT (Kuroda et al, 2009). Sugar doped MgB₂/Fe wire has about 10^4 A/cm² at 5 K and 10 T (Shcherbakova et al, 2007). Effect of stearic acid and stearate dopants on MgB₂/Fe tapes have better performances as compared to pure MgB₂ sample and transport J_c values are 2.02×10^4 Acm⁻² under 10 T for the sample doped with Zn stearate and 3.72×10^3 Acm⁻² at 4.2 K under 14 T for the sample doped with stearic acid (Gao et al, 2007b). Due to the deteriorating effect of excess MoSi₂ doping, amount of MoSi₂ dopant for MgB₂ tapes is limited to 2.5% and J_c value is 1.3×10^3 A cm⁻² at 4.2 K and 10 T for 2.5% doped MgB₂ tapes (Zhang et al, 2006). Addition of nano Si₃N₄ to MgB₂/Fe tapes enhances critical current density for greater than 5% providing a highest J_c value of 4.8×10^3 Acm⁻² at 4.2 K under 10 T (Jiang et al, 2005). Finally, Table 3.1 has been arranged for compound and element dopants to MgB₂ samples from researches in current literature and results of some studies are like this; WSi₂ addition to MgB₂/Fe tapes exhibits J_c of 2×10^3 A/cm² (5×10^3 A/cm²) under 10 T (8 T) (Ma et al, 2004), and ZrSi₂, ZrB₂ and WSi₂ dopants for MgB₂/Fe tapes reaches to J_c of 3×10^3 A/cm², 1.7×10^3 A/cm² and 1.9×10^3 A/cm², respectively under 10 T (Ma et al, 2003).

Table 3.1. List of the studied MgB₂ samples with type of dopants

Borides	Nitrides Silicides Hydrite	Oxides		Metals		Carbon
WB	AlN	Ag ₂ O	Bi ₂ O ₃	Al	Pt	C and nano C
AlB ₂	WSi ₂	ZnO	Y ₂ O ₃	Ag	Ru	CNT
TaB ₂	ZrSi ₂	CeO ₂	Al ₂ O ₃	Fe	Sb	B ₄ C
TiB ₂	SiCl ₄	GeO ₂	Eu ₂ O ₃	Ge	Sc	C ₁₅ H ₁₂ O ₂
NiCoB	Si ₃ N ₄	TiO ₂	(Bi,Pb)-2223	Co	Te	Li ₃ B ₄ C ₂
ZrB ₂	MoSi ₂	TeO ₂	Td ₄ O ₇	Mo	Sn	CNH
CeB ₄		Ho ₂ O ₃	Pr ₆ O ₁₁	Mn	Ti	C ₆₀
SmB ₆		Nd ₂ O ₃	CuFe ₂ O ₄	Ni	W	C ₁₆ H ₂ O ₃ N ₂
Ca ₃ B ₆ N ₄		Sb ₂ O ₃	YBCO	La	Zn	CaC
VB ₂		Co ₃ O ₄	Dy ₂ O ₃	Hf	Se	C ₄ H ₆ O ₄
h-BN		Fe ₃ O ₄	(Bi,Pb)-2212	Bi	Cu	C ₄ H ₆ O ₅
c-BN		CrO ₃		MNPs		BC ₂
FeB						Ti ₃ SiC ₂
Fe ₂ B						TiCl ₃
						CH ₄ N ₂ O
						Nano SiC
						C ₉ H ₁₂
						C ₁₈ H ₃₆ O ₂
						C ₁₂ H ₂₄
						Y(C ₂ H ₃ O ₂) ₃

3.2.4 The Annealing Temperature

The annealing process affects microstructure, physical homogeneity and chemical homogeneity diffusion of B, transition temperature, critical current and critical magnetic field of the prepared MgB₂ samples. Many researchers have performed deep investigations about heat treatment to improve superconducting properties of MgB₂ samples prepared by different methods. The commonly used route of preparing MgB₂ is to react the Mg and B powder mixtures in the range of 500-1000 °C (Larbalestier et al, 2001; Monteverde et al, 2001), following the chemical equation $Mg + 2B \rightarrow MgB_2$. Effect of heat treatment on T_c of ex-situ MgB₂/SS superconducting wires is shown in Figure 3.3 (Matsumoto et al, 2002) and critical current density values for different sheath materials (Fe and SS) are indicated in Figure 3.4 (Matsumoto et al, 2002; Fujii et al, 2002).

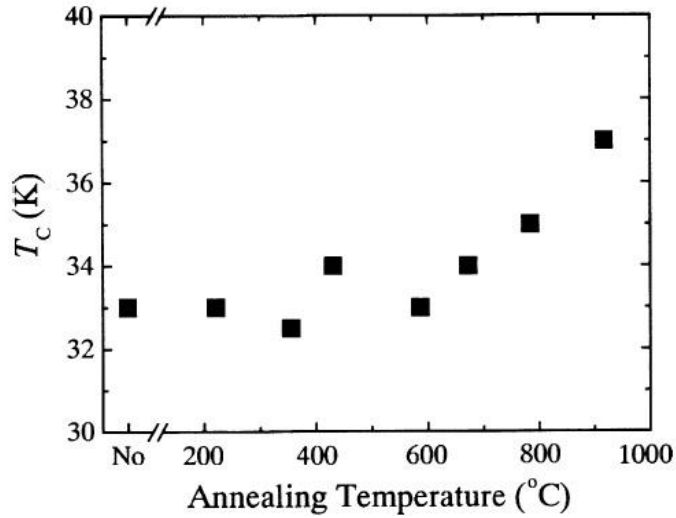


Figure 3.3. Annealing temperature versus T_c values for commercial $MgB_2/SUS316$ tapes (Matsumoto et al, 2002).

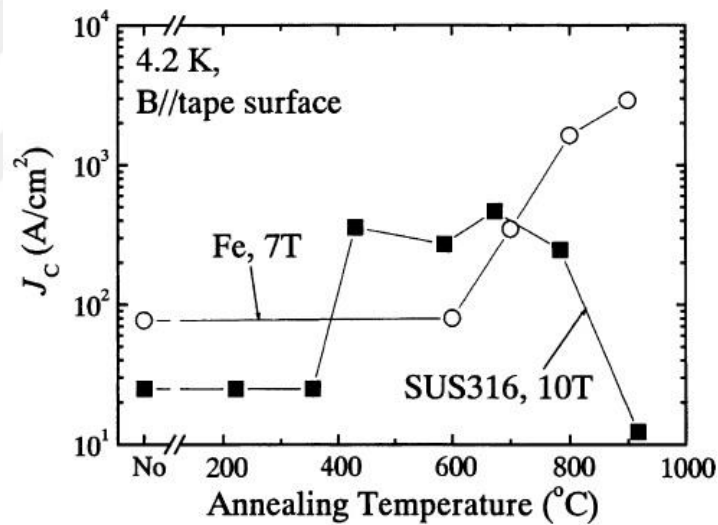


Figure 3.4. Annealing temperature versus transport J_c values for commercial $MgB_2/SUS316$ and MgB_2/Fe tapes for 1h (Matsumoto et al, 2002; Fujii et al, 2002)

Hence, the MgB_2 wires prepared with the ex-situ technique requires a heat treatment at approximately $950^\circ C$ while it is sufficient to sinter the wires prepared with the in-situ technique at lower temperatures of $600-750^\circ C$ (Dou et al, 2003a; Fu et al, 2003) to complete the reaction. A high transport current was obtained in the fabricated tapes using MgB_2 powder and Fe and Ni tube after annealing at 950 and $980^\circ C$ for 0.5 h in a pure argon atmosphere (Suo et al, 2001). The J_c of pure MgB_2 is

strongly influenced by heating rate, better J_c is obtained with slow heating rate (100 °C/h). Since the slower heating rate causes the samples more time at temperatures below the melting point of Mg and to form more MgB₂ through solid-state diffusion. The amount of free Mg is minimized on reaching 650 °C. Fast heating rates and high temperatures facilitate Mg loss and pores in the studied MgB₂ wire samples (Chen et al, 2005). Heat treatment time as short as 5 minutes is reported to be enough for formation of MgB₂ phase at temperature higher than 750 °C, and the highest J_c value ($\sim 10^6$ A/cm² at 10 K) was obtained at 800 °C for 15 minutes for un-doped MgB₂/Fe tapes (Suo et al, 2007b). Additionally, the MgB₂ wire samples annealed at 770 °C and 810 °C have more impurity phases and 830 °C and 850 °C are more suitable temperatures to form MgB₂ superconducting phase for 5-30 minutes sintering times. Heat treatment is optimized at 830 °C for 15 min (Suo et al, 2007a). However, that situation is different for the doped MgB₂ samples in terms of J_c value; annealing at temperatures higher than 900 °C is necessary for nanocarbon doped MgB₂ samples in order to get the better J_c at high field (Zhang et al, 2007; Yeoh et al, 2007). Nano-SiC doped MgB₂ requires annealing at temperature less than 650 °C (Yeoh 2007; Soltanian 2005). Sintering temperature of 850 °C is optimum for the Zn-stearate doped MgB₂ tapes (Gao et al, 2007a). MgB₂ sample doped with 10 wt.% silicone oil has the largest J_c in-field enhancement among the studied various samples sintered at 780 °C. The un-doped and silicone oil doped MgB₂ samples annealed in the range of 600–900 °C show better MgB₂ formation with less MgO impurity content. Silicone oil doped MgB₂ annealed at 600 °C for 4 h clearly indicates the presence of Mg₂Si phase (Wang et al, 2007).

3.2.5 Grain Connectivity

Investigations on critical field and grain connectivity of MgB₂ samples are presently in progress towards technological applications. A number of methods have been utilized to enhance superconducting properties of MgB₂ samples by hot isostatic pressing (HIP) and by use of finer and more pure powders of Mg (Takahashi et al, 2009) and Boron. Zhang et al reports that small sized Boron (B) increases the reaction rate (Zhang et al, 2008c) and the use of small sized B powder has a positive effect on mass density and homogeneity. Smaller B₄C (2.5µm) particles cause higher

T_c and significantly enhance J_c (Zhang et al, 2012). Chen et al. indicate that use of high purity B leads to increased J_c (Chen et al, 2009) and properties of initial precursor and particles size of B powder effect on superconducting properties of MgB₂ wires and tapes (Xu et al, 2016; Wang et al, 2015a). Moreover, J_c is enhanced by using cold compaction for ex-situ MgB₂ samples (Nakane et al, 2008) and cold high pressure for un-doped in-situ MgB₂ wires (Flukiger et al, 2009). Additionally, HIP method is used for obtaining denser MgB₂ core, easy formation of MgB₂ phase with Mg and B, better uniformity, small voids and improved connectivity between MgB₂ grains (Serquis et al, 2003; Gajda et al, 2013; Center et al, 2015; Kario et al, 2010; Gajda et al, 2014). Generally, high pressure may results in reduction of T_c (Monteverde et al, 2001) and at the same time J_c is increased by about 30% (Gajda et al, 2014). Carbon is effective as dopant for improving critical field and grain connectivity of MgB₂ at especially high magnetic fields (Dou et al, 2002; Kim et al, 2006; Hoassain et al, 2009), but homogeneity and mechanical problems for in-situ C doped MgB₂ materials were not completely solved. Investigation efforts for improvement of low field J_c for applications are also in progress.

3.3 MgB₂ Coils and Properties

Different types of superconducting coils such as solenoid, dipole, quadrupole, racetrack and toroid have been fabricated for various applications. Among them, the most widely used type is solenoid. Toroid coil generates a field in azimuthal direction and it used for superconducting magnetic energy storage (SMES). Finally, racetrack coil is obtained by combining of two parallel sides and two semi-circles at each end, and a pair can be assembled to approximate the field of a dipole being suitable for motors and maglev (MIT, 2003). Racetrack coils have important place due to its elliptical shape in applications such as MRI and accelerator. It is known that first commercial superconducting magnet producing 4 T magnetic field was manufactured by oxford instruments company in 1962 and the obtained racetrack coil by using MgB₂/Cu₃₀Ni monocore wire produces magnetic field 0.44 T at 12 K and 0.29 T at 20 K (Sumption et al, 2006). Many scientists struggle for applications using MgB₂ in order to obtain higher and more homogeneous magnetic fields.

Table 3.2. Magnetic field values of various coils for applications (MIT, 2003)

Type of coil	$B_{\max}(\text{T})$	Applications (partial list)
Solenoid	45	High-field research
	23.5	NMR
	5	MRI
	~1.5	Magnetic Separation
Dipole	~15	High-energy physics (HEP)
Quadrupole	0	HEP
Racetrack	4-5	Power Electric Devices
Toroid	~16	Fusion
	5-10	SMES

3.4 Importance of MgB₂ Applications

In recent years, the fabrication of MgB₂ wires by means of PIT process and other methods has attracted much attention for long length applications. A large number of studies are continued to develop MgB₂ strands, and considerable progress is made in improving the basic features such as transport J_c , B_{c2} and B_{irr} . Fabrication of high quality MF strand is crucial for use of MgB₂ in applications. MgB₂ has a significant potential in coil manufacturing and it can fill an important gap as an inexpensive, lightweight conductor able to operate at temperatures up to 20 K. These conductors may open up possibilities for transformers, motors, current leads (Panek et al, 2004) and generators, for the specific cases where 20 K operation is feasible. In particular, recent developments are leading towards light weight, superconducting exciter, stator, accelerator magnets, *LH2* sensors (Schlachter et al, 2006) and rotor coils for certain aircraft motors and wind turbines that could operate in *LH2*. The lighter weight coils, especially rotors, will enable the use of lighter weight support structures, and hence overall reductions in the specific weight of the power device. Large-scale applications for MgB₂ among superconducting materials essentially need development of superconductors with sufficiently good properties (Malagoli et al, 2010). However, MgB₂ have become available for magnetic resonance imaging (MRI) magnets (Li et al, 2007), having high marketing potential worldwide (Collins et al, 2008) at low field and relatively low-cost, when we compared to LTS wires which are in current use of industry, since late seventies (Edelson, 1973). MgB₂ can be fabricated at a lower cost with abundant raw materials of Mg and B (Zhou et al,

2009c). When compared with oxide HTS material, MgB₂ wires have some advantages such as lower cost, easier fabrication and smaller bending radius (Wen et al, 2015). Results show the potential for MgB₂ samples to be a good candidate for applications.

Table 3.3. Properties of technological superconducting materials at 4.2 K (Vinod and Upendran, 2010)

Material	T_c (K)	Anisotropy(γ)	J_c (A/cm ²)	B_{c2} (T)	$\xi(0)$ (nm)	ρ (at T_c) $\mu\Omega\text{cm}$
NbTi	9	Negligible	10^6	11-12	4-5	60
Nb ₃ Sn	18	Negligible	10^6	25-29	3	5
Nb ₃ Al	20	Negligible	10^6	30-45	4-5	10-60
MgB ₂	39	1.5-5	10^6	30-40	5-12	0.4
FeAs based	25-56	8-15	10^5	25-100	2-10	200-10 ⁴
Bi2223	110	50-200	10^7	>100	1.5	40-60
YBCO	92	5-7	10^6	>100	1.5	150-800

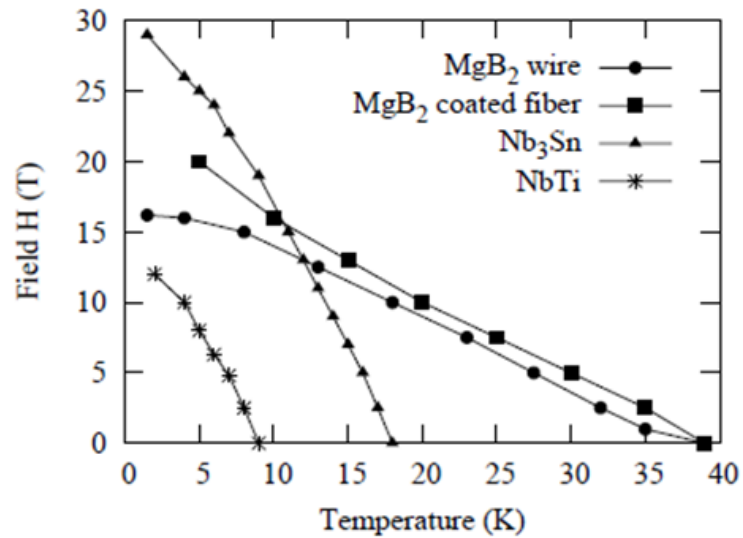


Figure 3.5. Comparison of H-T curves for MgB₂ and LTS wires (Vinod and Upendran, 2010).

4. AIM AND SCOPE OF THE STUDY

The purpose of this thesis is to produce monocoire and MF Fe sheated-MgB₂ carring on high J_c under self-field by in-situ and ex-situ PIT method. Examination of the mechanical, electrical and magnetic properties of these wires is also aimed. Another aim is to manufacture and test the racetrack coils which have a potential to be used in magnetic resonance imaging (MRI) and accelerator magnets systems by utilizing superconducting monocoire and MF Fe/MgB₂ wires produced by self. High quality MF wires in terms of their physical and electrical properties are required for production of racetrack coils. Towards this requirement, we have investigated the transport J_c (at 4,2K in self field) and irreversibility field (B_{irr}) of the wires produced within this thesis. Moreover, it is well-known that there are several parameters like heat-treatments and effective preparation conditions for the enhancement of superconducting properties of the MgB₂ wires and tapes. Briefly, when high performance MgB₂ wires have obtained by using original processes, we have provided a new insight with the obtained remarkable data within this work towards large scale applications of MgB₂ superconductors in our country.

5. EXPERIMENTAL TECHNIQUES

5.1 Preparation of Initial MgB₂ Powders

In this thesis, we used two different approaches for initial powders as in-situ and ex-situ without any addition or doping. Magnesium (Mg (Purity: 99 % , particle sizes: 100–200 mesh \approx 149-74 μ m)), amorphous boron (B (95–97 % , <1 μ m)), nano amorphous boron (nB (>98.5%, <250 nm)) and magnesium diboride (MgB₂ (99.99% - 325 mesh \approx 40 μ m)) powders are purchased from Pavezyum Kimya San. Dış. Tic. A.Ş. The use of reacted MgB₂ commercial powder in metal tubes is called the ex-situ method and the mixture of Mg and B powders with stoichiometric ratio is known as in-situ powder. Ex-situ powder is weighed in air atmosphere. The ex-situ powder and different sized agat balls with 1:4 mass ratio are filled into a glass bottle in argon atmosphere and tightly closed with a cap and sealed using parafilm. Then, the glass bottle is placed inside ball milling machine and milled for 3 hours as shown in Figure 5.1. Agate mortar is also used to grind this homogenous mixture for 1 hour. Those weighing, mixing and grinding processes as mentioned above are same for the preparation of all the powders used in this thesis. Filling process with the use of the MgB₂ powder after milling stage is called Filling 1 as seen in Figure 5.2. The MgB₂ powder is pressed under 2 tonnes for 10 seconds to obtain cylindrical bulks (pellets) 8.8 mm in diameter and about 1.5 mm thick. Preparation of pellets was same for all different powders used for filling iron tube. Filling process with the use of the MgB₂ pellets is named Filling 2 as shown in Figure 5.2. Filling 1 is a powder in tube (PIT) process and Filling 2 which is pellet in tube process is abbreviated as PLIT throughout this thesis. Moreover, mixture of Mg and B in stoichiometric ratio of 1:2 are prepared and pellets are obtained by using the in-situ powder as mentioned steps above. While the in-situ powder is filled via Filling 1, the in-situ pellets are filled via Filling 2 as explained in section 5.2.3.1. Also, the samples are obtained by using the in-situ pellets (PLIT) are coded as F6 as described in section 5.2.5. Finally, other mixture is prepared by utilizing Mg, B and nB powders. The mixture includes Mg, B and nB with 1:1:1 molar ratio giving stoichiometry of MgB₂. The obtained in-situ

powder with the mentioned process above is filled to the metal tube in the form of PIT and MgB_2 wires produced this way are coded F5 as given in detail in section 5.2.3.2.



Figure 5.1. Image of ball milling machine

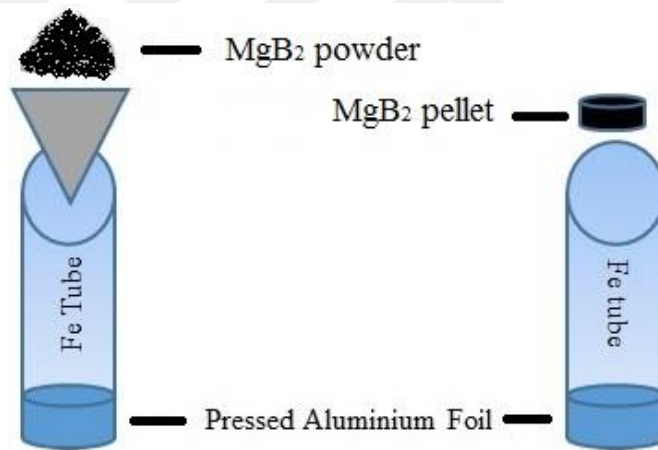


Figure 5.2. Filling processes for ex-situ and in-situ MgB_2

5.2 Fabrication of MgB_2 Wires and Tapes

In wire production process, MgB_2 monocoire wires are produced by means of Filling 1 or Filling 2 methods. The used Fe tube has 12 mm outer diameter and 9 mm inner diameter. Initially, the Fe tube is cleaned with acetone and methanol for 30 minutes in ultrasonic machine (Transsonic 460/H). The cleaned Fe tube is closed with an aluminum plug at one end by pressing Aluminium (Al) foil pieces into the tube with a piston. The MgB_2 powders or pellets which are prepared beforehand are filled into

the Fe tube closed at one end. The remaining open end of the filled tube through which powder or pellet are fed is closed with aluminum plug in the same manner. The obtained sample is drawn from 12.00 mm down to 1.00 mm diameter by passing it through many circular dies. Cross-sectional area reduction ratio between successive round dies which are shown in Figure 5.3 was kept between 5-10%. We use wire pointing machines to decrease the diameter of the front end of the composite to feed the wire through the drawing dies. The wire pointing machine is seen in Figure 5.5. Also, total length of the wire depending on the drawing diameter through the drawing process can be seen in Table 5.1. Due to excessive deformation, mechanical work hardenings occur and intermediate annealing (IA) was applied to remove the induced strain. We performed IA of drawn wire at 1.00 meter/hour speed through a homemade furnace 280 cm in length. In-situ MgB₂ tapes were made pressing the fabricated round wires between polished hardened steel blocks using a hydraulic press operated manually.



Figure 5.3. Photograph of the dies used in drawing process

Table 5.1. Drawing process of ex-situ MgB₂/Fe sample

Diameter of die (mm)	Length of wire (cm)	Diameter of die (mm)	Length of wire (cm)	Diameter of die (mm)	Length of wire (cm)	Diameter of die (mm)	Length of wire (cm)	Diameter of die (mm)	Length of wire (cm)
12	21	6.80	51.8	5.50	76.9	4.40	118.8	3.45	180.9
8.35	35.5	6.60	55.3	5.30	81.6	4.15	129.4	3.25	202.4
8.10	37.2	6.40	57.3	5.15	85.9	4.00	138.4	3.15	213.9
7.85	38.3	6.20	60.7	5.00	94.3	3.90	145.0	3.05	227.2
7.60	43.5	6.00	66.4	4.85	97.3	3.80	151.0	2.95	241.5
7.40	47.5	5.80	69.9	4.70	104.6	3.70	156.9	2.85	260.6
7.00	49.5	5.65	72.4	4.55	110.3	3.55	171.7	2.70	262.9

5.2.1 Production of Ex-situ MgB₂ Monocore Wires

The ex-situ MgB₂ powder was milled for 3 hours with 200 rpm in ball milling system as in Figure 5.1 and mixed for 1 hour in agate mortar before filling. MgB₂/Fe monocore wires were fabricated using ex-situ MgB₂ powder. Filling process into a Fe tube is completed in two ways; either by Filling 1 or Filling 2 in air atmosphere as seen in Figure 5.2. Outer and inner diameters of the iron tube are 12.00 mm and 9.00 mm and consequently the wall thickness is 1.5 mm. Open ends of the tube were plugged with aluminum as explained in section 5.2. Length of the iron tube was about 20 cm. Size and weight of each MgB₂ pellets obtained as described in section 5.1 were approximately same. Their thickness, diameter and approximate masses were 1.3 mm, 8.8 mm and ~0.120 g, respectively and their mass density was about 1.5 g/cm³. The MgB₂/Fe samples prepared with pellets or powders of MgB₂ were drawn from 12.00 mm to 2.00 mm with IA to remove mechanical work hardening of the wire. Wire drawing system (17 m in length) is seen in Figure 5.4, wire pointing machine is shown in Figure 5.5 and a photograph of programmable tube furnace is given in Figure 5.6. Microhardness measurements were taken from the polished sections of wire samples cut at various diameters throughout drawing process from 12.00 mm to 2.00 mm without IA and the wire was produced by using MgB₂ powder. Elongation values of the MgB₂ wire depending on diameters can be seen in Table 5.1. The produced wires by two different methods were sintered at 850 °C for 1 hour (850-1h) under 5-10 bar argon pressure with heating rate and cooling rates of 5 °C/min. Mechanical, structural and superconducting properties of these wires were examined by means of vickers microhardness, x-ray diffractometer (XRD) and cryocooler system (down to 4.2 K) to compare the methods of filling either with pellets or powder.



Figure 5.4. Wire drawing machine



Figure 5.5. Wire pointing machine



Figure 5.6. Programmable tube furnace

5.2.2 Production of Ex-situ MgB₂ Multifilamentary Wires

Ex-situ MgB₂/Fe monocoire sample was prepared and drawn from 12.00 mm to 2.95 mm diameter. From this monocoire wire, 10 cm long six pieces were cut, and then the remaining wire was further drawn to 1.70 mm in a number of steps. 10 cm long six pieces cut from 2.95 mm diameter monocoire wire were used to obtain seven (6+1) filamentary ex-situ MgB₂/Fe wire. After the completion of the drawing process until 1.70 mm diameter, 10 cm long eighteen pieces were cut off from the drawn wire to obtain nineteen (18+1) filamentary ex-situ MgB₂/Fe wire. 10 cm long copper wires with 2.95 mm diameter for MgB₂/Fe (6+1) MF and with 1.70 mm diameter for MgB₂/Fe (18+1) MF MgB₂ samples were placed at the center of the iron tube as seen in Figure 5.7 (a). Drawing process for production of monocoire and MF wires is similar with some differences in drawing sequences and IA conditions. This MF MgB₂/Fe wires with 6+1 and 18+1 filaments were drawn down to diameters of 2.25 mm and 2.00 mm, respectively as shown in Figure 5.7 (b) and (c). The MF wires were annealed at 800 °C and 900 °C temperatures for 1 hour (800 °C or 900 °C /1h) in argon pressure and examined by various measurement systems as I-V in LH, cryocooler and SEM.

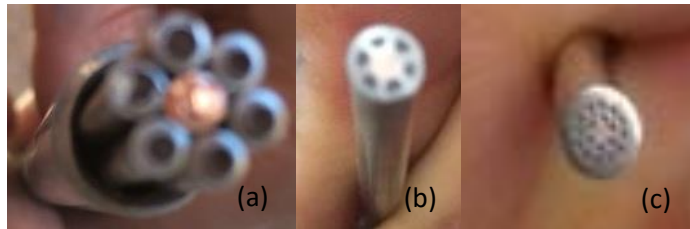


Figure 5.7. Photograph of (a) preparation of ex-situ MgB₂/Fe 7 filamentary wire, (b) ex-situ MF MgB₂/Fe wire and (c) ex-situ MF MgB₂/Fe wires

5.2.3 Production of In-situ MgB₂ Monocore Wires

5.2.3.1 Preparation of Fe/MgB₂ Monocore Wire With Pelletized In-situ Powder

The monocore Fe/MgB₂ superconducting wires were prepared from Mg powder and B powder. The stoichiometric precursor Mg+2B powder was mixed in a ball milling for 3 hours and, the resulting mixture was stirred manually in an agate mortar for an additional 1 hour. An equal amount of homogenous powder weighing 4.6 g was filled into pre-cleaned two identical iron tubes with lengths of 20 cm. A special attention was paid to the tube filling process and two tubes with different initial powder filling densities were prepared in argon atmosphere. One tube with 50% (via Filling 1 method) and the other one with 60% (via Filling 2 method) of theoretical mass density of Mg+2B powder mixture were filled (Flukiger et al, 2009). A cold drawing method with several intermediate heat treatments under argon pressure or argon flow was applied to fabricate the wire samples. Two wires with the same diameter of 1.90 mm were annealed in a three-zone programmable tube furnace (Protherm-Model PZF12/75/700) at two different temperatures of 800 °C and 900 °C for 1 hour. The wire samples were heated and cooled with a rate of 5 °C/min under 5-10 bar argon atmosphere.

Moreover, the unreacted MgB₂ wires obtained by pellet-in-tube initial filling method (Filling 2) underwent cold drawing to a diameter of 0.9 mm (Akdoğan et al, 2015). Unreacted MgB₂ wires were sintered by hot isostatic pressing (HIP) process at the Institute of High Pressure Research in Warsaw. Samples A was annealed at 740 °C for 40 min under 0.1 MPa (1 bar) argon pressure as a reference sample for comparison. Samples B was sintered at 740 °C for 40 min at pressure of 1.1 GPa as indicated in Table 5.2. The HIP process was applied under 5N argon atmosphere in high gas pressure chamber (Cetner et al, 2015). Transport Resistivity vs Temperature ($R-T$) and transport normal state resistance vs applied magnetic fields (R_N-B) were obtained for the sample A and B using a test current of $I_c = 100$ mA.

Table 5.2. The HIP process of parameters for unreacted MgB₂ wires.

Sample identifier	Annealing time [min]	Annealing Temp. [°C]	Pressure [Pa]
A	40	740	0.1 M
B	40	740	1.1 G

5.2.3.2 Preparation of In-situ Fe/MgB₂ Monocore Wires With Mixture of Different Two Borons

The starting materials in this work were commercially available Mg, B, and nB powders. The accurately weighted powders (Mg = 8.00026 g, B = 3.53823 g, and nB = 3.53846 g) as to yield Mg+2B stoichiometric ratio were homogeneously mixed by means of rotary ball milling for 3 hours under argon atmosphere. After mixing, the powder was filled into an iron tube of 351 mm in length under by Filling 1. Both ends of the tube were closed by aluminum plugs. Starting mass density of the Mg+2B inside the tube was estimated to be around 1.5 g/cm³. Cold drawings through progressively decreasing die diameters were applied with several intermediate heat treatments (600 °C, 1 h) under argon pressure to fabricate the wire samples. Wire samples with the outer diameter of 1.00 mm were cut to about 150 mm long pieces and annealed in a three-zone programmable tube furnace at five different temperatures of 800 °C, 850 °C, 900 °C, 950 °C, and 1000 °C for 1 hour under 5-10 bar argon atmosphere with 5 °C/min heating/cooling ratios. 20 mm long pieces from both ends of the sintered wires were cut off to avoid any irregularities due to open ends, only middle parts of the wires were used for investigation. Wire samples were named to indicate sintering temperature as F5E900, the last three digits being sintering temperature in degree celsius.

5.2.4 Production of In-situ MgB₂ Monocore Tapes

The monocore Fe/MgB₂ superconducting wires were prepared from Mg, B, and nB powders by using the in-situ solid state reaction and Filling 1 methods. The starting boron powder is composed of 50 % amorphous boron and 50 % amorphous nano boron. This initial stoichiometric precursor of Mg + 2B powder was mixed by ball milling for 3 h. The ball milled homogenous powder weighing 15.1 g was filled into

a 350 mm long pre-cleaned iron tube as detailed in section 5.2. Cold wire drawing method with several IA under argon pressure and/or argon flow was applied to fabricate the wire samples. The wires of 1.00 mm diameter were cut to 120 mm pieces and sintered in series in a three-zone programmable tube furnace at temperatures of 800°C, 850°C, 900°C, 950°C, and 1000°C for 1 h under 5–10 bar argon pressure. The mechanical deformation with manual hydraulic press and subsequent heat treatment processes were applied to these in-situ fabricated wire samples. The wire samples heat treated at different temperatures were tested in the cryostat to measure their transport properties. The same samples were then cleaned to remove soldering and were brought into the tape form by applying a pressure of around 1 GPa (calculated for the area of the pressed tape dimensions 2 mm x 20 mm) between two hardened steel plates. After pressing the samples, transport properties were measured again in the cryostat to investigate the effect of pressing. These tapes were re-cleaned after measurements and a final heat treatment at 850 °C for 1 h was carried out in 5–10 bar argon atmosphere. Each data is analysed on the basis of processing steps; before pressed (*BP*): Fabrication of initial in-situ Fe/MgB₂ monocoresh wires, after pressed (*AP*): Mechanical deformation of the initial wire samples, and post annealed (*PA*): Heat-treatment on excessively deformed samples.

5.2.5 Preliminary Coil Production of In-situ Fe/MgB₂ Monocore wire

A 400 mm long piece of iron sheathed MgB₂ monocoresh wire 1.10 mm outer diameter fabrication is given in detailed in section 5.2.3.1. The MgB₂ monocoresh wire by the Filling 2 process as detailed in section 5.1 and 5.2 is called as F6 obtained. Using this 400 mm long F6 MgB₂/Fe wire, we made a solenoid coil with 12 turns, 10 mm inner diameter, 12.77 mm outer diameter, and 23.45 mm length, as shown in Figure 5.8 (b). After the demo coil was annealed at 850 °C for 1 hour under argon pressure, it was coated with G-varnish for turn to turn insulation to prevent short circuit. Totally, eight (8) electrical contacts were made at various points on the coil. These contact points shown in Figure 5.8(a) are named as T, M, G, F, C, L, D, S and they were used for current connections and remaining points were utilized as potential taps. This coil was tested in helium gas-contact Cryo-Industries cryostat system. The critical current values with various voltage contacts were measured at different

temperature values from 20 K to 36 K under applied magnetic field strengths up to 7 T. Microstructure properties of the superconducting MgB_2/Fe coil were investigated by XRD analysis and a scanning electron microscope (SEM, JEOL 6390-LV).

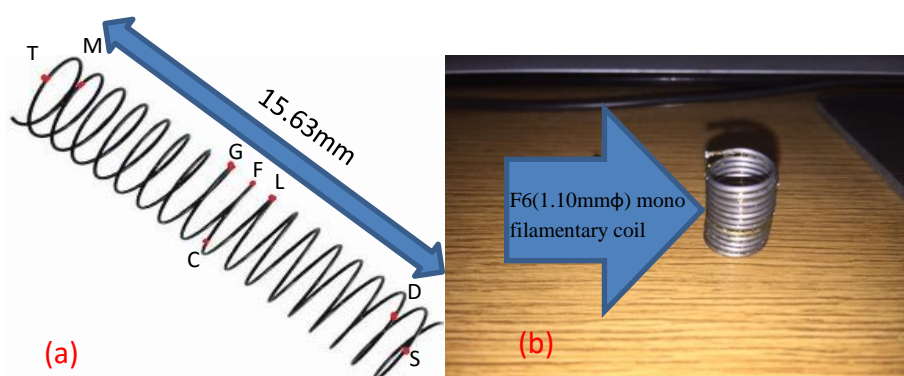


Figure 5.8. Presentation of voltage and current contacts (a), image of the preliminary solenoid coil covered by G-vanish before measurement (b)

5.2.6 Production of In-situ MgB_2 Multifilamentary Wires

18 pieces of monocoil wires cut from the wire given in section 5.2.3.2 and inserted into an iron tube together with a Cu wire in the center for making 18+1 MF wire. The MgB_2/Fe monocoil wire 1.19 mm diameter was obtained with the use of F5 powder. Then, MgB_2/Fe MF wire were drawn from this composite down to 1.00 mm diameter. The initial composite of 18+1 MF wire was produced from 1.19 mm diameter monocoil MgB_2 wire pieces and a 1.22 mm diameter copper wire in the center. Each inserted wire was 110 mm length at the beginning of the MF configuration. The prepared composite with 18+1 wires were made by inserting the monocoil MgB_2 wires and the Cu wire into an iron tube in a geometrical perfect manner as in Figure 5.7(a). The MgB_2/Fe MF 18+1 wire were fabricated by cold drawing down to 1.00 mm with a few IA steps. Four pieces each of which was 7 cm in length were cut from the obtained MF wire and these MF MgB_2 wire samples were sintered at different temperatures, namely; at 700 °C, 750 °C, 800 °C, 850 °C for 1 hour and 700, 750 °C for 2 hours under argon pressure (5-10 bar). The produced MgB_2/Fe 18+1 MF superconducting samples were named as MF5E meaning that these multifilamentary wires were obtained by using the unreacted F5 monocoil wires.

5.2.7 Bending Process of In-situ Fe/MgB₂ Multifilamentary Wires

In this part, the tested samples were MF5 wires produced by utilizing F5 monocoire wire fabrication details of which are given in section 5.2.3.2. As indicated in Figure 5.9, the unreacted MgB₂/Fe 18+1 wire 1.00 mm and 0.56 mm in diameter were bent to 35mm and 25 mm radius (r_b) using cylindrical formers. Then, we cut 3.5 cm long pieces from these bent wires as seen in Figure 5.10 and sintered at 700 °C for 1 hour. Our 18+1 filament Fe/MgB₂ wires (OD = 1 mm and 0.56 mm) were tested by using our cryocooler system (4.2 K) in magnetic fields up to 7 T and examined by SEM.

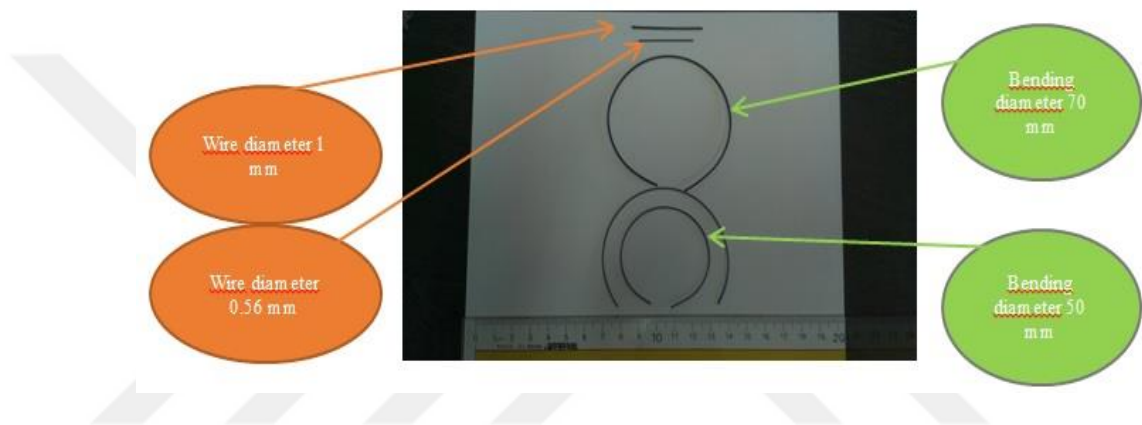


Figure 5.9. Image of the MgB₂/Fe (18+1) wires bent to different diameters

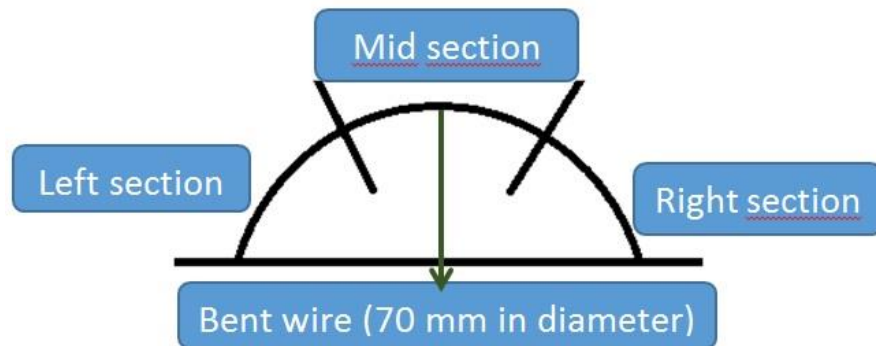


Figure 5.10. Schematic illustrations of wire pieces taken for measurement from different sections of the bent MgB₂/Fe (18+1) wires

5.2.8 S-Glass Insulation Process of Long MgB₂ Wires

S-glass fiber is used for electrical isolation of MgB₂ wires. S-Glass fiber is known to be durable sample at high temperature. We used two type S-glass fibers with 0.15 mm and 0.30 mm thickness and an Ex-Themp glue to coat on the S-Glass fiber isolation layer. This adhesive liquid is claimed to be capable of enduring high temperatures. Initially, the Fe clad MgB₂ wires which are about 25 m in length seen Figure 5.11(a) were continuously isolated with S-glass fiber (0.15 mm) as seen in Figure 5.11(b) using a braiding machine (Figure 5.12) granted by Basoglu Kablo San. Tic. A.S.



Figure 5.11. Images of the fabricated long MgB₂/Fe wires before (a) and after (b) S-Glass braiding.



Figure 5.12. Terz M. Expo Braiding Machine



Figure 5.13. Image of the produced wire 1.10 mm in diameter after braiding with S-glass fiber

A 14 m long MgB_2 wire was wound onto a steel former and impregnated with the liquid glue as shown in Figure 5.14. This solenoid coil was sintered at 800 °C for 1 hour under argon flow in a box type furnace. Figure 5.15 shows this coil after sintering, some pieces of wires were cut off from the coil windings and their superconducting properties were investigated. Moreover, some pieces of wires of 1.10 mm diameter isolated using S-glass fibers with or without liquid adhesive coating were sintered under argon pressure at temperatures of 850 °C and 900 °C. Photographs of these wires after sintering are shown in Figure 5.16.



Figure 5.14. Image of the solenoid coil wound on a steel former and coated with EX-THEMP glue before heat treatment.

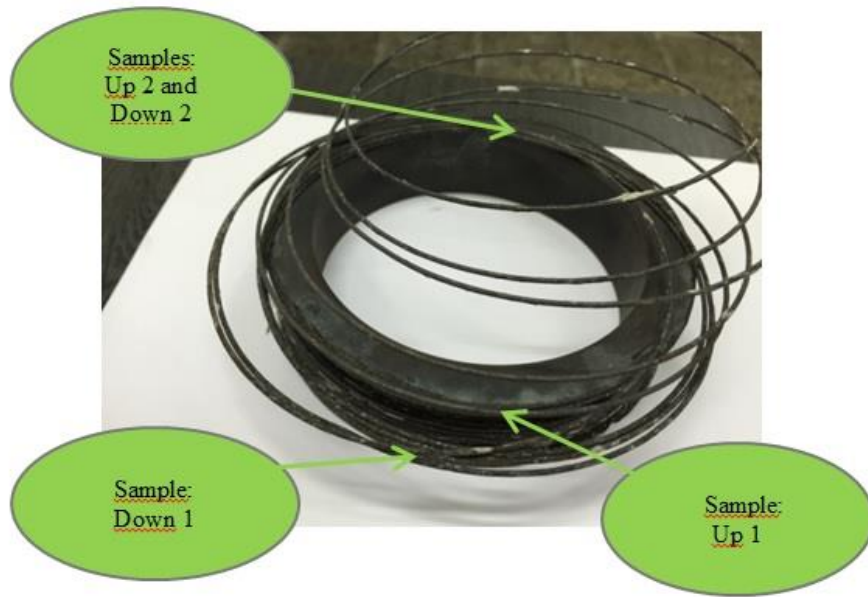


Figure 5.15. Photograph of the solenoid coil after sintering under argon flow



Figure 5.16. Images of the isolated wires after sintering under different conditions.

5.2.9 Fabrication of Racetrack Coils

We have fabricated two MgB_2/Fe monocoil (F5B and F5D) and two MF wires (MF6 (18+1) and MF5D (8+1)) each of which was approximately 25 m in length. These four wires were isolated by 0.15 mm thick S-glass fiber braiding as detailed in section 5.2.8. The isolated wires are wound on racetrack coil formers (24cmX10cm) as seen in Figure 5.17. The manufactured racetrack coils without liquid adhesive in Figure 5.18 (a) are sintered at 700 °C for 1 hour under 5-15 bar argon pressure. Transport current of the sintered racetrack coils and the produced magnetic field of the chosen racetrack coil at its center shown in Figure 5.18 (b) were measured at 4.2 K (*LH2*) in ILHMFLT, Wroclaw, Poland.

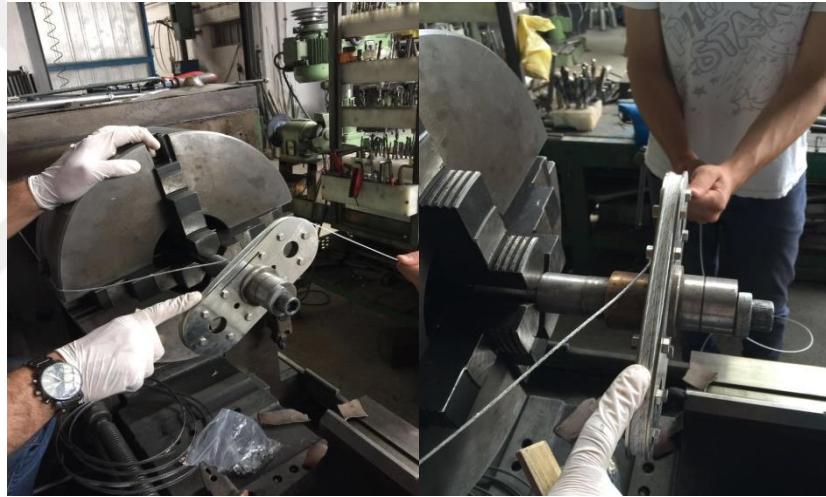


Figure 5.17. Winding process of racetrack coils.

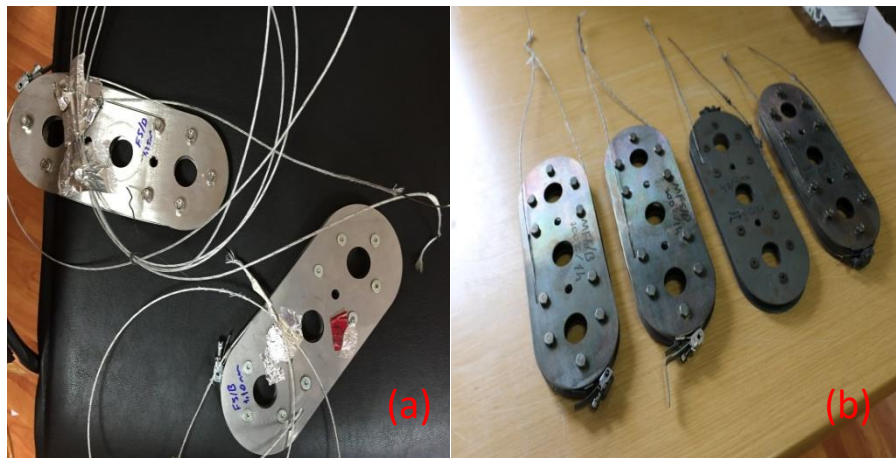


Figure 5.18. The manufactured racetrack coils before (a) and after (b) sintering.

5.2.10 Sintering Processes

All sintering heat treatments of the MgB_2 wire samples and some of the IA heat treatments were performed using a Protherm Controller/ Three Zone Programmable tube furnace seen in Figure 5.19. All the samples were heat treated in a stainless steel tube at various temperatures for different periods in high purity argon atmosphere. This 1.5 m long stainless steel tube with 35 mm outer diameter and a wall thickness of 3 mm was used for heat treatment of wire samples under argon pressure. Connections for vacuum and argon inlets are attached to this stainless steel tube with T type connections. The furnace was kept under vacuum for 10 minutes and filled with argon. This process was repeated for three times to remove any trace of oxygen before heat treatment. All heat treatments of the samples were done under high purity argon (Ar) pressure to achieve superconducting phase formation of MgB_2 wires or under argon (Ar) flow for IA processes of long wires.



Figure 5.19. Three Zone Programmable Furnace.

5.3 Characterization Techniques

5.3.1 X-Ray Diffraction (XRD) Technique

Examination of phase composition and crystal structure of the obtained MgB_2 samples were characterized by Rigaku MultiFlex 2kW diffractometer using $\text{Cu K}\alpha$ radiation ($\lambda=1.5418 \text{ \AA}$) in the range $2\theta=10\text{--}90^\circ$ at a scan speed of $5^\circ/\text{min}$ with step

increments of 0.02° at room temperature. Iron sheath of the MgB_2 wires was removed and the MgB_2 core was taken out of either as cylindrical bulk or powder for XRD measurements. The measurements were carried out under beam acceleration conditions of 38 kV/28 mA. Phase purity and lattice parameters were estimated from the XRD patterns. The accuracy in determining the lattice parameters (a , b and c) is found to be $\pm 0.0001 \text{ \AA}$. In addition, the average grain sizes of the MgB_2 samples are inferred from the Scherrer - Warren approach (Cullity, 2001) as a result of the broadening nature of the XRD peaks.

5.3.2 Scanning Electron Microscopy (SEM)

A scanning electron microscope (SEM, JEOL 6390-LV) with the accelerating voltage of 20 kV was used to investigate the surface morphology of the monocoresh and multifilamentary MgB_2/Fe wires. SEM images were obtained from the fracture surface (fcs) and the polished surface (pls) of the wires. There are two type of measurements as backscattering electron (BSE) and second electron (SE). Also, This SEM instrument has electron dispersive spectroscopy (EDS) system for elemental chemical analysis. After the interaction between the incident electrons and atoms in the material, a signal containing the information about porosity of the samples, microstructures of the samples occurs. Microstructure examinations using SEM provide us with valuable data about the grains, voids, cracks and pores in the studied samples.

5.3.3 Resistivity-Temperature ($R-T$) and Current-Voltage ($I-V$) Measurements

The dc resistivity measurements ($\rho-T$) and current voltage ($I-V$) measurements of the samples were performed with the four point resistivity method using Keithley nanovoltmeter (Model 2182A) and a Keithley current source (Model 238). A constant DC bias current of 50-100 mA was run through the samples between 10 and 50 K in a closed cycled He cryostat. A programmable temperature controller (Lakeshore 340) is used for the accurate monitoring of the temperature with a

stability and accuracy of ± 0.01 K. Standard Pb-Sn solder was used for soldering of the current and voltage contacts to surface of the wire. The current was applied to the two outer electrical contacts and the voltage drop across the two inner electrical contacts was measured against temperature. Transport currents in magnetic fields were measured by standard four-probe configuration with constant direct current (DC) between 0 and 1 A at cryogenic temperatures below T_c . Magnetic fields up to 7 T were created by a solenoid type superconducting magnet and applied to these wires. The applied magnetic field was perpendicular to the current direction. The current-voltage (I - V) characteristics of the samples were measured at various temperatures with the standard four-probe method under self or applied field to determine the critical current densities (J_c) of the wires. The $1 \mu\text{Vcm}^{-1}$ criterion was used for critical current determination. The transport J_c was defined as I_c divided by the cross-sectional area of the MgB_2 wire which was accurately measured with a micrometer. All the data were recorded using the Labview computer software.

Critical current of the 20 mm long wire samples after sintering was also measured in liquid helium with the four probe method up to 200 A in perpendicular magnetic fields at ILHMFLT in Wroclaw using a Bitter 14 T magnet. The magnetic field was applied perpendicular to the wire axis and $1 \mu\text{Vcm}^{-1}$ criterion was used for evaluation of critical current.

5.3.4 Magnetization (M - H) Measurements

Resistance measurements (15 Hz AC current, $I_{AC} = 100$ mA) of the wires were performed from 10 to 35 K using a physical properties measurement system (PPMS Model 7100, Quantum Design) with a magnetic field sweep rate of 0.050 T/s and the amplitude of up to 14 T in the ILHMFLT. The values of B_{irr} , T_c and B_{c2} have been determined with the criterion of 10 %, 50 % and 90 % of normal state resistivity before transition, respectively. Analysis of the microstructure was performed at the Institute of High Pressure Physics PAS in Warsaw.

5.3.5 Mechanical Tests

Vickers / Microhardness method is considered to be very useful for testing on a wide variety of materials, including metals, composites and ceramics. Microhardness measurements can also be used for applications such as testing thin materials like foils, or measuring the surface of a part, testing individual microstructural features and measuring the depth dependence of hardening by sequential sectioning a part and making a series of indentations. It is necessary make the specimen's surface smooth to permit a regular indentation shape for accurate and good measurement. The sample to be measured should be held precisely perpendicular to the indenter. Vickers microhardness measurements of the mounted and the polished MgB₂ wire samples were performed using digital microhardness tester (SHIMADZU HVM-2). The applied loads were between 0.245 and 2.940 N and duration of the load was 10 s. A square base pyramid shaped diamond is used for testing in the Vickers scale. Diagonals of indentations were measured with an accuracy of $\pm 0.1 \mu\text{m}$. Average of three readings at different locations of the specimens' surfaces was taken to obtain reasonable mean values for each load.

5.3.6 Metallographic Process

Small pieces of MgB₂/Fe wires and tapes were placed longitudinally or vertically with copper acrylate powder in the mounting machine seen in Figure 5.20 (a). The small pieces vertical or horizontal sections of MgB₂ wires and tapes were polished using a polishing machine (Hergon MP 200) shown in Figure 5.20(b). The polishing of mounted specimens was carried out with SiC grinding papers of 240, 600, 800, 1200, 2400 and 4000 a followed by polishing with 1 μm and 1/4 μm diamond pastes. After polishing, the surface structures of these samples were examined by SEM and OLYMPLUS GX41 optical microscope seen in Figure 5.21.



Figure 5.20. a) Mounting Machine, b) Polishing Machine.



Figure 5.21. Optical Microscope OLYMPLUS GX41.

6. RESULTS AND DISCUSSIONS

6.1 Investigation of Ex-situ MgB₂ Monocore Wires

We were performed measurements on two different types (Filling 1 and Filling 2) of the Fe/MgB₂ monocore wires. Filling 1 has normal filling density and Filling 2 has higher filling density by using the ex-situ pellets. Initially, the aim of microhardness measurements is to test whether or not the prepared ex-situ MgB₂/Fe tube by filling 1 method can be drawn from 12.00 mm to 1.00 mm diameter without any IA. The ex-situ monocore MgB₂/Fe composite ready for drawing has aluminum plugs at both ends with MgB₂ powder packed in the middle. The pieces of wires taken from the sample at different stages of drawing with different diameters were examined for Vickers microhardness at room temperature as seen in Figure 6.1 and 6.2. The microhardness of the sheath materials increases with larger applied load. This situation is defined as reverse indentation size effect (Sangwal et al, 2011). Microhardness value of the iron sheath with of 8 mm diameter wire MgB₂ powder inside is half of that of the sheath at 2 mm diameter for applied loads $\geq 0.98\text{N}$. Microhardness value of the sheath is reduced by 75% after drawing from 8.00 mm to 2.00 mm diameter for applied loads $\leq 0.49\text{ N}$. This difference in microhardness values measured under various loads is probably due to elastic deformation which is proportionally more important for smaller loads. Elasticity of the sheath material decreases due to elongations of grains and loss of good mechanical connectivity between grains of iron sheath (Sangwal et al, 2011) throughout drawing 12.00 mm to 2.00 mm diameter. Additionally, we can say that this causes increment of plasticity and decrement of microhardness (Geng and Liu, 2013). On the other hand, the microhardness of the Al pressed Fe sheath doesn't change significantly as depending on diameter. Briefly, we can say that the effect of ex-situ MgB₂ powder on the microhardness of the Fe sheath is higher when compared to that of Al foil.

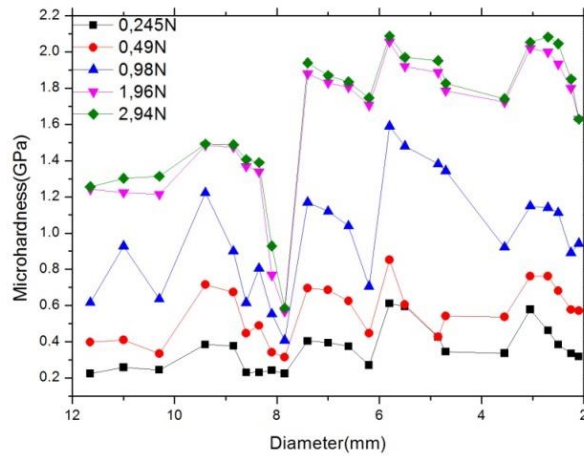


Figure 6.1. Microhardness values of ex-situ monocore MgB₂/Fe wires of different diameters (crosssection includes Al material in core)

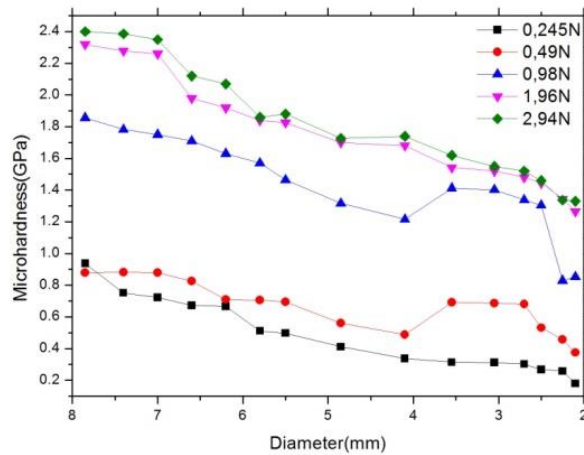


Figure 6.2. Microhardness values of ex-situ monocore MgB₂/Fe wires (Filling 1) of different diameters (crosssection includes MgB₂ powder in core)

Then, ex-situ MgB₂/Fe wires obtained by filling 1 and filling 2 methods, and drawn wires to 2.00 mm diameter were annealed at 850 °C for 1 hour under argon pressure at 5-10 bars. Structural, morphological and electrical properties of these MgB₂/Fe wires were examined by means of XRD, SEM and cryocooler system. Figure 6.3 shows that XRD pattern of MgB₂ core has a high count rate and this pattern can be indexed as MgB₂ phase with only MgO impurity phase which has a very low counts rate. Evaluating the XRD results in Figure 6.3, we can claim that the main peaks of the ex-situ MgB₂/Fe samples prepared by both filling methods are

almost the same. Full width at half maximum (FWHM) and count rate of the sample made by Filling 2 (0.4120) has higher than those of the sample made by Filling 1 (0.3814) while Bragg angle of the MgB_2/Fe by Filling 2 (42.39) is similar to that of the MgB_2/Fe by Filling 1 (42.46). Broader peak gets smaller crystallite size. We did not observe any significant difference between unit cells/lattice parameters of both samples. In XRD data, dark line belongs to Fe sheath the sintered at 850 °C for 1hour. Especially its main peak can be seen as impurity phase in the both samples with small count rate because of no reaction between Fe and MgB_2 powder in this temperature. We can see sometimes iron peak in XRD data due to iron particles on surface of cylindrical bulk sample after removing iron sheath material from the wire.

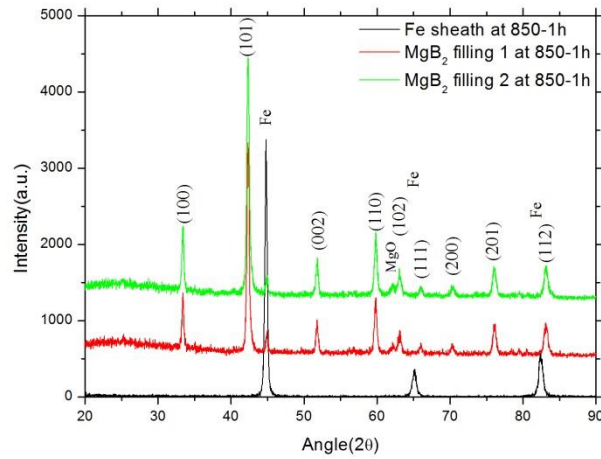


Figure 6.3. XRD patterns of ex-situ monocoire MgB_2/Fe (2.00mm ϕ) wires and iron sheath sintered at 850°C for 1 hour.

When we look at Figure 6.4, the resistance of the MgB_2 wire by filling 2 (525 $\mu\Omega$) is higher than that of the MgB_2 by Filling 1 (400 $\mu\Omega$) at normal state. This difference may be the effect of crystallite size by supporting the XRD results. The greater crystallite size means more grain boundaries in a sample and these grain boundaries cause more resistance. T_c of the former (38.33 K) is similar to that of latter (38.83 K). Also, width of transition temperature (ΔT) is same as 0.70 for filling 2 and 0.67 for filling 1. As expected, we can say that ex-situ MgB_2 monocoire wires having similar characteristic properties can be produced by using PIT and PLIT techniques as seen Figure 6.3 and Figure 6.4.

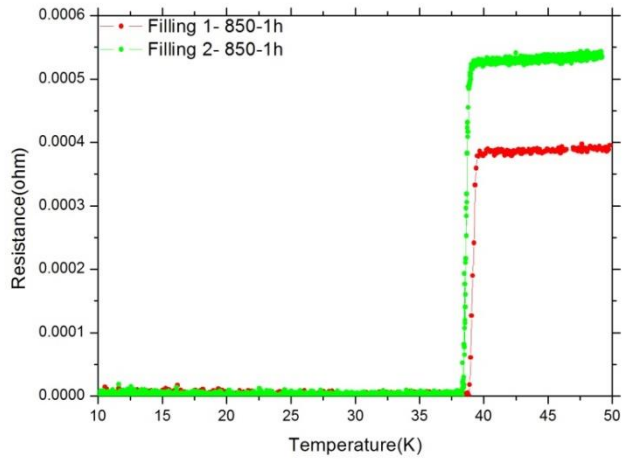


Figure 6.4. Resistance vs Temperature graph of Ex-situ moncore MgB_2/Fe wire 2.00 mm ϕ .

As seen in SEM images at low magnifications (30x for Filling 2 sample and 45x for Filling 1), no significant fluctuations due to the cold drawing process at the inner surface of the sheath are observed in the both wires (in Figure 6.5 and 6.6). Irregularities of inner surface of the sheath, if present, would indicate uneven mechanical deformations which are potentially deteriorating for long length wires.

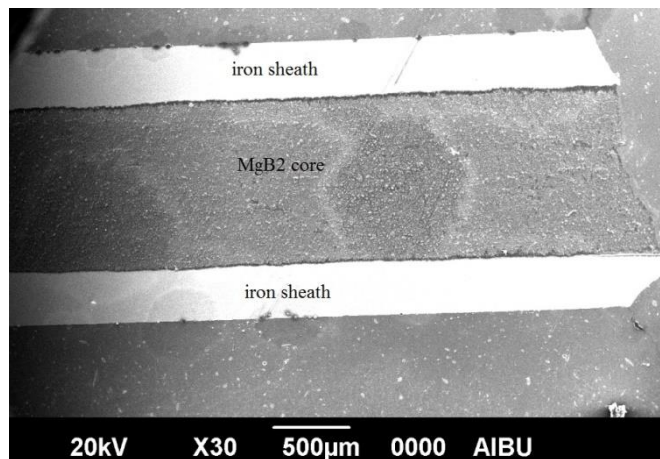


Figure 6.5. SEM image ;Ex-situ moncore MgB_2/Fe wire (2.00mm ϕ -850-1h) longitudinal region (Filling 2).

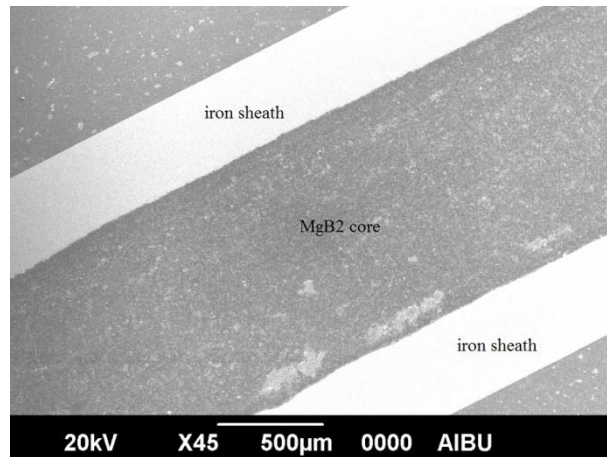


Figure 6.6. SEM image; Ex-situ monocore MgB₂/Fe wire (2.00mm φ -850-1h) longitudinal region (Filling 1)

In our cryocooler system, I_c values of both wires were measured at a constant temperature close to T_c as seen in Figure 6.7. In performing these measurements, we intended to find a way of predicting low temperature (such as 4.2 K) I_c values of our samples before sending them to Poland for transport I_c measurements in liquid helium (LH). While I_c value of ex-situ MgB₂/Fe by Filling 2 is 0.55 A at 1.1 K below T_c in self-field, that of ex-situ MgB₂/Fe by Filling 1 is 0.45 A at 1.5 K below its T_c in self-field. The effect of Filling 2 on especially transport I_c can be clearly seen in Figure 6.7.

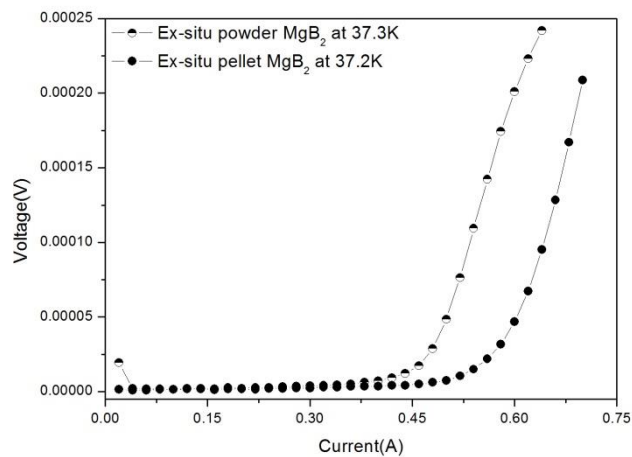


Figure 6.7. Current vs Voltage curves of Ex-situ monocore MgB₂/Fe wires measured at temperatures closed to T_c . These wires were produced by PIT and PLIT filling methods with 2 mm diameter and sintered at 850°C for 1 hour

6.2 Examination of Ex-situ MgB₂ Multifilamentary Wires

We produced MF MgB₂/Fe wires with assumption that MF wires of the same diameter would carry larger supercurrent. The resistivity versus temperature graph of ex-situ MgB₂/Fe MF wires obtained by filling 1 with different diameters sintered at 800 °C and 900 °C for 1 hour are given in Figure 6.8. All of the studied MgB₂/Fe wires have the same T_c (37.5 K). Normal state ρ of the ex-situ MgB₂/Fe (18+1) wires increases with increasing sintering temperature. Increasing the sintering from 800 °C to 900 °C does not affect normal state ρ at around 40 K due to probably larger Cu stabilizer ratio in MgB₂/Fe (6+1) MF wire in Figure 6.8. Resistivity of the iron sheath increases with decreasing filament diameter and increasing sintering temperature due to B diffusion into iron sheath. This amount of B is apparently lost from MgB₂ core reducing normal state connectivity of the core. Therefore, we can say that inter-sheath connections of the studied wires are directly proportional to resistance value of them at normal state. Also, diameter of copper in the ex-situ MgB₂/Fe (6+1) wire is greater than that of ex-situ MgB₂/Fe (18+1) wire. While diameter of copper is inversely proportional with resistance at normal state, amount of metal-metal connections is directly proportional to resistance at normal state. Resistivity values of the samples sintered at different temperatures and having different diameters range from 1 $\mu\Omega$.cm to 7 $\mu\Omega$.cm as seen Figure 6.8.

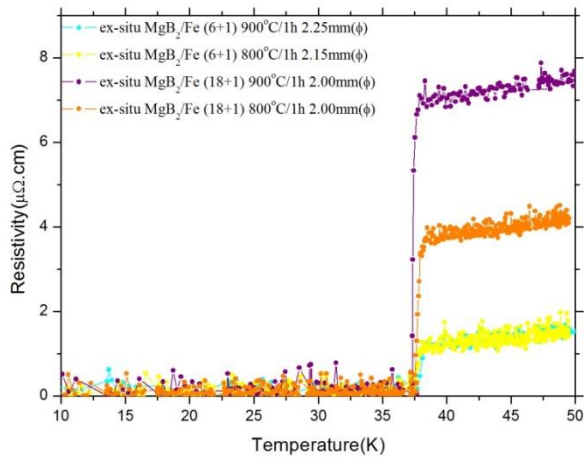


Figure 6.8. Resistivity vs Temperature graphics of MgB₂/Fe (6+1) and MgB₂/Fe (18+1) filamentary wires sintered at different temperatures.

After the production of the ex-situ MgB_2 MF wires was completed, as shown in Figure 6.9, the SEM images of the cross sections of these wires were taken to analyze the geometrical morphology of these samples. As seen in the micrographs, the fabrication of ex-situ MgB_2/Fe MF wires was completed successfully with regularly shaped and evenly distributed filaments. Only exception is the wire cold drawn without intermediate strain relief annealing from 12.00 mm down to 1.00 mm diameter. This wire had an irregularly shaped cross section despite the copper filament used in the center of MF configuration.

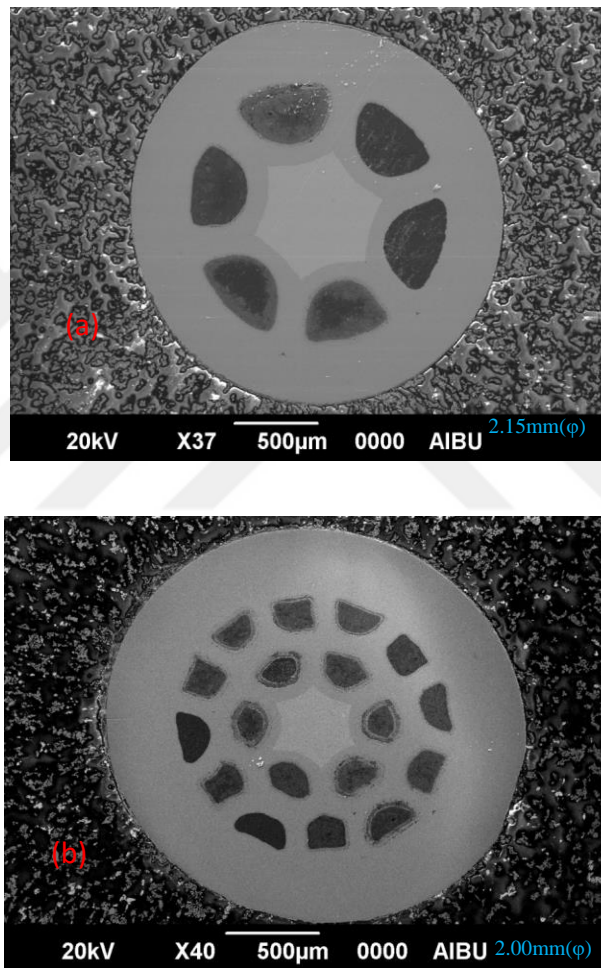


Figure 6.9. SEM Images taken from the cross sections of the MgB_2/Fe wires sintered at 900 °C for 1 hour with (a) (6+1) and (b) (18+1) filaments

Transport critical current of the MgB_2/Fe (18+1) and (6+1) wire with 2.00 mm diameter were tested in LH. While the MgB_2/Fe (18+1) wire carried 5 A at 5.5 T and 50 A at 3.5 T, the MgB_2/Fe (6+1) wire did not carry any current under applied magnetic field as shown in Figure 6.10 (a) and (b). The MgB_2/Fe (18+1) MF wire is better than the MgB_2/Fe (6+1) MF wire. But, the difference between both wires is

seen due to locally homogeneity problem of long wires through drawing process. Because, this measurement was carried out only once test for a part of the wire.

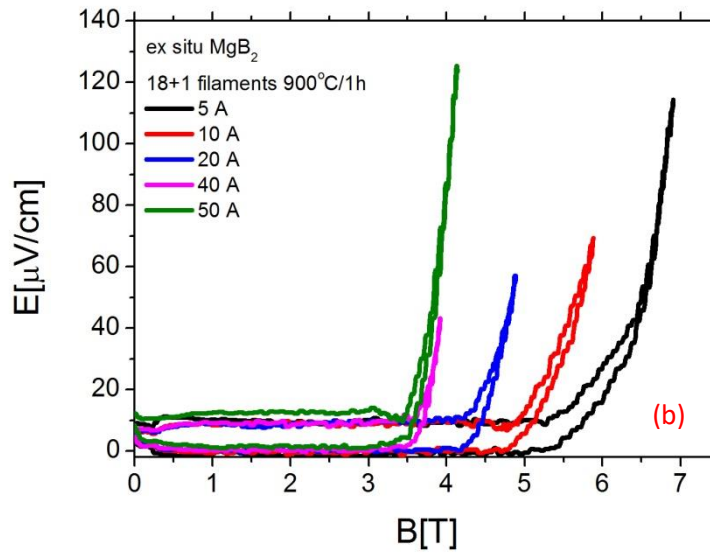
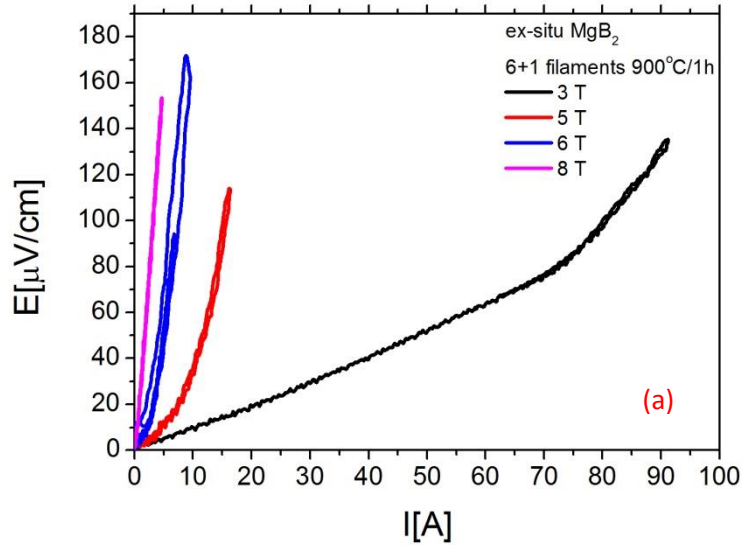


Figure 6.10. Graphics of dependence of resistive transition upon (a) applied current for different values of constant magnetic fields the MgB_2/Fe (6+1) and (b) applied magnetic field for different values of constant transport currents (18+1) wires.

6.3 Investigation of In-situ MgB₂ Monocore Wires

Figure 6.11 shows XRD analysis of the in-situ MgB₂/Fe monocore wires with 1.90 mm diameter obtained by Filling 1 and Filling 2 at different annealing temperatures of 800 °C, 850 °C and 900 °C for 1 hour. XRD graph of the paste material used for holding the cylindrical MgB₂ cores is shown as an insert graph in Figure 6.11. There are some peaks appear between $10^\circ < 2\theta < 25^\circ$ resulted from the paste material on the sample holder and there isn't any peaks belonging to MgB₂ phase in this range. When the results of the in-situ MgB₂ wires prepared at all temperatures were examined, it can be said that Bragg angle (2θ) of in-situ MgB₂ wires by filling 2 shifts to left when compared to those of in-situ MgB₂ wires by Filling 1. XRD patterns of the studied MgB₂ monocore wires at different temperatures may show peaks belonging to MgB₂ phase together with a minor amount of MgO as impurity and a peak belonging to Fe due to Fe particles from the sheath material. Some XRD peaks belonging to phases of Fe₂B or FeB due to high sintering temperature, but it is not to distinguish these peaks since their count rate is low, they overlap with some of the XRD peaks of MgB₂ phase and main peak of Fe iron phase.

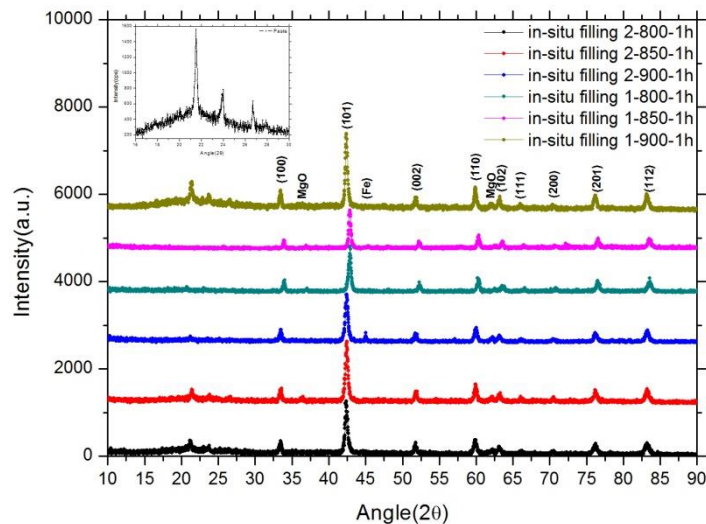


Figure 6.11. XRD graph of in-situ monocore MgB₂/Fe wire 1.90 mm Φ sintered at various temperatures and the used paste to hold samples in the inserted graph.

In Figure 6.12, ρ vs T graph for the in-situ MgB₂/Fe monocore wires sintered at various temperatures are shown. 40 K resistivity of the in-situ MgB₂ wires made by Filling 2 are less influenced by sintering than those of the in-situ MgB₂ wires made by Filling 1. While resistance of the Filling 2 changes from 145 to 160 $\mu\Omega$.cm, those of Filling 1 are in the range of 80 $\mu\Omega$.cm and 140 $\mu\Omega$.cm depending on sintering temperatures. T_c values of the all studied wire samples are same (37 K) except for a small difference for Filling 1 at 800°C (37.5 K) (see Figure 6.12).

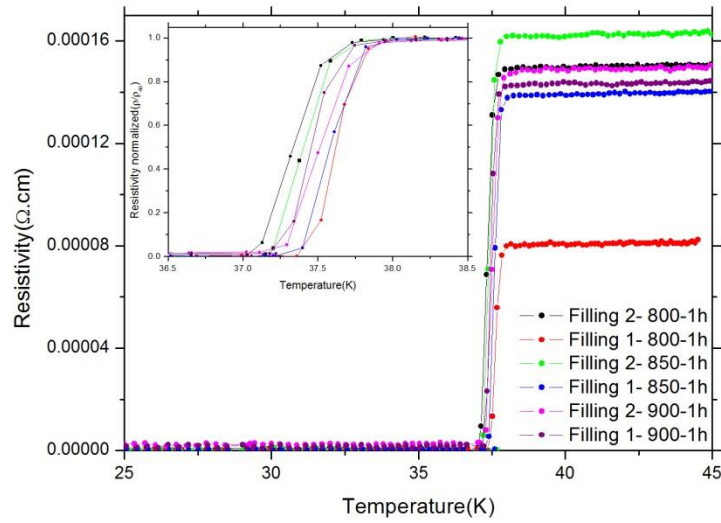


Figure 6.12. ρ vs T graph and Resistivity normalized (ρ_n) vs T inserted of in-situ monocore MgB₂/Fe wire at 1.90 mm Φ sintered at different temperatures.

The I_c measurement of the Fe/MgB₂ monocore wires under magnetic fields ranging from $B = 3$ T to 10 T is indicated in Figure 6.13, 6.14 and 6.15. The magnetic field was applied perpendicular to the wire axis in a Bitter magnet. It was found that a high I_c (4.2 K) = 140 A (9.8×10^3 A/cm²) at $B = 5$ T was obtained for the Filling 2 wire, sintered at 900 °C in Figure 6.14. While Filling 1 wire sintered at 900 °C carries 52 A under 4 T in Figure 6.13, Filling 2 wire sintered at 800 °C carries 118 A under 4 T in Figure 6.15. Transport critical current measurements were obtained in liquid helium for the wires sintered at temperatures of 800 °C and 900 °C. It can be said that the best temperature for the in-situ monocore MgB₂/Fe wire 1.90 mm diameter is 900 °C based on these results.

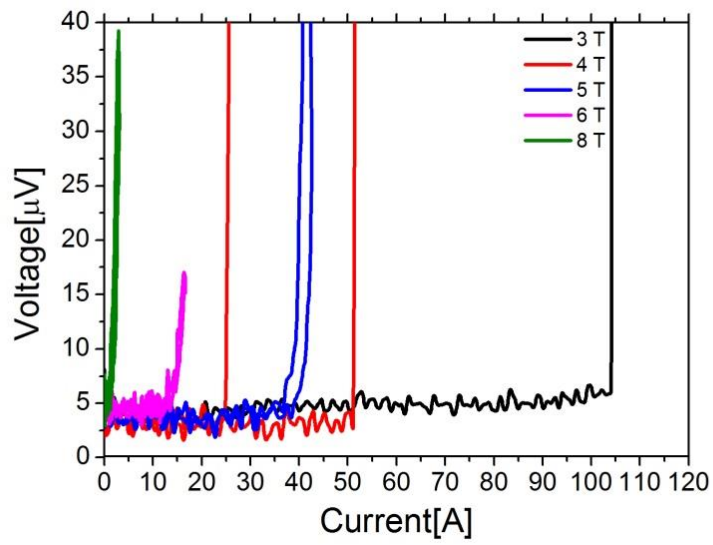


Figure 6.13. In-situ monocoire MgB_2/Fe wire 1.90 mm Φ sintered at 900 °C for 1h (Filling 1).

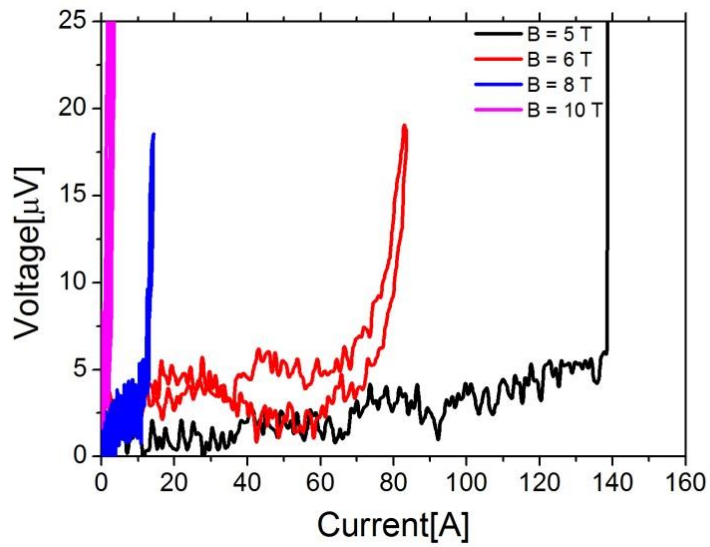


Figure 6.14. In-situ monocoire MgB_2/Fe wire 1.90 mm Φ sintered at 900 °C for 1h (Filling 2).

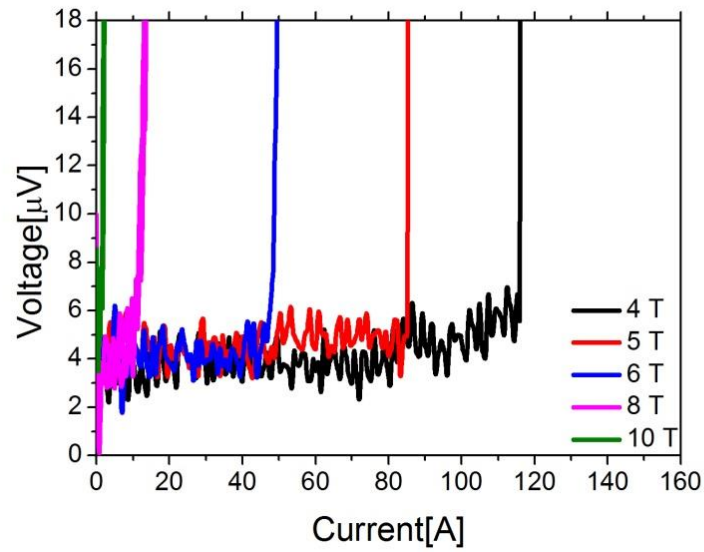


Figure 6.15. In-situ monocore MgB_2/Fe wire 1.90 mm Φ sintered at 800 °C for 1h (Filling 2)

In Figure 6.16, we present the best results in terms of the magnetic field dependence of the critical currents for the Filling 1 and Filling 2 wires. We found that the transport properties of the insitu Fe/MgB_2 wires were improved when the initial filling density is increased from 50% to 60% of the theoretical limit. The effect of sintering temperature of the wires made by PLIT is more apparent at the magnetic fields below 8 T and the best J_c results were obtained for the Filling 2 – 900 °C wire sample. It has been reported that Fe/MgB_2 monocore wires are sintered at temperatures between 600 °C and 800 °C to avoid the formation of FeB_2 and improve the grain connectivity which is related to transport properties of the MgB_2 wires (Varghese et al, 2011). The high J_c values at lower sintering temperatures for in-situ processed wires are usually attributed to the formation of the smaller grain size. However, iron is the most promising cladding material for the heat treatments above 900 °C and high transport J_c values have also been reported for copper cladded Fe/MgB_2 , sintered at 900 °C for 1 h (Glowacki and Majoros, 2001a; Jin et al, 2001).

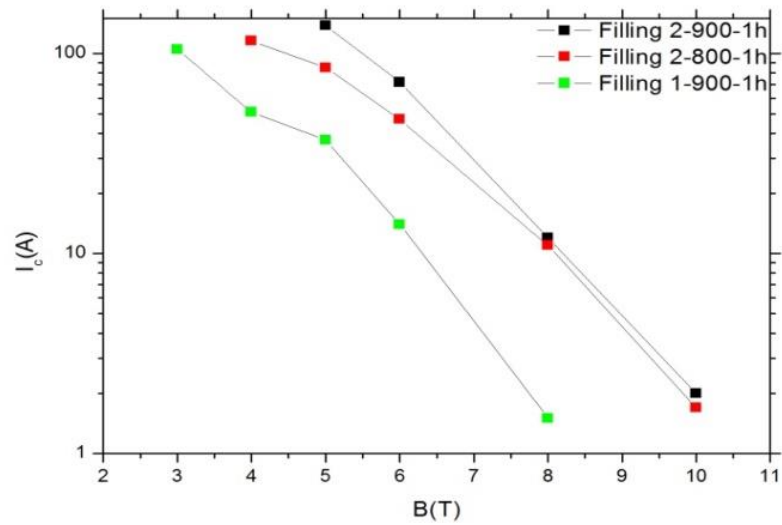


Figure 6.16. Magnetic field dependence of the critical currents of the in-situ Fe/MgB₂ wire samples at 4.2 K.

Moreover, a line scan of SEM-EDX analysis of the Filling 2 samples also revealed that a certain amount of boron diffuses into the Fe sheath material as shown in Figures 6.17(a) – 6.17(b). A line scan of SEM – EDX analysis of the Filling 2 samples clearly showed that no reaction layer was formed between the MgB₂ core and Fe surface and a small amount of boron diffused into the iron-sheath during the reaction process. However, a line analysis of the Filling 1–900 °C wire revealed that more boron penetrated into iron-sheath as shown in Figure 6.17(c). Boron diffusion may cause no voids at the core region but leads to presence of some Mg and somehow causes lower transport properties.

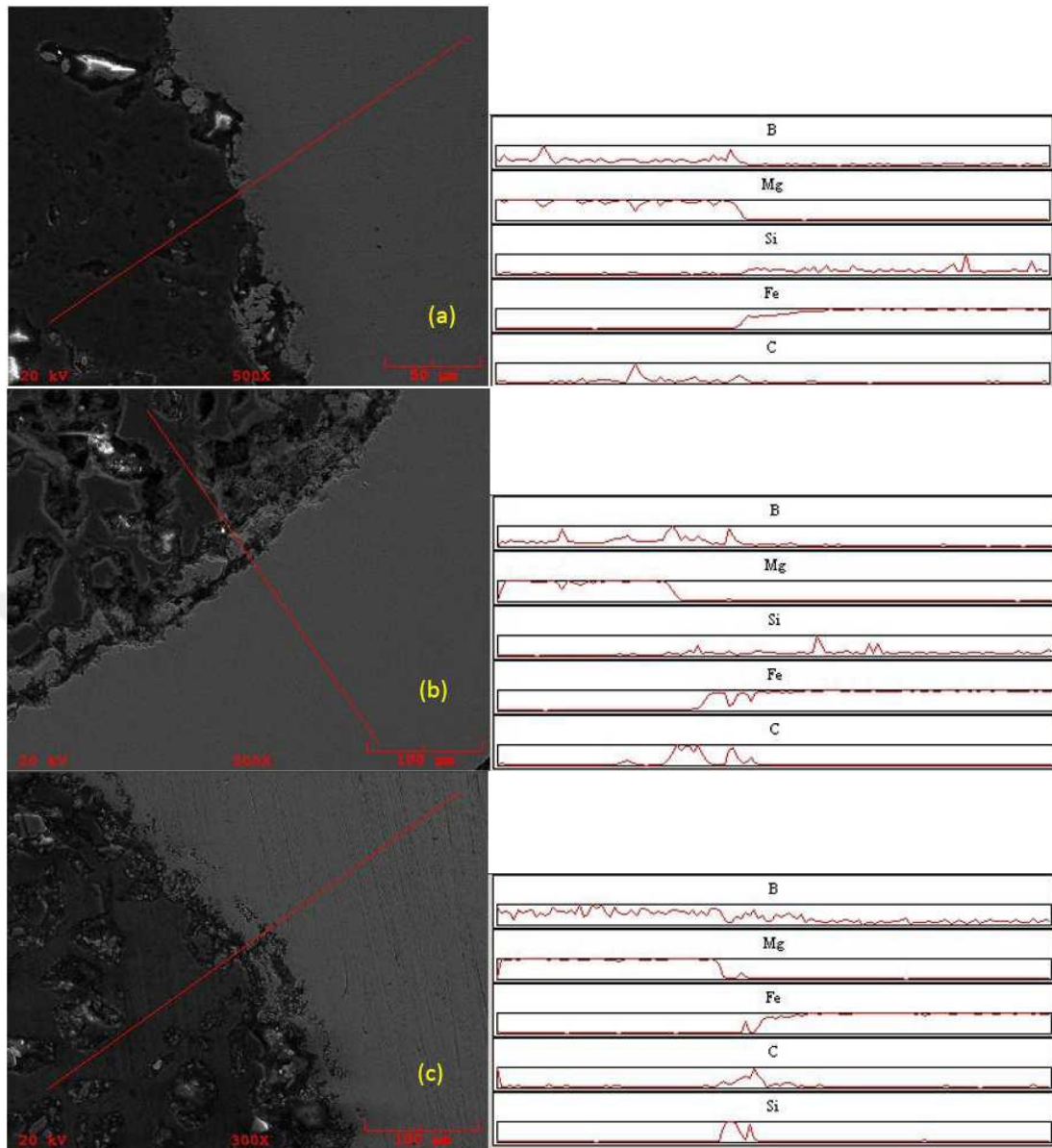


Figure 6.17. The line scan of SEM-EDX analysis of the (a) Filling 2 – 800 °C, (b) Filling 2 – 900 °C samples, (c) Filling 1 – 900 °C for 1 hour samples.

The Figures 6.18 shows the polished cross sectional SEM images of the in-situ MgB_2/Fe wires Filling 1 – sintered at 900 °C (a, d and g), Filling 2 – sintered at 800 °C (b, e and h), and Filling 2 – sintered at 900 °C (c, f and i) at different magnifications. The SEM analysis showed that a dense MgB_2 core with the micro scale voids was formed for the in-situ reacted Filling 2 – 900 °C wire sample, rather than a granular structure with the porosity. This indicates that the formation of good grain connectivity was achieved during the reaction process. For the Filling 2 – 900 °C sample, several voids ($< 30 \mu\text{m}$) were present in the core region and these voids may be associated with a complete reaction between large size magnesium (>100

μm) and boron. An unavoidable Mg diffusion caused the formation of some voids with a well – formed MgB_2 phase at the wire core. The SEM analysis of the Filling 2 – 800 °C sample showed more voids at the core region in comparison to that observed for the Filling 2 – 900 °C sample. This result may also justify the difference between the critical current values of the Filling 2 – 800 °C and Filling 2 – 900 °C wire samples as shown in Figure 6.17. Filling 2 – 900 °C gives better J_c results at $B=8$ T in comparison to those obtained for the Filling 2 – 800 °C indicating that a better grain connectivity was achieved without reducing density of the grain boundaries significantly because this sample carried highest I_c at high magnetic fields.

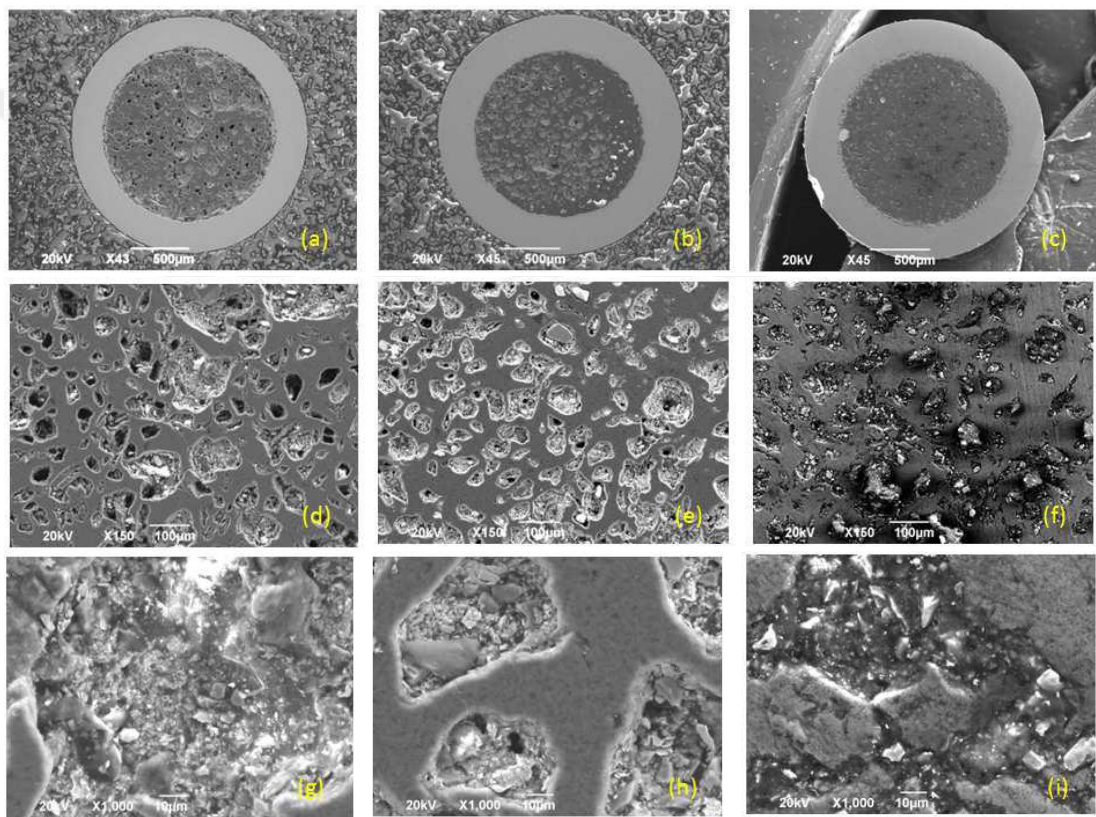


Figure 6.18. Polished cross-sectional SEM images of the in-situ Fe/MgB_2 wires. Columns belong to Filling 2-900, Filling 2-800 and Filling 1-900°C from left to right.

In analysis of the sample named as F6 by HIP process, energy dispersive spectrometry (EDS) analysis given in Figure 6.19 (a) and Figure 6.19 (b) show that MgB_2 material has a good purity after annealing in low pressure. Carbon (C) and oxygen (O) atoms were introduced during preparation of samples for SEM analysis. A small amount of iron atoms diffused in to the core material during annealing process at atmospheric pressure. Annealing under high pressure produced MgB_2

material with higher phase purity (Figure 6.19 (c)) by lowering the diffusion of iron atoms in to the superconducting MgB_2 core and decreasing the amount of voids. This suggests that high pressure slows down the diffusion rate of the Fe atoms from iron sheath to the MgB_2 core. Also, HIP accelerates the rate of reaction in the MgB_2 material and leads to the formation of more superconducting phase.

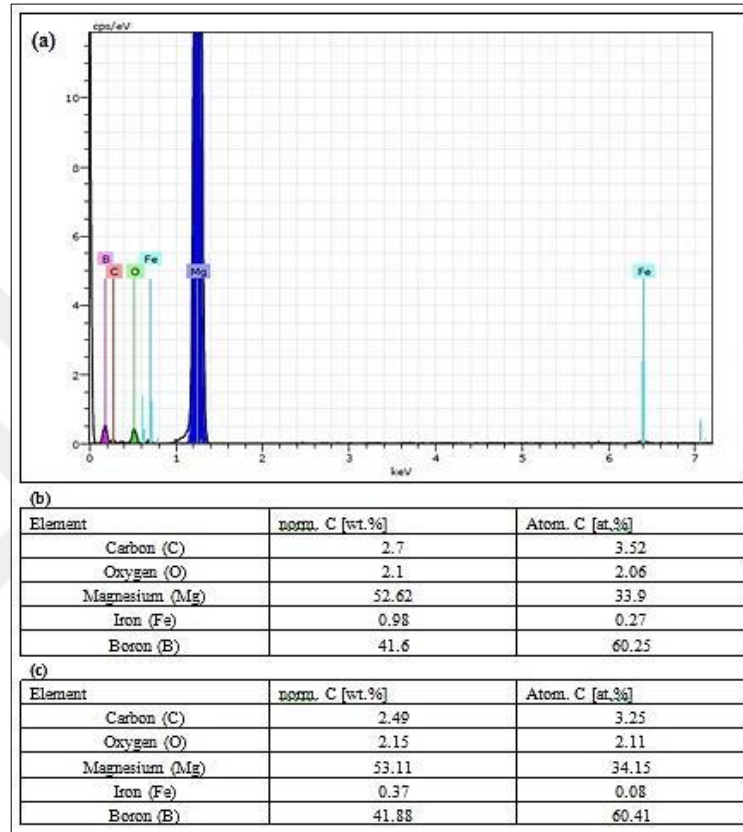


Figure 6.19. The EDS analysis of samples cross-section for (a) and (b) sample A (0.1 MPa) and (c) sample B (1 GPa).

The results in Figure 6.20 (a) show that a T_c of 37.9 K (in $B = 0$ T) is obtained by HIP at 1.1 GPa while a lower T_c of 36.6 K (in $B = 0$ T) is obtained for annealing at atmospheric pressure (0.1 MPa). This indicates that HIP at 1.1 GPa increases the T_c by about 1.3 K in zero field and even more in magnetic fields from 1 T to 5 T. Temperature dependence of B_{irr} and B_{c2} values for different applied magnetic field strengths also favors the use of HIP method. At the same magnetic field strength HIPped samples exhibit same B_{irr} and B_{c2} values at a higher temperature by about 5 K. As shown in Figure 6.20 (b), B_{irr} of the sample A is less than 10 T (at 4 K) while that of the sample B is higher than 12 T (above 6 K). Measurements in zero fields indicate that the sample A has the resistance in the normal state higher than in sample

B by about 5 %. The magneto-resistivity measurements of sample A indicate that increase of the magnetic field from 0 T to 14 T increases the normal state resistance (R_N) by about 18% (Figure 6.20 (c)). Moreover, Figure 6.20 (c) shows that the R_N increases linearly with the applied magnetic field. In addition, the results for sample A in Figure 6.20 (a) and Figure 6.20 (b) show that increase of temperature causes decrease of resistance in normal state. On the contrary, the magnetoresistivity results for sample B show that the normal state resistance does not increase with increasing magnetic field or increasing temperature (Figure 6.20 (a) and Figure 6.20 (b)).

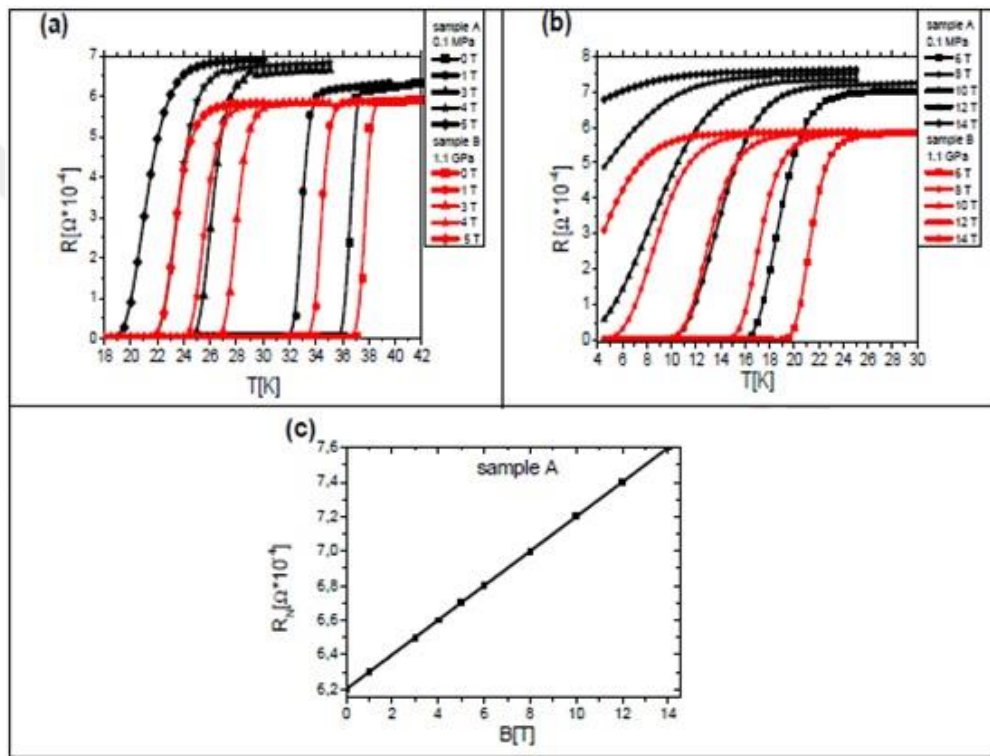


Figure 6.20. Transport R - T curves for samples A and B, (a) in low magnetic fields, (b) in high magnetic fields and (c) Transport R_N - B curves for samples A.

HIP process significantly increases the critical current density (J_c) and pinning force (F_p) at 4.2 K; four times in 5 T, six times in 7 T and by one order magnitude in 9 T (Figure 6.21). At 20 K, 1.1 GPa pressure also allows for significant increase of J_c (six time – Figure 6.21(b)).

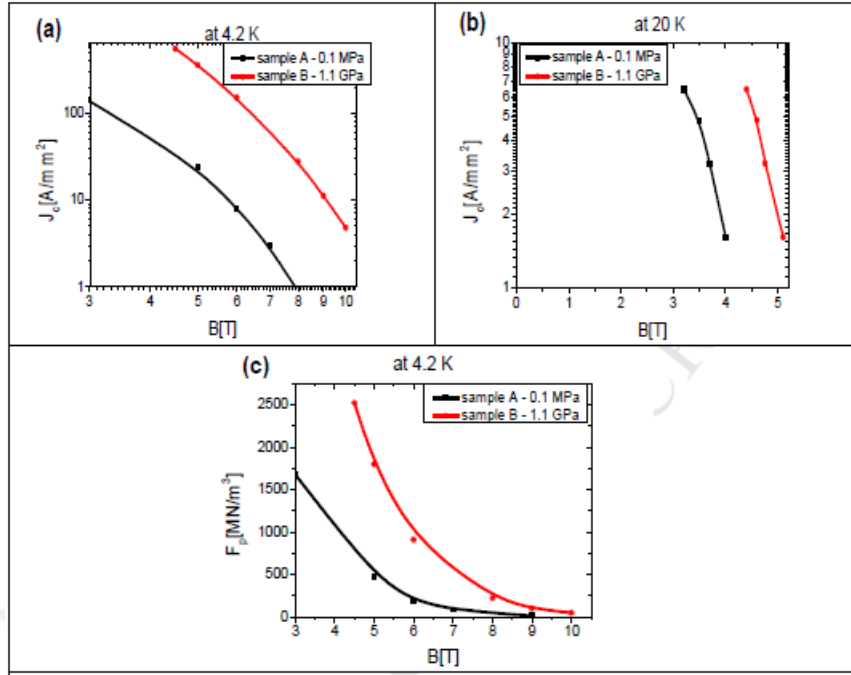


Figure 6.21. Transport $J_c - B$ curves for samples A and B (a) at 4.2 K, (b) at 20 K and (c) Transport $F_p - B$ curves for samples A and B.

All images in Figure 6.22 were obtained by using the SEM in secondary electron (SE) mode. SEM images given in Figure 6.22 (a) show that annealing in low pressure creates a lot of big voids which are unevenly distributed throughout the structure of MgB₂ wire. In Figure 6.22 (b) we see that low pressure results in the formation of large grains and a reduction in the number of connections between the grains. Application of HIP significantly reduces the amount of voids in the core structure of wires (Figure 6.22 (c)) and increases the density of the MgB₂ material. This finding indicates that mechanically forced compaction through isostatic pressure during sintering is important in achieving high performance MgB₂ wires. The results given in Figure 6.22 (d) show that high pressure allows for obtaining smaller grains, leading to an increase in the number of connections between the grains i.e. to more current paths.

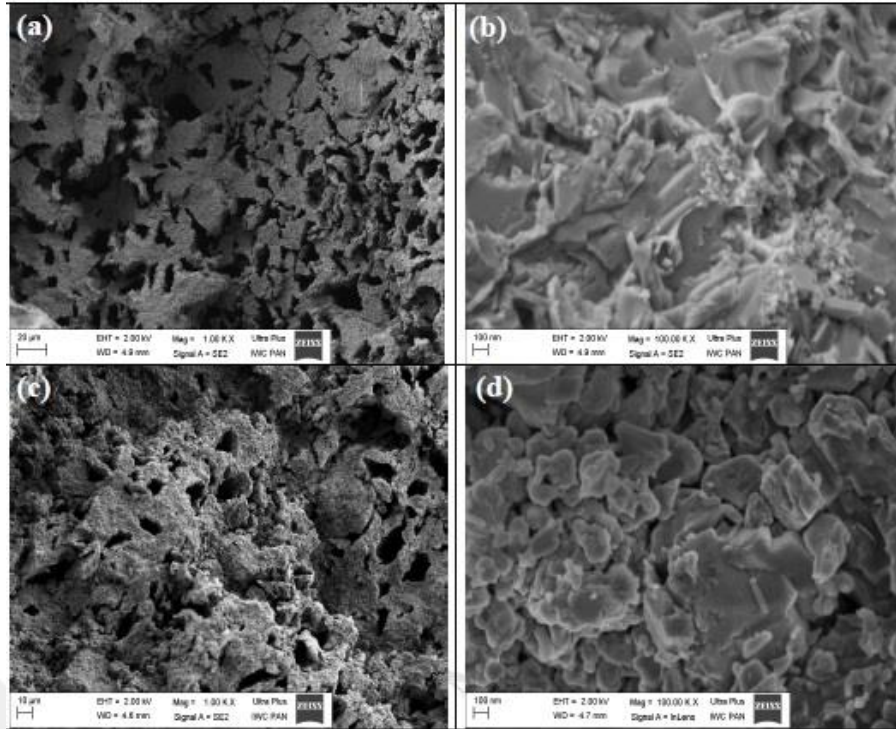


Figure 6.22. The SEM images of samples' cross-sections in the mode of secondary electron (SE), (a) and (b) show sample A, (c) and (d) indicate sample B.

Backscattering electron (BSE) analysis shows that annealing at atmospheric pressure results in the formation of large areas of unreacted Mg (light areas) which exhibit inhomogeneous distribution in the wire core (Figure 6.23 (a) and Figure 6.23 (b)). This might indicate a smaller ratio of superconducting MgB_2 phase. As shown in Figure 6.23 (c) and Figure 6.23 (d) HIP process results in lower amount of unreacted Mg particles hence greater amount of MgB_2 phase with better homogeneity. The effect of HIP process can be seen from the decrement of bright areas in Figure 6.23 (a) and (c) indicating magnesium rich regions. Topology of the samples' surfaces may also have an affect on appearance of bright areas since these surfaces are not polished surfaces. Despite this, the SE and BSE images in Figure 6.23 were taken from same regions and they constitute good evidence for presence of unreacted Mg particles. BSE image of sample B has more uniform gray appearance with less white regions in contrast.

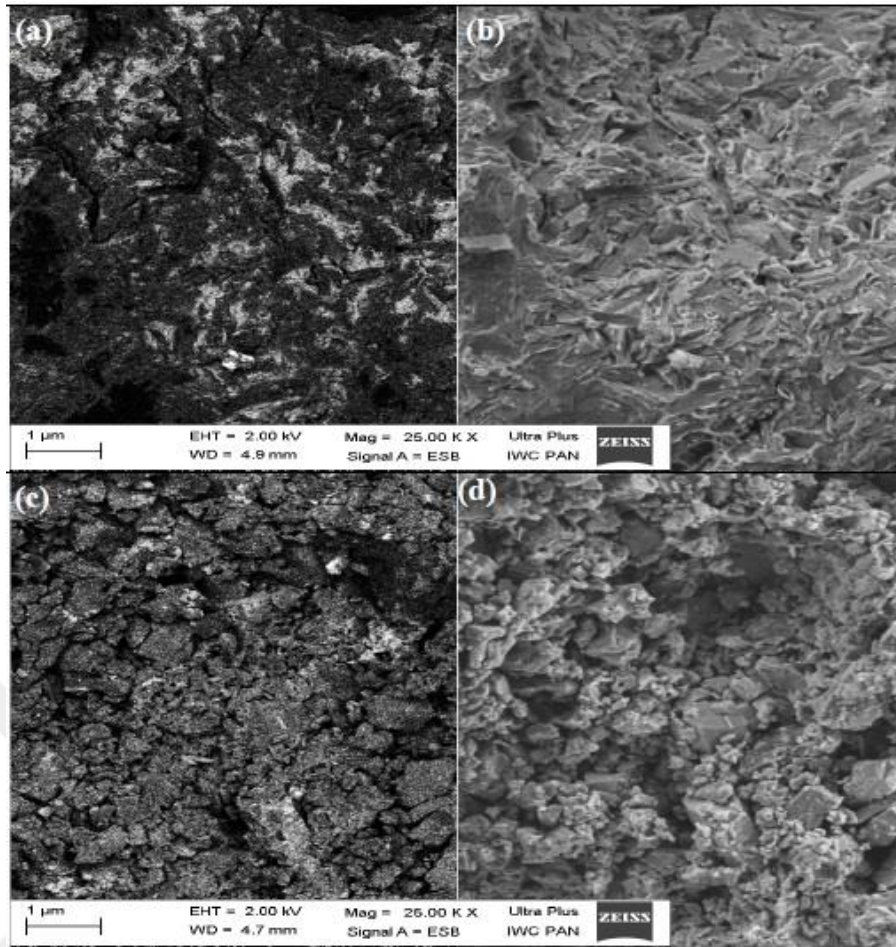


Figure 6.23. The SEM analysis of samples cross-section in the BSE mode for sample A(a) and sample B(c). Sample A(b) and sample B(d) in the SE mode.

The Figure 6.24 shows the transport measurements of the 1.00 mm diameter MgB_2/Fe monocoire F5E850 and F5E900 wire samples measured in PPMS. The $T_{c,\text{offset}}$ is 36.5 K ($\Delta K = 1.5$ K) and 37.1 K ($\Delta K = 1.0$ K) for F5E850 and F5E900 wire samples, respectively. The F5E850 sample has a lower T_c and a wider transition width in the transport measurement but the difference in the transition width of both samples could have been determined with better precision if more data taken with smaller temperature intervals. The $\Delta\rho$ value of the F5E850 sample is higher than the value of the F5E900 sample. This may be an evidence of relationship between sintering temperature and superconducting properties as well as boron depletion into the iron sheath causing Mg rich core with better connectivity.

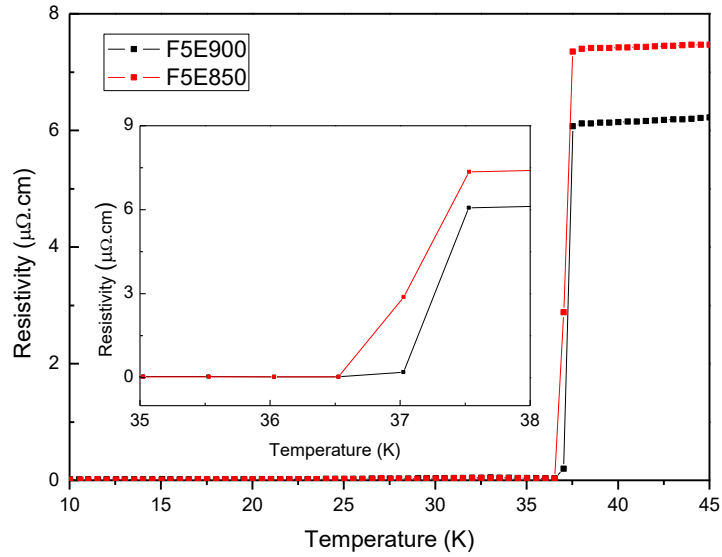


Figure 6.24. Transport measurements of the F5E850 and F5E900 in-situ monocore MgB_2/Fe wire samples.

The effect of the applied magnetic field on the resistivity has been examined in the temperature range between 10 K and 35 K. Figure 6.25 shows a set of the $\rho(B, T)$ curves for several applied field strengths for F5E850 and F5E900 wire samples. As can be seen from Figure 6.25, the B_{irr} of both samples are almost equal at 35 K and B_{irr} of the wire F5E850 gradually becomes better as the temperature decreases. This behavior may be attributed to higher pinning ability of the wire F5E850 due to higher granularity since the wire F5E900 are more crystallized.

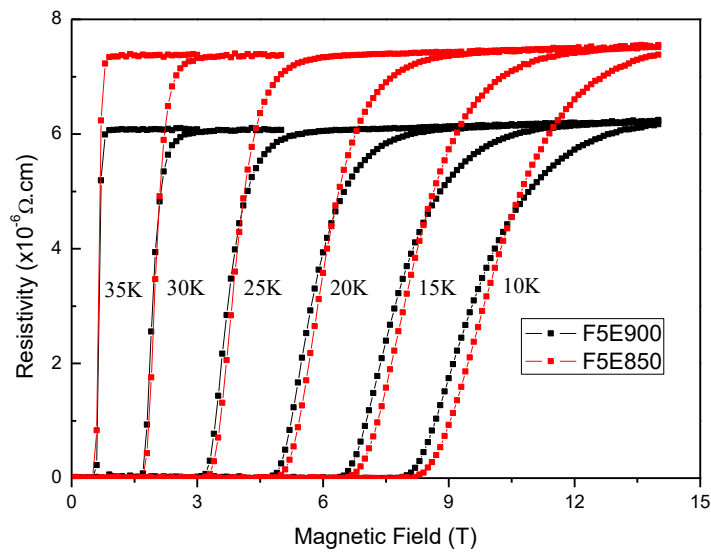


Figure 6.25. Magneto-resistivity measurements of the F5E900 and the F5E850 in-situ monocore MgB_2/Fe wire samples.

Figure 6.26 presents the transport I_c measurements of F5E850 and F5E900 monocoire wires under high magnetic fields ranging from $B = 3$ T to 9 T. The magnetic field was applied perpendicular to the wire axis. It was found that a high I_c (4.2 K) > 150 A ($J_c > 1.91 \times 10^4$ A/cm²) at $B = 3$ T was obtained for F5E850 wire, sintered at 850 °C. Critical current measurement was also applied for F5E900 sample and measurement results can be seen as inset in Figure 6.26. The critical current values of both samples at $B = 3$ T are above 150 A but the I_{cc} values of the F5E850 wire are higher than the F5E900 wire at magnetic fields higher than 3 T.

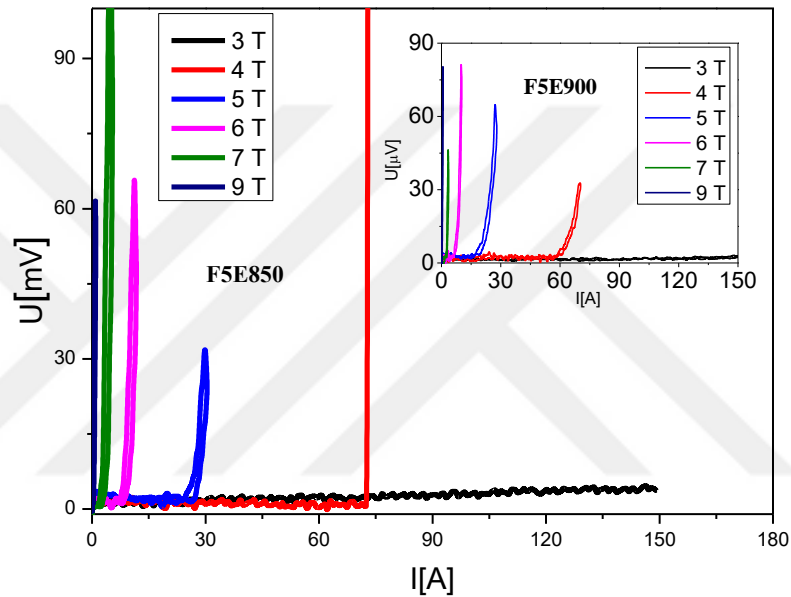


Figure 6.26. Transport I_c measurements of the F5E850 and F5E900 in-situ MgB₂/Fe monocoire wire samples at 4.2 K under different magnetic field strengths up to 9 T.

The Figure 6.27 indicates the transport engineering J_c values of the F5E850 and F5E900 at 4.2 K under different magnetic field strengths up to 9 T. The J_{cc} - B performance of F5E850 wire is significantly better than that of F5E900 wire. This situation indicates that the flux pinning ability of F5E850 is better for higher magnetic field strengths (Zhang et al, 2006).

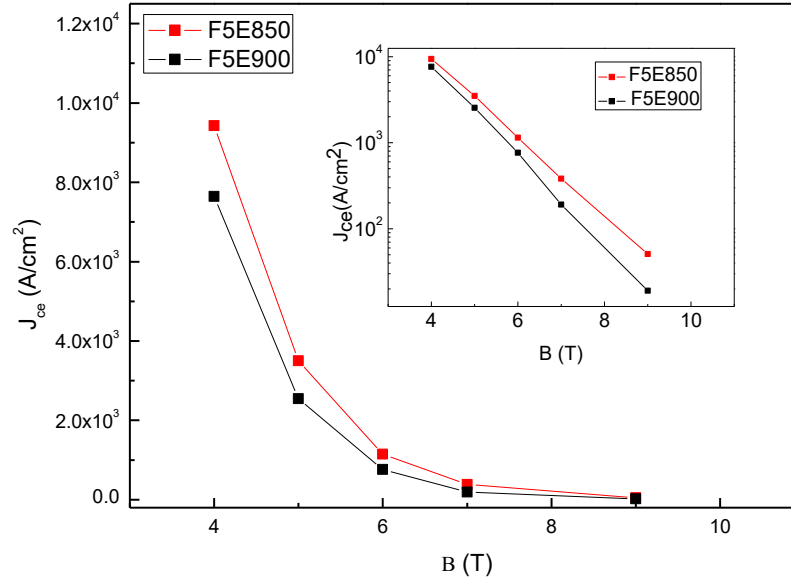


Figure 6.27. Transport engineering J_c measurements of F5E850 and F5E900 in-situ MgB_2/Fe wire samples at 4.2 K with different magnetic field strengths up to 9 T.

Since it is not possible in our laboratory to perform transport measurements with currents as large as 200 A in LH, It is very important to predict transport critical current value of the MgB_2/Fe wires when transport currents up to 200 A were run through them under magnetic field at 4.2 K. For that purpose, we decide to compare the transport current values obtained in ILHMFLT in LH with transport critical current the results obtained in our cryostat at temperatures just below T_c running transport currents upto 1 A through the samples in magnetic field as seen Figure 6.28(a) and 6.28(b). Inhere, the studied samples are the samples tested in Poland. Critical current values of the wires with T_c of ~ 37.5 K are 0.3 A for F5E900 and 0.48 A for F5E850 when measured 0.5 K below T_c . F5E900 wire carries 0.55 A supercurrent 1 K below T_c and critical current value of F5E850 wire is higher than 1 A at 1 K below T_c (Figure 6.28). While F5E850 and F5E900 carry supercurrents of 0.48 A and 0.3 A respectively at 37 K in our system, the critical current value of F5E850 and F5E900 are ~ 72 A and ~ 57 A at 4.2 K under 4 T, respectively (see Figures 6.26 and 6.28). So, the results are in agreement with measurements performed in ILHMFLT and we can clearly say that an MgB_2 wire which carries a large critical current at 4.2 K should also have a critical current value of about 1 A at 1 K below its $T_c(0)$ in our gas contact cryostat system.

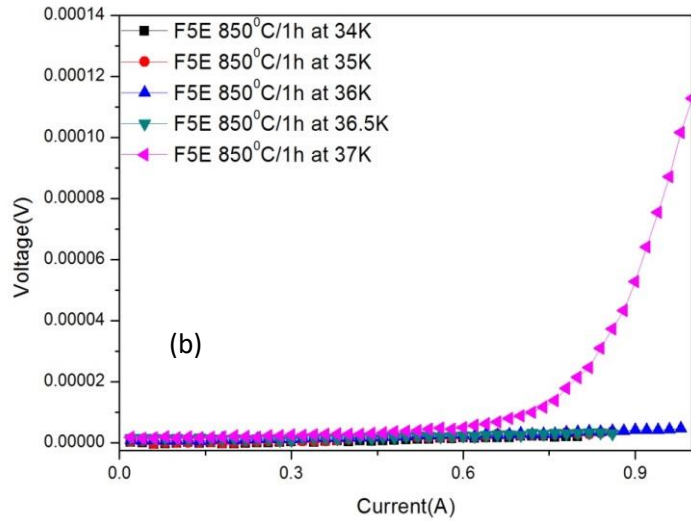
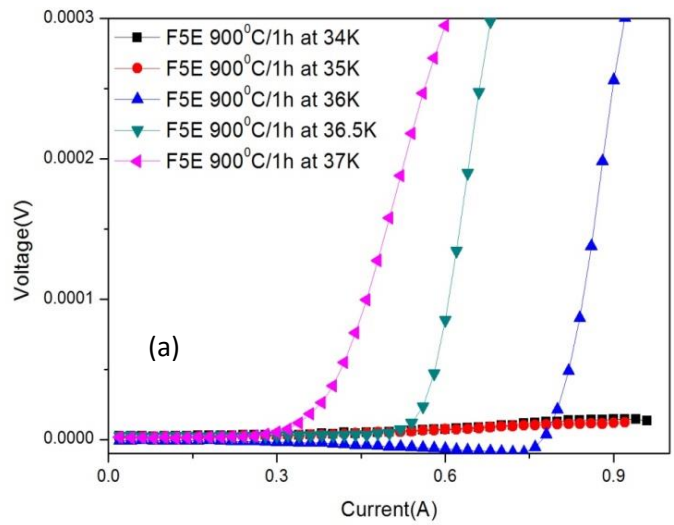


Figure 6.28. Transport I_c measurements of F5E900 (a) and F5E850 (b) in-situ MgB_2/Fe wire samples at constant temperatures just below T_c in self-field.

In Figure 6.29, some XRD patterns of both samples and paste material are given. The detailed information about the paste material can be seen in section 6.3 and in Figure 6.11. In the present study, XRD analysis of F5E850 and F5E900 wires show that there are Fe_2B and Fe phases for F5E900 with small intensities. It is known that the interface reaction layer (Fe_2B) doesn't act as a diffusion barrier to prevent more/further reaction (Grivel et al, 2006). Moreover, MgO peaks appeared at both patterns and their intensity is higher in the F5E900 sample. It is clear that the

desired MgB_2 phase formed in the cores of both samples and F5E900 showed better crystallinity of MgB_2 phase as evidenced by higher count rate in the XRD.

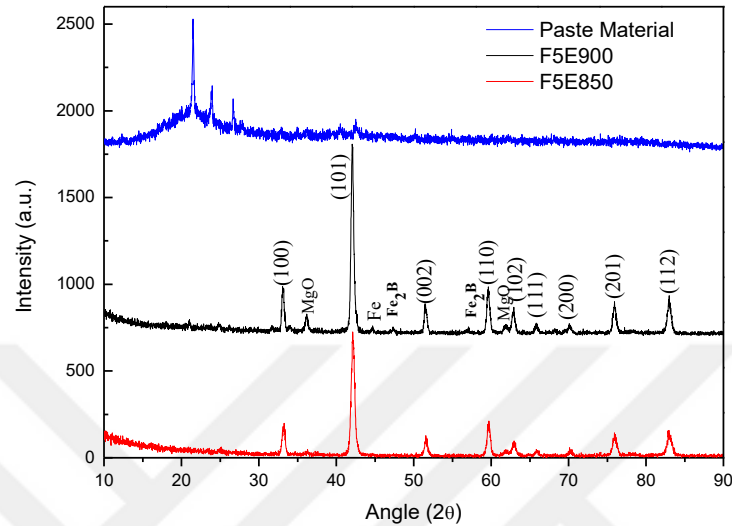


Figure 6.29. X-Ray Diffraction analyses of the wire samples after the Fe sheath material was extracted mechanically.

In Figure 6.30(a) and 6.30(b), fracture cross sections images of F5E900 and F5E850 are seen after the mechanical removal of Fe sheaths. Figures 6.31(a) – 6.31(d) show SEM images of these fracture cross sections of F5E850 and F5E900 wires respectively at higher magnifications. All samples had a crack free microstructure and grain size appeared to be sub-micron size. Figures 6.31(c) and 6.31(d) are SEM pictures which are taken from fracture cross-sections show granular structure and powdery appearance. For F5E900 sample (Figures 6.31(a) and 6.31(b)), the microstructure of superconducting core transforms to a more web-like network of interconnected MgB_2 interspersed with voids (Susner et al, 2007). The voids at F5E900 may be attributable to the complete reaction between large size magnesium and boron. An unavoidable Mg diffusion caused the formation of some voids with a well-formed MgB_2 phase in the wire core. The SEM analysis showed that a dense MgB_2 core with the micro scale voids ($<30 \mu\text{m}$) was formed for the in-situ reacted F5E900 wire sample, rather than a granular structure with the porosity. Furthermore, F5E850 wire sample shows granular structure with smaller porosities in comparison to that observed for the F5E900 wire sample. For both samples, SEM images show

different levels of crystallinity for two samples. Better crystallized sample F5E900 had sharper transition while the sample sintered at 850 °C had wider transition but better in field transport behavior due to a finer grain structure.

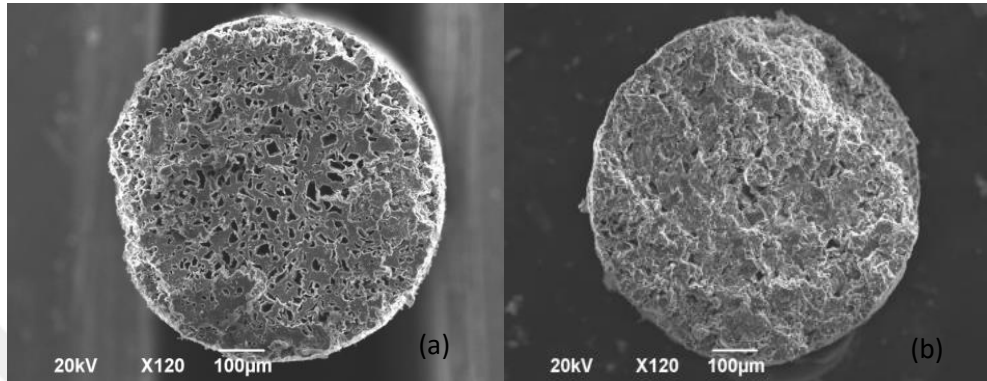


Figure 6.30. SEM images as cross sectional of F5E900 wire core (on left) and F5E850 wire core (on right).

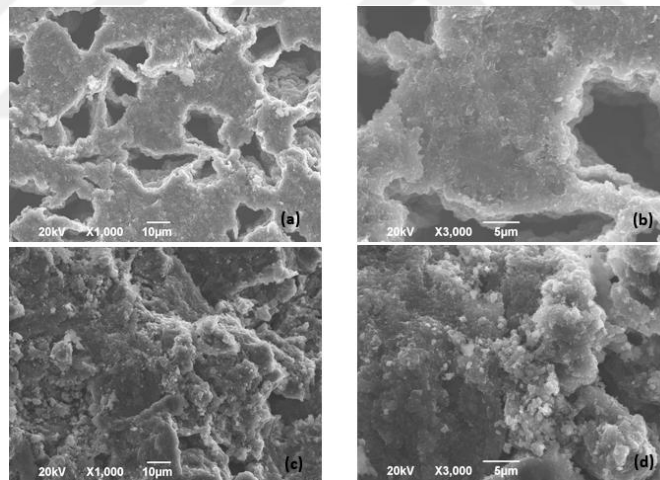


Figure 6.31. SEM images of a-b) F5E900 and c-d) F5E850 wire samples at 10 µm and 5 µm scales.

6.4 Examination of In-situ MgB₂ Monocore Tapes

Figure 6.32 shows the $\rho - T$ curves obtained from dc electrical resistivity measurements of the sample, initially sintered at 950 °C, before and after additional processing steps. The in-situ BP-950 wire sample has a sharp superconducting transition with a $T_c = 38.3$ K. The same sample after mechanical deformation (*AP*-

950) is found to possess a lower T_c with a broadening in the superconducting transition. Besides that the mechanical deformation also affected the resistivity values at 40 K (ρ_{40K}). It is found that ρ_{40K} value measured for the *AP*-950 sample is greater than that of the *BP*-950 sample. This behaviour is also consistent to the results obtained from the other samples. As an example, the same results are presented in the inset in Figure 6.32 indicating the resistivity measurements of the *BP*-800, *AP*-800, and *PA*-800 samples. At final step, additional annealing at 850 °C recovered the superconducting features to some extent although not fully. The broadening of the superconducting transition was improved a lot, but the T_c was still below the initial values together with a higher resistivity at 40 K. In contrary, the inset in Figure 6.32 is clearly seen that the *PA*-800 sample has a lower 40-K resistivity in comparison to that of the *BP*-800, unlike samples the *PA*-950 and the *BP*-950.

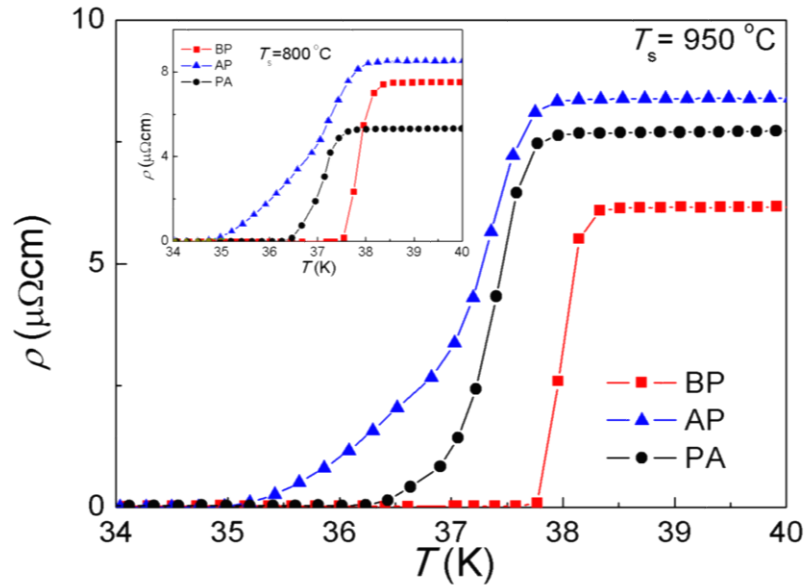


Figure 6.32. The ρ - T curves of the Fe/MgB₂ wire sample sintered at 950 °C and the insert graph for the Fe/MgB₂ wire sintered at 800 °C for PA of both samples was performed at 850 °C for 1 hour each experimental step.

Figure 6.33 indicates the details of the superconducting transition by means of onset critical temperatures ($T_{c,onset}$), offset critical temperatures ($T_{c,offset}$) and transition width (ΔT) curves for all samples at every step. Figure 6.33(a) shows that the samples have similar $T_{c,onset}$ values in each step as functions of the initial

sintering temperature. The only anomaly for which we don't have an explanation was found for the sample initially sintered at 850°C. In Figure 6.33(b), effect of excessive mechanical deformation on offset critical temperatures is quite evident for all samples. It is also remarkable that the final annealing process improves transition temperatures of the pressed samples considerably. In Figure 6.32, the resistivity curves showed a tail behaviour in the $T_{c,offset}$ due to excessive mechanical deformation. Figure 6.33(a) indicates that such a case is not to be presumed to exist in the onset of the superconducting transition, again 850°C samples are exceptions. As readily seen in Figure 6.33(c), the broadening of the superconducting transition occurs at $T_{c,offset}$ end of the curves. This finding indicates that mechanically induced cracks do not lower onset T_c so any decrease in onset critical temperature is more likely to be related with chemical effect rather than mechanical effect. This type of broadening arises due to the formation of a large number of micro-cracks which contribute to weak-link behaviour and the subsequent heat treatment highly eliminated the tail behaviour as shown in Figure 6.33(c). We suggest that the heat treatment re-joined the grains and improved the microstructure of the sample by a considerable amount.

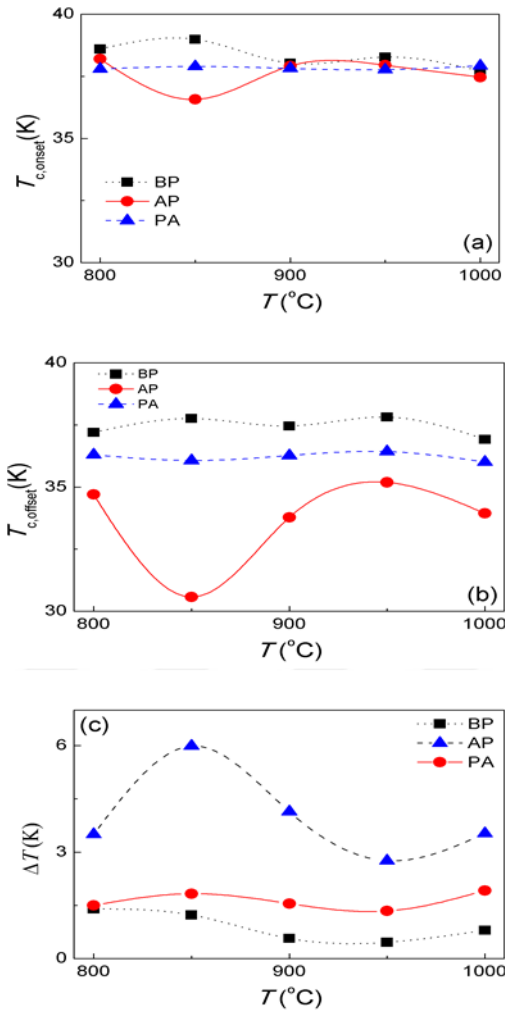


Figure 6.33. Variation of $T_{c,onset}$ (a) $T_{c,offset}$ (b) ΔT (c) of the five sintered Fe/MgB₂ samples in the *BP*, *AP*, and *PA* steps.

Figure 6.34 exhibits the XRD patterns of the sample initially sintered at 950 °C at different processing steps. These patterns were obtained from different samples which were fabricated in an exactly same manner. A silver base was used as holder in XRD measurements in order to eliminate broadening background reflection effects which prevent small diffraction peaks, such as Mg and MgB₄ to be seen. The analysis of XRD patterns revealed the presence of a well-formed MgB₂ phase at all stages of the experiments. The XRD peaks obtained from the samples sintered above 900 °C showed some MgB₄ phase which is difficult to avoid at high sintering temperatures (Mustapic et al, 2013). The Fe peak in XRD patterns appeared for only *AP* and *PA* samples because the MgB₂ cores were mechanically removed from the iron-sheath.

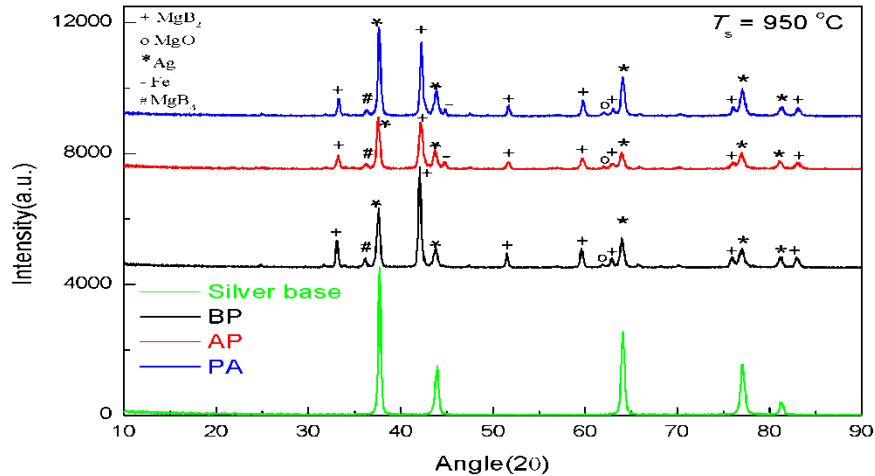


Figure 6.34. XRD patterns of (black) the Fe/MgB₂ samples initially sintered at 950°C, (red) after pressing and (blue) after post annealing at 850 °C.

Figure 6.35 show the results of the transport I_c measurements of the sample initially sintered at 950 °C before pressing as virgin sample (BP), after pressing (AP) and after post annealing at 850 °C (PA). The current vs. voltage (I-V) measurements were done at the temperatures of $T = 36.5$ to 37.3 K, Step 1-BP in Figure 6.35(a), $T = 32.5$ to 34.5 K, Step 2-AP in Figure 6.35(b) and $T = 34$ to 35.7 K, Step 3-PA in Figure 6.35(c). In all measurements the temperature range for I_c measurements were determined from $T_{c,offset}$ at the lowest temperature at which critical current is $I_c \geq 1$ A. The I_c values were determined using $1 \mu\text{V}/\text{cm}$ criterion for transport currents of up to maximum 1 A. The results were found to be consistent with the results of resistivity measurements. A large degradation was observed in the I_c values after mechanical deformation and they were increased by additional post annealing heat treatment process. This directly indicates that an excessive mechanical deformation is desirable to fill the voids, but leads to the formation of many new grain boundaries inside the sample.

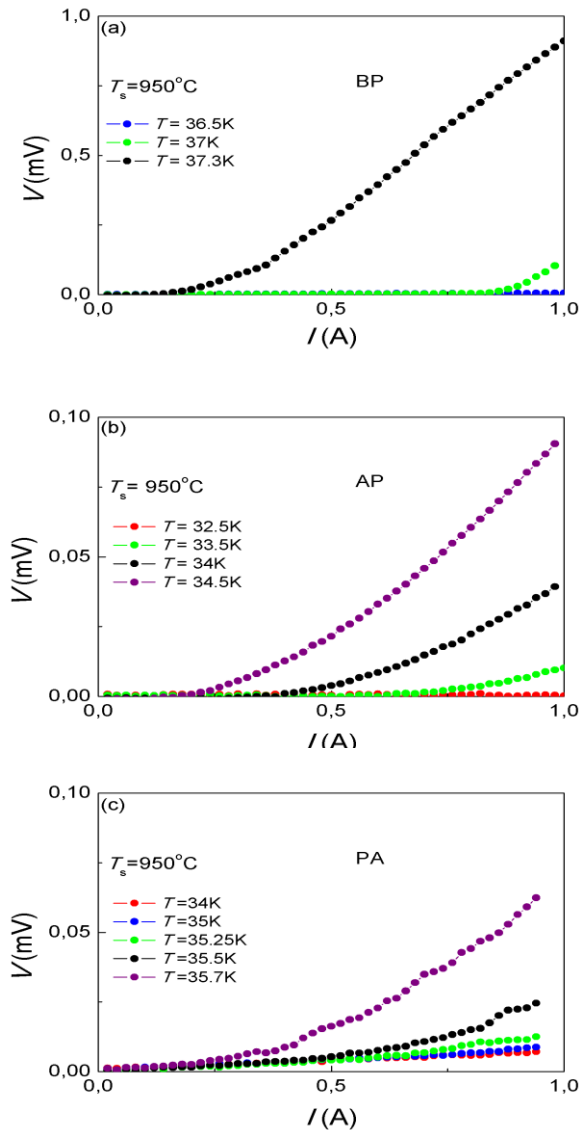


Figure 6.35. I - V curves of (a) the Fe/MgB₂ wire sample initially sintered at 950 °C (b) the sample after pressing and (c) the sample after post-annealing at 850 °C.

The transport J_{ce} of the samples are represented in Figure 6.36 (a)–(c). The J_{ce} values of the post-annealed samples at 850 °C are almost as large as those of the initial Fe/MgB₂ wire samples. On average the total cross-section area of any pressed sample is 15 % less than that of an initial sample and almost all of this reduction comes from compaction of superconducting core making the ratio of the superconducting cross section of the wire smaller. Due to this fact, it is expected that J_{ce} values of *PA* samples must be larger than their J_{ce} values due to decrement of the total cross-sectional area from 0.00785 to 0.00667 cm². By considering the high rate of J_{ce} re-gains in our work, it is suggested that a small degradation of J_{ce} may be

compensated and even exceeded by sintering the wires initially at a temperature which is lower than the post annealing temperature.

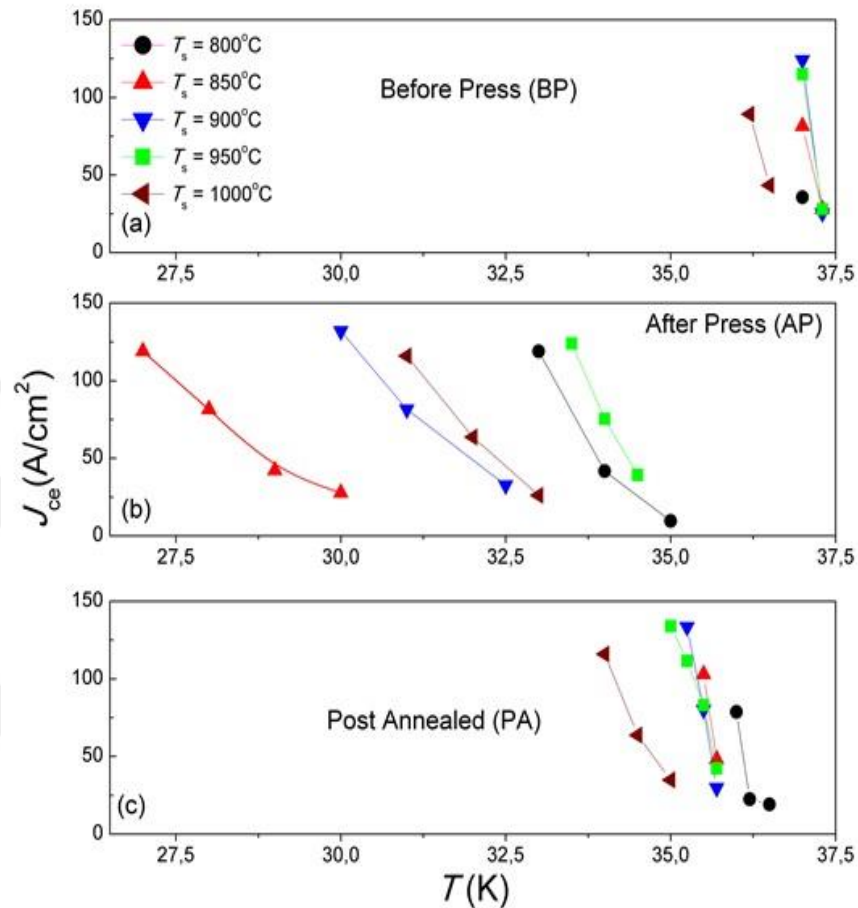


Figure 6.36. T vs J_{ce} curves of a) BP, b) AP, and c) PA at 850 °C for the samples initially sintered at different temperatures from 800 °C to 1000 °C

The SEM images in Figure 6.37 (a)–(c) are very suggestive in further processing of the wire samples. These images represent that a dense MgB_2 core with micro scale voids is achieved for the in-situ reacted BP-950 wire sample which has a dense superconducting core with some voids as shown in Figure 6.37(a). This is a significant result in terms of the accomplishment of fine grain connectivity during the reaction process for the BP-950 sample. Figure 6.38 (a), (b) and (c) shows the microstructures of the samples BP-950, AP-950 and PA-950 before mechanical deformation, after mechanical deformation and after post annealing, respectively. It seems that these voids were almost totally removed, and the core density was further

increased after pressing the sample. Densification upon mechanical deformation corresponds to about 30 % volume reduction in superconducting core. Mass density difference between $\text{Mg} + 2\text{B}$ and MgB_2 leads to ~23 % void formation. The rest of the volume reduction is expected to be due to incomplete densification during drawing. Nano pores may be present in the MgB_2 core even after pressing but the mass density of the core in our samples is near full density according to SEM examinations. Our transport measurements also revealed the existence of grain boundaries arising from the crushing of superconducting grains/clusters into smaller pieces which was supported by grain size values such as 283.9 Å (*BP*), 184.6 Å (*AP*), and 284.3 Å (*PA*) obtained from XRD patterns. The poor connections between the grains impeded the J_{ce} , a subsequent heat treatment is very promising in order to upgrade the microstructure as seen in Figure 6.36(c). Samples initially sintered at 800°C showed the highest percentage of recovery in terms of critical current density near T_c , indicating that a final heat treatment at a higher temperature can help to obtain better performance when sintering temperature prior to final mechanical deformation is kept lower. The need for fully dense MgB_2 wire is not only important for critical current density considerations, but also crucial for preventing mechanical damage during its use since voids in the core cause mechanical weakening.

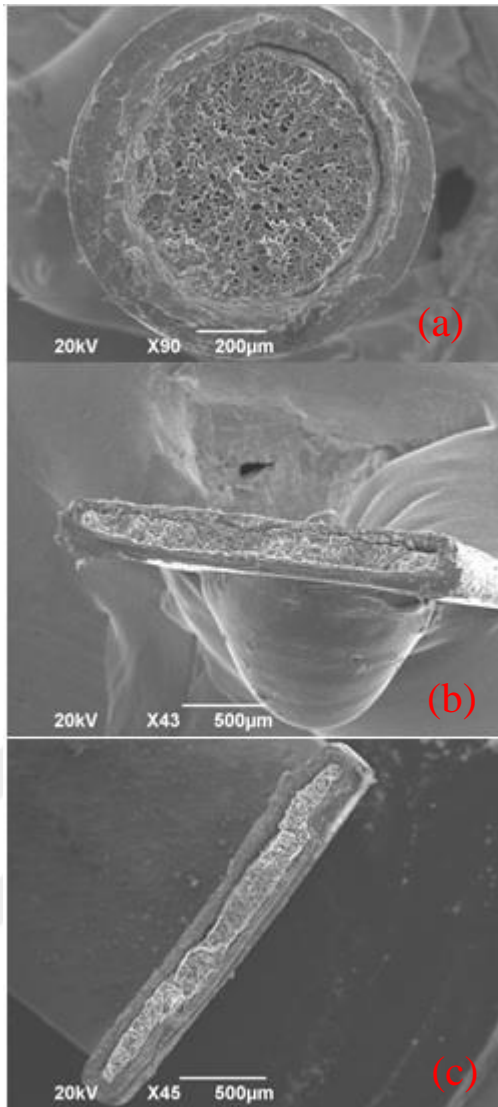


Figure 6.37. SEM images taken from fracture cross sections of Fe/MgB₂ samples initially sintered at 950 °C after steps for (a) *BP*, (b) *AP* and (c) *PA* at 850 °C.

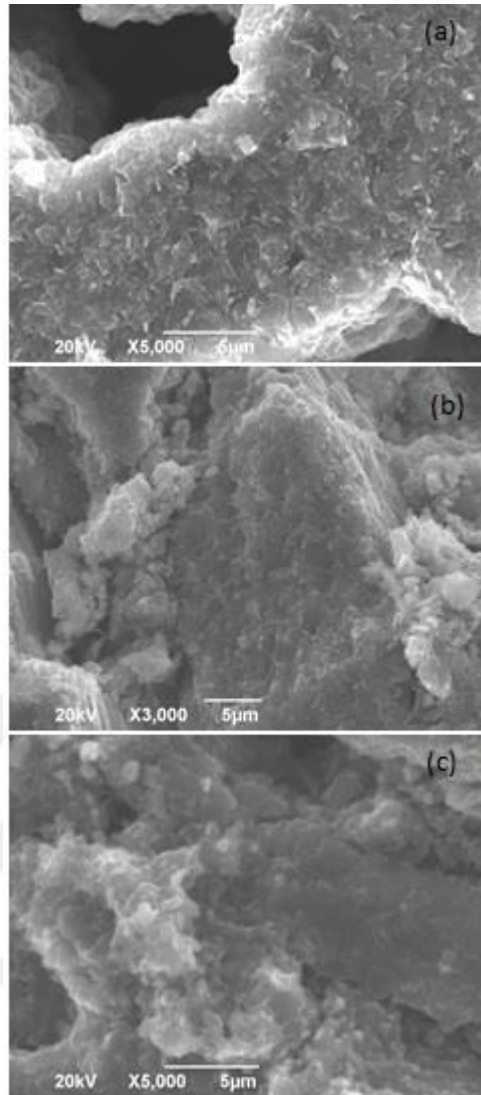


Figure 6.38. Microstructural SEM images of Fe/MgB₂ samples initially sintered at 950 °C after a) *BP*, b) *AP*, and c) *PA* at 850 °C.

6.5 Investigation of In-situ MgB₂ Multifilamentary (18+1) Wires

Figure 6.39 and 6.40 indicates resistivity vs temperature curves of two sets of MgB₂/Fe (18+1) wire samples produced using same procedures. For both sets, we can say that normal state resistivity of the MF wires sintered in range of 700 and 800 °C for 1 hour increases with enhancement of annealing temperature. Annealing temperature of 850 °C (for 1 hour) is higher than optimum for the MF wires having superconducting filament with about 150 µm diameter as shown in Figure 6.39 and 6.40. While, their resistivity values differ between 2 µΩ.cm and 4.3 µΩ.cm, transition temperatures are between 31 K and 36 K for all sintering temperatures.

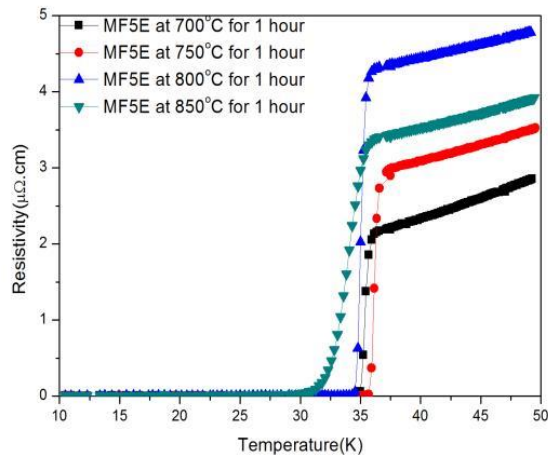


Figure 6.39. Resistivity vs temperature curves of MgB_2/Fe 18+1 in-situ filamentary wire sample for the first set sintered at different temperatures.

Transition temperature values of the whole studied wires are approximately same (between 34.5 K and 35.5 K) except for the wire sintered at 850 °C for 1 hour and normal state resistivity values just above transition range between 2 $\mu\Omega\cdot\text{cm}$ and 4.5 $\mu\Omega\cdot\text{cm}$ for all samples as seen Figure 6.40. Sintering temperature is more effective on normal state resistivity than sintering time.

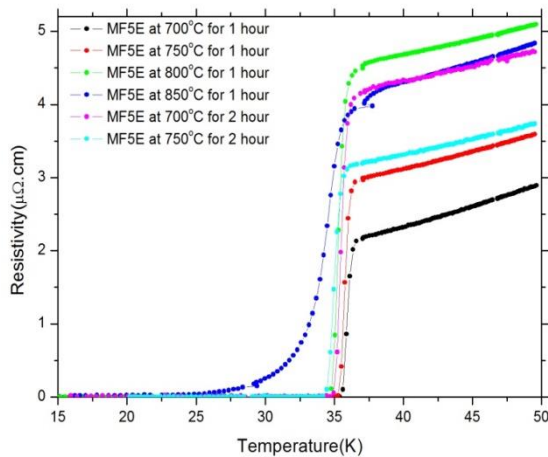


Figure 6.40. Resistivity vs temperature curves of MgB_2/Fe 18+1 in-situ filamentary wire samples for the second set sintered at different temperatures for 1 and 2 hours heat treatment durations.

Figure 6.41 shows the critical current values taken at constant temperatures 0.5 K – 1 K below T_c for the studied MF wires. Annealing temperature between 700

and 800 °C for 1 hour is more suitable. The wire samples annealed in range of 700-800 °C for 2 hours are not very bad. Critical current value is the most important parameter of MgB₂ superconducting wires for racetrack coil production, in this respect sintering at 850 °C for 1 hour is detrimental. Briefly, the most useful temperatures for MgB₂/Fe (18+1) wires which have 1.00 mm outer diameter are 700 and 750 °C for duration of 1 hour in terms of transport superconducting properties.

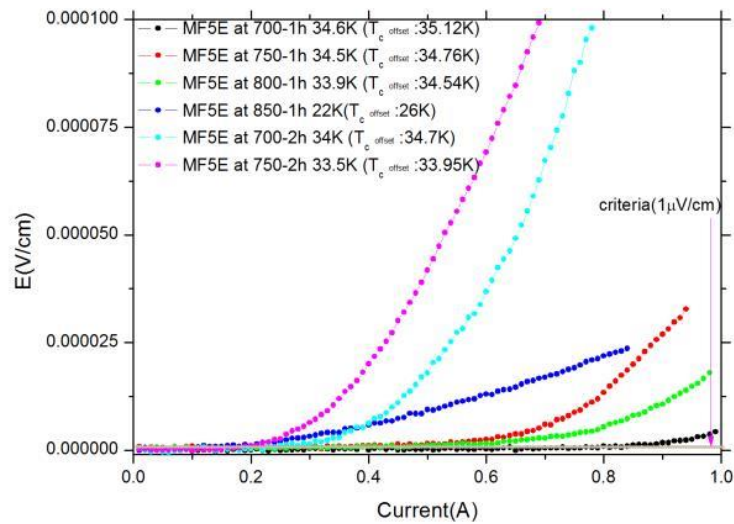


Figure 6.41. Current vs voltage curves of second set in-situ MgB₂/Fe 18+1 filamentary wires at a constant temperature slightly below their $T_{c,offset}$.

In Figure 6.42 (a) and (b), the polished and fracture cross sectional surface (fcs) of the best MgB₂/Fe MF wires can be clearly seen with perfect geometrical arrangement of filaments. In addition, the MgB₂/Fe (18+1) wires are produced with good morphological structure and superconducting properties at temperatures lower than 800 °C. The samples with better grain connectivity were produced by sintering at 700°C-750 °C for 1 hour as seen in Figure 6.42 (c) and (d).

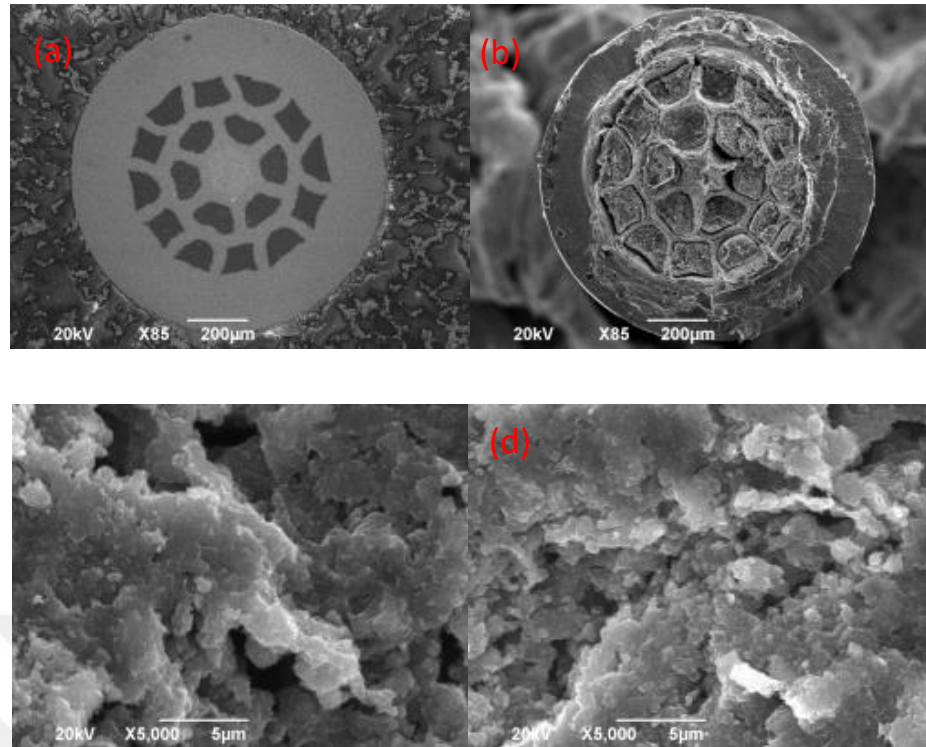


Figure 6.42 (a) Polished surface of MF5E at 700 °C/1h, (b) fcs of MF5E at 750°C/1h, (c) fcs MF5E 700 °C/1h and (d) MF5E 750 °C/1h in 5 μm scale.

6.6 Examination of Preliminary Coil Wound with In-situ Fe/MgB₂ Monocore Wire

R versus T graph was obtained by using fixed current contacts at the ends and 5 different voltage contacts as shown in Figure 6.43. MD, ML, LD, FL and FC codes in Figure 6.43 indicate different $R-T$ curves obtained by measuring the potential difference between different potential taps with various distances between each pair. MD and FC connections have the longest and shortest wire segments. $T_{c,offset}$ value of the monocore MgB₂/Fe coil for all voltage connections is 37.18 K with a $\Delta K=1.1$ K transition width. Normal state resistance depends on the distance between the potential taps and these values are compatible and changes from 2.4 mΩ to 21 mΩ as seen Figure 6.43.

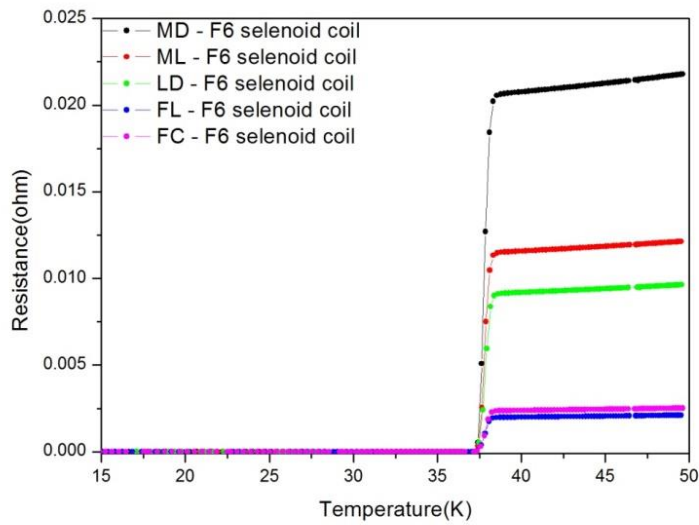


Figure 6.43. R vs T graph for various potential links on preliminary solenoid coil.

When we measure I_c values for potential taps pairs with longest or shortest distance in between in order to test the wire entirely, we haven't seen any significant difference between critical current values at 30 K under different applied external magnetic fields. In this experiment, the applied magnetic field was parallel to the axis of preliminary coil. While I_c value of the coil measured with FL contacts is 0.36 A under 2.5 T, I_c value of the coil measured with MD links is 0.38 A under 2.5 T as indicated in Figure 6.44 (a) and (b). Also, we can say that the coil carried higher current than 1 A under 2.30 T at 30 K.

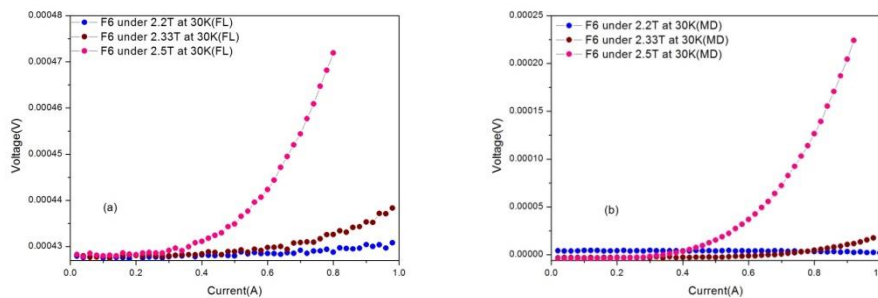


Figure 6.44. Current vs voltage graph for the solenoid coil with FL (a) and MD (b) voltage contacts under various applied magnetic fields.

Figure 6.45 shows current vs voltage curves of the preliminary coil when the potential taps are at FL. These measurements were performed at different

temperatures under different magnetic fields which were arranged in such a way that superconducting to normal transition due to transport current took place at or below 1 A. The preliminary coil carries a critical current of $I_c = 0.7$ A at 22 K under 7 T external magnetic field. These results constitute the evidence that these wires can be used below 5 T at *LH2* temperature (~ 20 K).

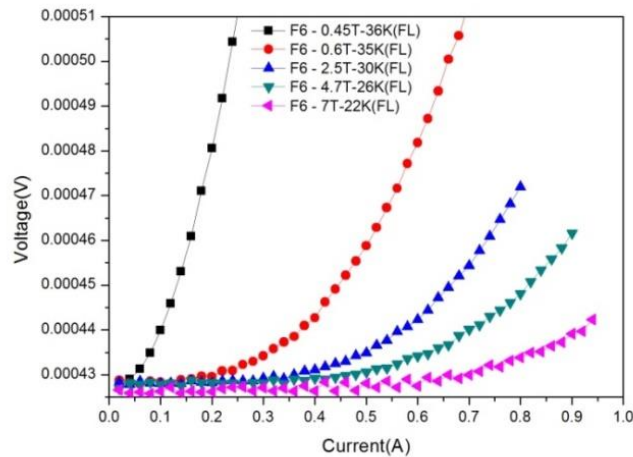


Figure 6.45. Transport I_c of the preliminary solenoid coil at different temperatures under different magnetic fields.

Figure 6.46 presents SEM images of bent and straight MgB_2/Fe monocoire wires. There is not any mechanical degradations or cracks and extra reaction layers when the polished longitudinal sections of the straight and bent MgB_2/Fe monocoire wires are examined. So, the MgB_2 wire 1.10 mm in diameter can be easily bent to diameters as small as 15 mm.

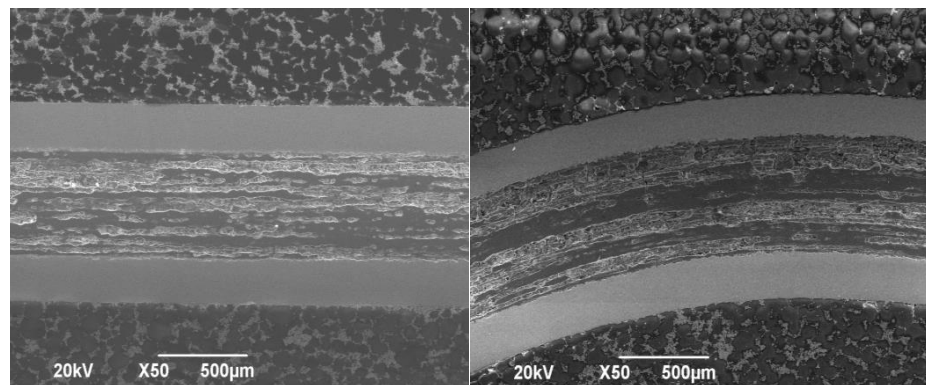


Figure 6.46. SEM images of the produced MgB_2/Fe monocoire wire for the solenoid preliminary coil before and after bending.

XRD patterns were taken from the MgB_2 powders obtained from the wire pieces of preliminary coil and shown in Figure 6.47. Most of the peaks in this XRD patterns are indexed to MgB_2 phase and some peaks belonging to Mg and MgO phases are also present in the pattern. For the wire sintered at 800 °C for 1 hour, peaks belonging to Fe_2B , FeB and FeB_2 phases do not appear on the XRD pattern in Figure 6.47 (Feng et al, 2003). This may be because sintering temperature is not high enough or sintering duration is not long enough (Grivel et al, 2006) or count rates for the peaks of these phases are inefficiently low. Peaks belonging to MgO impurity phases are clearly observed in the XRD patterns due to sensitiveness of Mg to oxygen which may come either during handling in air or sintering. Presence of Mg peaks in the xrd pattern may be a sign of incomplete reaction due to short sintering time at the studied temperature since there is not any sign of Mg peaks in the XRD patterns of the MgB_2 samples sintered at 850 and 900 °C for 1 hour as seen in Figure 6.29.

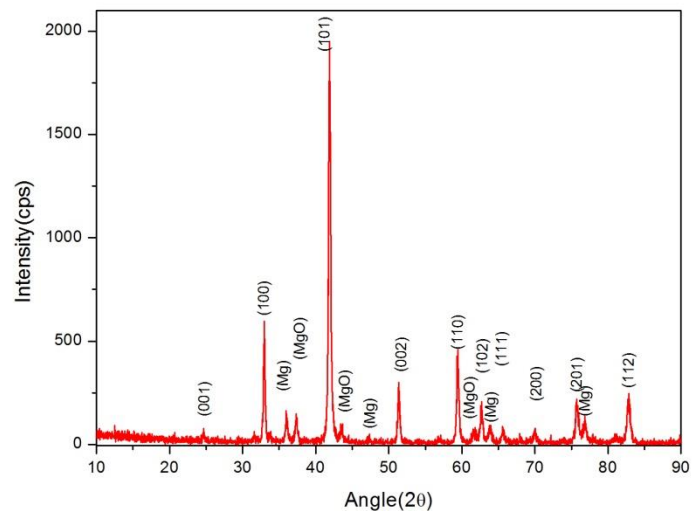


Figure 6.47. XRD taken from MgB_2/Fe monocore wire for the solenoid preliminary coil.

6.7 Bending test of In-situ Fe/MgB_2 Multifilamentary(18+1) wires

As an addition to section 6.5, effect of bending which is unavoidable in most applications of superconducting wires were investigated for the MgB_2/Fe (18+1)

wire with 1.00 mm diameter. Figure 6.48 shows resistance vs temperature behavior of straight and bent wire. Bending strain of the wire 1.00 mm in diameter after being bent to 35 mm radius was calculated as 1.41% using the formula given in (Thomas et al, 2012). T_c of straight and bent wires sintered at 700 °C for 1 hour are both 35.5 K. However, there is some difference in the normal state resistances of straight and bent wires, their normal state resistivities are 610 and 880 $\mu\Omega$, respectively. It may be said that resistance difference between the straight and bent wire can be also observed in wind and react process by depending on bending angle and the produced wire diameter when compared to react and wind process as seen in Figure 48 and Figure 6.52. But, bending angle is more dominant for React&Wind process in terms of superconducting properties of the wire.

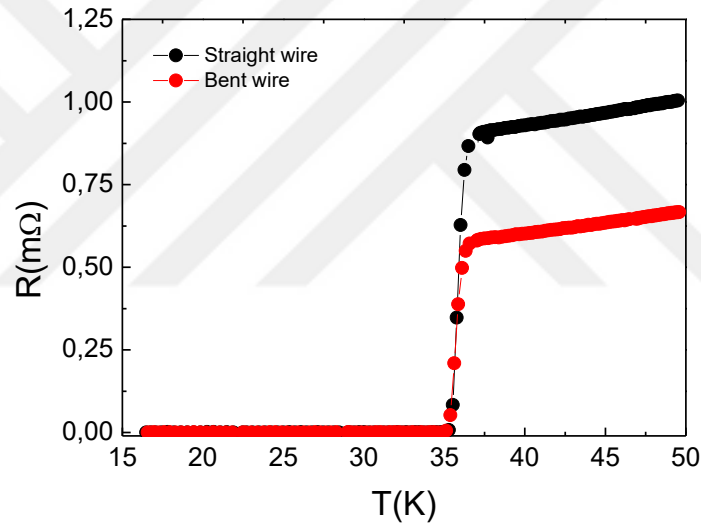


Figure 6.48. R vs T graph of straight (black) and 70 mm bent (red) F5 multifilamentary 1.00 mm in diameter annealed at 700 °C for 1 hour.

Figure 6.49 indicates that there is a small difference in I_c value at 22 K under external parallel magnetic field to the wires at 6 T for both wires. Critical current value of straight wire and bent wire are 0.40 A and 0.35 A at 22 K under 6 T, respectively. Considering these results, we may argue that no significant degradation occur in critical current of the in-situ MgB_2/Fe , when the bending of the wire is applied before sintering (Salama et al, 2005).

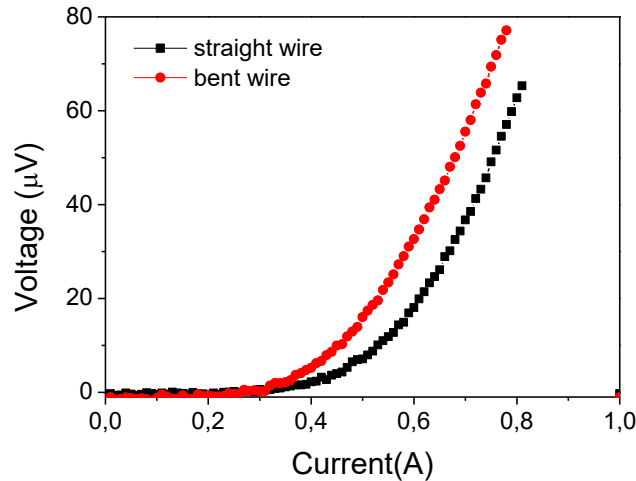


Figure 6.49. I_c values of F5 (18+1) filamentary straight (black) and 70 mm bent (red) wire with 1.00 mm diameter at 22 K under 6 T.

Longitudinal sections of the wires were polished after mounting then etched before SEM micrographs in Figure 6.50 were taken. As seen in these SEM images, bending strain has not caused any significant micro-cracks in the in-situ MgB_2/Fe wires and there is not any apparent interfacial reaction between the MgB_2 core and sheath material in both wires.

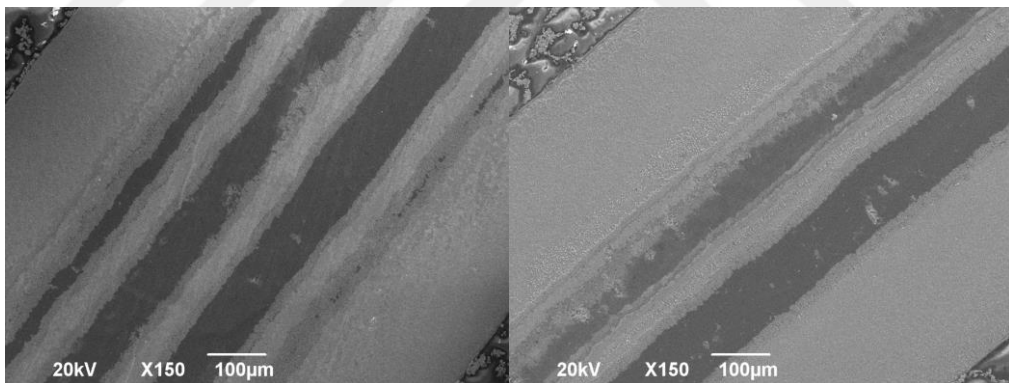


Figure 6.50. SEM images of the polished (a) three filaments of MgB_2/Fe (18+1) straight wire, (b) two upper filaments of 7 cm bent wire 1.00 mm in diameter.

Figure 6.51 and 6.52 indicate R vs T curves of the MgB_2/Fe (18+1) wires with 0.56 mm outer diameter bent to 70 mm and 50 mm diameters. Bending strain of the 0.56 mm diameter wire bent to these two diameters are calculated respectively as 0.8% and 1.11% by using the formula given in (Thomas et al, 2012). T_c of straight and bent wires sintered at 700 °C for 1 hour is almost same and about 34 K. Normal state resistance of straight and wire bent to 70 mm diameter is same and about 1.67

mΩ, normal state resistance of straight and wire bent to 50 mm diameter is little different 1.67 and 1.50 mΩ, respectively.

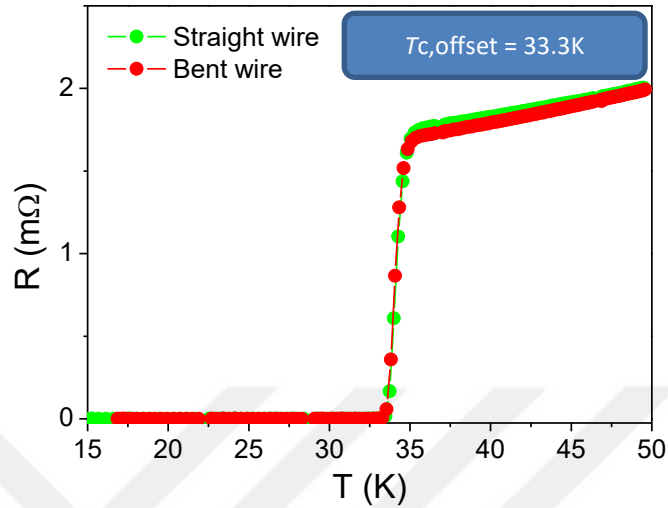


Figure 6.51. R - T graph of 0.56 mm (OD) MgB₂/Fe MF straight and bent to 70 mm wires

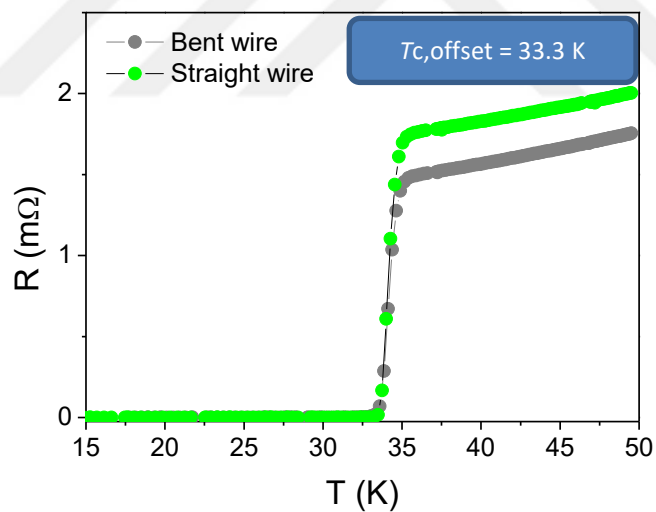


Figure 6.52. R - T graph of 0.56 mm (OD) MgB₂/Fe MF straight and bent to 50 mm wire

In Figure 6.53, we see that the bent wires have critical current value of 0.7 A under 3.5 T at 22 K and the straight wire has critical current value of 0.6 A under 4 T at 22 K. Also, the straight wire carries a current greater than 1 A under 3.5 T at 22 K. However, the bent wire 1.00 mm in diameter can carry a supercurrent up to 1 A at 6 T magnetic field and for bent wire with 0.56 mm diameter this magnetic field strength reduced to 3.5 T as compared both of Figure 6.49 and 6.53.

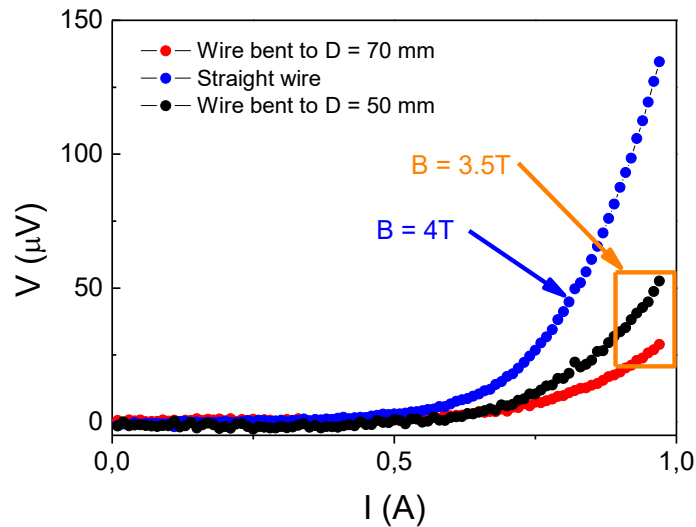


Figure 6.53. *I-V* graphs of 0.56 mm (OD) MgB_2/Fe MF straight, bent wires at 22 K under external magnetic field.

We have succeeded in producing MgB_2/Fe (18+1) wires having diameters as small as 0.56 mm with good morphological features by suitable intermediate strain relief annealings. Figure 6.54 (a) and (b) show the cross sectional pictures of SEM clearly revealing Fe sheath boundaries on polished cross section MgB_2/Fe MF wire. The MF wires have filaments with the sizes of 80 μm in diameter. We can see that each filament has fine pores and intersurface of Fe sheath materials belonging to monocoresh are not bonded at the studied sintering temperatures.

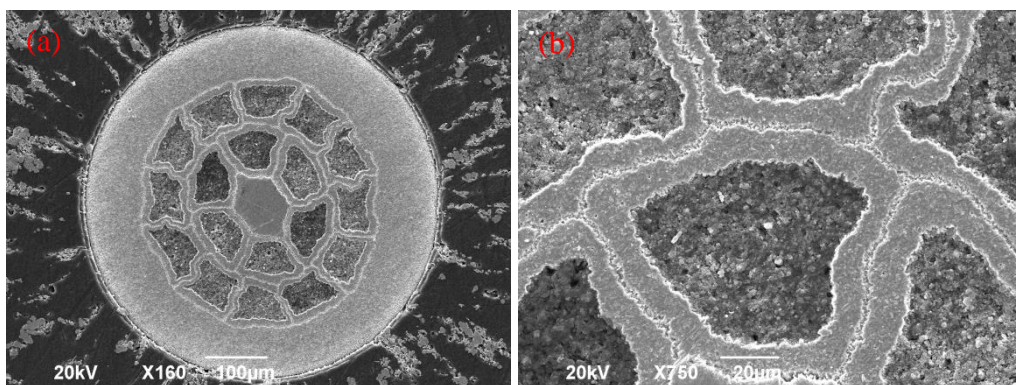


Figure 6.54. SEM images of polished and etched cross section of 0.56 mm (OD) MgB_2/Fe MF wire at two different magnifications.

Pores in MgB_2 core in monocoresh wires are much larger than the pores in these MF wires proving that Mg particles are further elongated during drawing of MF wires. These thin fibers of Mg leave a pore in the superconducting core when reacted with B to form MgB_2 .

6.8 Test of The Fabricated Racetrack Coils

In Figure 6.55, V - A curves belonging to the fabricated four racetrack coils are shown. The test was obtained at 4.2 K (LH) in ILHMFLT in Poland. Both of the racetrack coils were produced by MF Fe/MgB₂ wires such as the prepared MF6 (18+1) with F6 monocoil wires and the MF5D (8+1) by using F5 monocoil wires. The others were fabricated by monocoil Fe/MgB₂ wires such as the named F5D and F5B wires. F5D and F5B monocoil wires were obtained with different mixing and milling process of the same mixture powder. The F5B racetrack coil was sintered at 700 °C for 2 hours and the other coils were sintered at 700 °C for 1 hour under pure argon pressure 15 bars as shown in Figure 6.55. As a result, F5B and F5D racetrack coils carried on greater currents than 100 A and 150 A in self-field in LH, respectively. While MF6 racetrack coil has maximum transport current about 65 A, that of MF5D racetrack coil is about 50 A in self-field in LH.

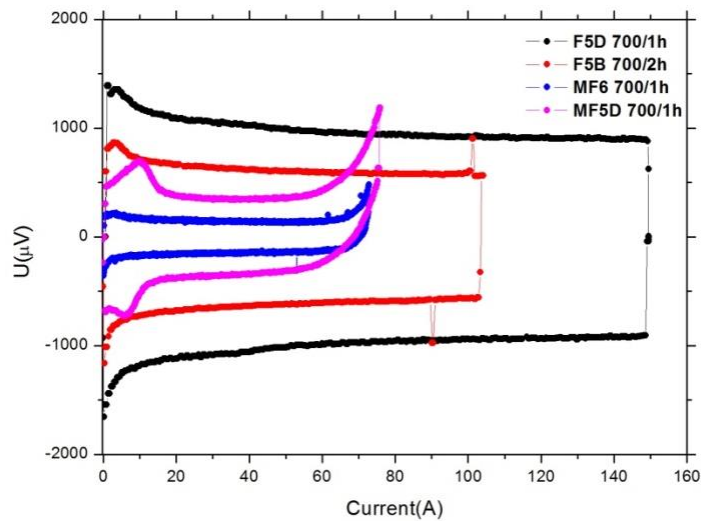


Figure 6.55. I - V curves at room temperature of the racetrack coil before (black) and after (red) sintering

Moreover, the produced magnetic field at the center of a racetrack (F5B) coil was measured in ILHMFLT in Poland. Potentiel value of the used hole sensor reached linearly to about 240 μ V with increase of the applied transport current. It means that 240 μ V equals to approximately 30 mT. That is, we saw that the F5B

racetrack coil carrying on a current of 90 A produced about 30 mT magnetic field at itself center in self-field in LH as indicated in Figure 6.56.

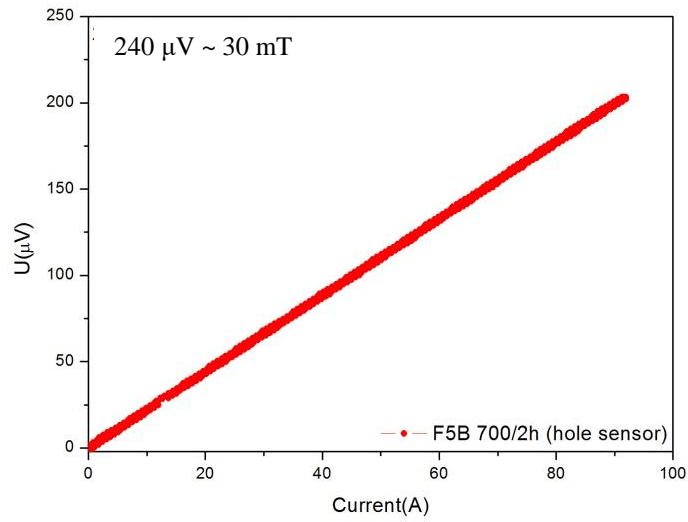


Figure 6.56. The measured magnetic field at the center of F5B racetrack coil

7. CONCLUSIONS

Our investigations show that MgB₂/Fe wires made with large grain sized boron and small grain sized boron, without chemical diffusion barrier and carbon or carbon related powder addition have good performance in terms of J_c . Although this process has several disadvantages such as large pores, large voids, diffusion of iron atoms, a small number of connections between the grains and large areas of unreacted Mg. When HIP is applied to the moncore MgB₂/Fe wires produced with same processes as above, we obtained smaller grains with more connections between grains, eliminated diffusion of iron atoms in to the superconducting core significantly and achieved the improved J_c values. Initially, we found that initial mass density of the filling has a direct influence on the I_c of the MgB₂ wires and increment of I_c (4.2 K) at $B = 5$ T from 40 A (2.8×10^3 A/cm²) to 140 A (9.8×10^3 A/cm²) was observed when the filling density was increased from 50% to 60% of theoretical mass density of Mg+2B. Diffusion of iron atoms into MgB₂ grains at the interface between materials usually reduces T_c , B_{irr} , B_{c2} and J_c . Even though Mg was in liquid state during the reaction process, the presence of large areas of pure Mg indicates decreased amount of MgB₂ phase in the sample. Because of these disadvantages, wires sintered in low pressure have limited possibility of application. HIP process improves the connections between the grains and reduces the amount of unreacted Mg indicating that it accelerates the formation of MgB₂ phase. We emphasize that improvement of T_c , J_c , B_{irr} , and B_{c2} properties of HIP processed wire is related with a increased number of connections between the grains, lack of diffused iron atoms and increased amount of MgB₂ phase. Application of HIP process permits to obtain Fe/MgB₂ wires from low cost boron powder with larger particle size and lower purity of 95 – 97 % and without using any high cost chemical barriers. HIP improves the transport properties of the moncore in-situ Fe/MgB₂ wire with 1.00 mm diameter at high applied magnetic fields. High pressure of 1.1 GPa significantly increases T_c in high magnetic fields. The mixture of amorphous boron and nano amorphous boron powders with 50-50% weight ratio has improved the magneto-transport properties of the iron clad moncore MgB₂ wires. It is also possible to improve transport properties further through different weight ratio values of amorphous boron and nano

amorphous boron powders. The monocoil in-situ Fe/MgB₂ wire has good transport properties (with $I_c > 150$ A at $B = 3$ T) at low and moderate applied magnetic fields. Application of excessive mechanical deformation on Fe-sheathed MgB₂ wire samples removes the internal voids and causes the formation of smaller grains and additional grain boundaries. This deformation leads to a fast degradation of J_{ce} and T_c values. Because, cracking of MgB₂ material with the mechanical deformation after sintering destroys the percolation paths for current flow. On the other hand, heat treatment after mechanical deformation re-joined the grain structure and highly improved the grain boundaries. Transport measurements reveal that the transport J_{ce} values of the tapes were increased to a certain extent, but not totally recovered in comparison to that obtained for initial Fe/MgB₂ wire. However, the use of lower sintering temperature and higher annealing temperature after pressing may produce fully dense tapes potentially applicable to superconducting coil fabrication. The monocoil MgB₂ wires are also very promising for a usage at *LH2* temperature and manufacturing a racetrack coil with low and middle magnetic field range. When we consider the MgB₂/Fe MF wires obtained by using the monocoil MgB₂ wires having high performance as mentioned above, MgB₂/Fe (18+1) in-situ Fe/MgB₂ wire with 1.00 mm diameter has better transport properties in comparison to those of the MgB₂/Fe (18+1) wire with 0.56 mm in diameter. Sintering at a temperature of 700 °C for 1 hour time duration are the most suitable for MF (18+1) 1.00 mm diameter wires to obtain good superconducting properties. Bending of the unreacted monocoil and MF wires does not cause any significant degradation in I_c values of the wires (Bend&React). In this thesis, cross-sectional appearance of monocoil MgB₂/Fe wires distribution of the filaments in MF Fe/MgB₂ wires could be obtained in a perfect manner in all wires with even smallest diameters and these wires carried large critical currents. Finally, four racetrack coils made with the produced superconducting MgB₂/Fe wires have been fabricated successfully. While MF6 and MF5D MF racetrack coils carried on current of about 65 A and 50 A, respectively, F5B and F5D racetrack coils have a transport current greater than 100 A and 150 A in LH (at 4.2 K), respectively. We measured that the F5B racetrack coil carrying a current of 90 A produced about 30 mT at its center at 4.2 K.

8. REFERENCES

Agatsuma K, Furuse M, Umeda M, Fuchino S, Lee WJ, Hur JM (2006) “Properties of MgB₂ Superconductor by Doping Impurity of SiC, Graphite, C-60, and C Nano-tube”, IEEE Transactions on Applied Superconductivity, 16(2):1407.

Akdoğan M, Yetiş H, Gajda D, Karaboğa F, Ülgen AT, Demirtürk E, Belenli İ (2015) “Effect of The Initial Filling Density on The Critical Current of In-situ Fe/MgB₂ Wires”, Journal of Alloys and Compounds, 649:1007.

An JM, Pickett WE (2001) “Superconductivity of MgB₂: Covalent Bonds Driven Metallic”, Physical Review Letters, 86(19):4366.

Bardeen J, Cooper LN, Schrieffer JR (1957) “Theory of Superconductivity”, Physical Review, 108(5):1175.

Barua S, Patel D, Alzayed N, Shahabuddin M, Parakkandy JM, Shah MS, Ma Z, Mustapić M, Al Hossain MS, Kim JH (2015) “Correlation Between In-Field *J_c* Enhancement and Grain Connectivity in Co-Doped MgB₂ Superconductor”, Materials Letters, 139:333.

Ban E, Sakaguchi R, Matsuoka Y, Goto T, Watanabe K, Nishijima G (2005) “Carbon Nanohorn Doping in MgB₂ Wire Prepared by Suspension Spinning”, Physica C: Superconductivity and Its Applications, 426:1249.

Bean CP (1962) “Magnetization of Hard Superconductors”, Physical Review Letters, 8(6):250.

Bohandy J, Kim BF, Phillips TE, Adrian FJ, Moorjani K (1990) U.S. Patent No. 4,904,929., Trademark Office, Washington, DC: U.S.

Bordet P, Mezouar M, Nunez-Regueiro M, Monteverde M, Nunez-Regueiro MD, Rogado N, Regan KA, Hayward MA, He T, Loureiro SM, Cava RJ (2001) “Absence of A Structural Transition up to 40 GPa in MgB₂ and The Relevance of Magnesium Nonstoichiometry”, Physical Review B, 64(17):172502.

Bray JW (2009) “Superconductors in Applications; Some Practical Aspects”, IEEE Transactions on Applied Superconductivity, 19(3):2533.

Braccini V, Nardelli D, Penco R, Grasso G (2007) “Development of Ex-situ Processed MgB₂ Wires and Their Applications to Magnets”, Physica C: Superconductivity, 456(1):209.

Braccini V, Gurevich A, Giencke JE, Jewell MC, Eom CB, Larbalestier DC, Pogrebnikov A, Cui Y, Liu BT, Hu YF, Redwing JM, Li Q, Xi XX, Singh RK, Gandikota R, Kim J, Wilkens B, Newman N, Rowell J, Moeckly B, Ferrando V, Tarantini C, Marre D, Putti M, Ferdeghini C, Vaglio R, Haanappel E (2005) “High-

Field Superconductivity in Alloyed MgB_2 Thin Films”, *Physical Review B*, 71(1):012504.

Bud’ko SL, Canfield PC, Kogan VG (2002) “Magnesium Diboride: Basic Physical Properties and High Upper Critical Field Anisotropy”, *Physica C: Superconductivity*, 382(1):85.

Bud’Ko SL, Lapertot G, Petrovic C, Cunningham CE, Anderson N, Canfield PC (2001a) “Boron Isotope Effect in Superconducting MgB_2 ”, *Physical Review Letters*, 86(9):1877.

Bud’Ko SL, Petrovic C, Lapertot G, Cunningham CE, Canfield PC, Jung MH, Lacerda AH (2001b) “Magnetoresistivity and $H_{c2}(T)$ in MgB_2 ”, *Physical Review B*, 63(22):220503.

Burdusel M, Aldica G, Popa S, Enculescu M, Badica P (2012) “ MgB_2 with Addition of Sb_2O_3 Obtained by Spark Plasma Sintering Technique”, *Journal of Materials Science*, 47(8):3828.

Buzea C, Yamashita T (2001) “Review of The Superconducting Properties of MgB_2 ”, *Superconductor Science and Technology*, 14(11):R115.

Canfield PC, Bud’ko SL, Finnemore DK (2003) “An Overview of The Basic Physical Properties of MgB_2 ”, *Physica C: Superconductivity*, 385(1):1-7.

Canfield PC, Finnemore DK, Bud’Ko SL, Ostenson JE, Lapertot G, Cunningham CE, Petrovic C (2001) “Superconductivity in Dense MgB_2 Wires”, *Physical Review Letters*, 86(11):2423.

Cetner T, Morawski A, Adamczyk K, Rindfleisch M, Tomsic M, Zaleski A, Gajda D, Presz A (2012) “Improvement of Critical Properties of Undoped, Multifilamentary MgB_2 Wires in Nb/Cu After Annealing Under High Gas Pressure”, *High Pressure Research*, 32(3):419.

Cetner T, Morawski A, Gajda D, Häßler W, Rindfleisch M, Tomsic M, Zaleski A, Czujko T, Żuchowska E, Przysłupski P (2015) “Hot Isostatic Pressing of Multifilamentary MgB_2 Wires in Solid State Media for Large Scale Application”, *Superconductor Science and Technology*, 28(4):045009.

Chen SK, MacManus-Driscoll JL (2009) “Enhanced Critical Current Densities in MgB_2 by Mixing Relatively Impure Boron Powders”, *Superconductor Science and Technology*, 22(6):065009.

Chen SK, Wei M, MacManus-Driscoll JL (2006) “Strong Pinning Enhancement in MgB_2 Using Very Small Dy_2O_3 Additions”, *Applied Physics Letters*, 88:92512.

Chen SK, Tan KS, Glowacki BA, Yeoh WK, Soltanian S, Horvat J, Dou SX (2005) “Effect of Heating Rates on Superconducting Properties of Pure MgB_2 , Carbon Nanotube and Nano-SiC Doped In-situ MgB_2/Fe wires”, *Applied Physics Letters*, 87:182504.

Chen Y, Yang C, Jia C, Feng Q, Gan Z (2016) “Thickness Dependence of $J_c(0)$ in MgB_2 Films”, *Physica C: Superconductivity and Its Applications*, 525:56.

Cheng C, Zhao Y (2006) “Enhancement of Critical Current Density of MgB_2 by Doping Ho_2O_3 ”, *Applied Physics Letters*, 89(25):2501.

Cheng CH, Zhang H, Zhao Y, Feng Y, Rui XF, Munroe P, Zeng HM, Koshizuka N, Murakami M (2003) “Doping Effect of Nano-diamond on Superconductivity and Flux Pinning in MgB_2 ”, *Superconductor Science and Technology*, 16(10):1182.

Collings EW, Lee E, Sumption MD, Tomsic M, Wang XL, Soltanian S, Dou SX (2003) “Continuous and Batch-Processed MgB_2/Fe Strands Transport and Magnetic Properties”, *Physica C: Superconductivity*, 386:555.

Collings EW, Sumption MD, Bhatia M, Susner MA, Bohnenstiehl SD (2008) “Prospects for Improving The Intrinsic and Extrinsic Properties of Magnesium Diboride Superconducting Strands”, *Superconductor Science and Technology*, 21(10):103001.

Collins J (2008) “Letter From The Editor: The History of MRI”, In *Seminars in Roentgenology*, 43(4):259.

Cullity BD (2001) *Element of X-ray Diffraction*, 3rd Edition, Reading MA., Wesley.

Da Silva LB, Vianna AA, Manesco AL, Hellstrom EE, Rodrigues D (2016) “The Influence of Stearic Acid Addition on The Superconducting Properties of MgB_2 ”, *IEEE Transactions on Applied Superconductivity*, 26(3):1.

Da Silva LBS, Serrano G, Serquis A, Metzner VCV, Rodrigues Jr D (2015) “Study of TaB_2 and SiC Additions on The Properties of MgB_2 Superconducting Bulks”, *Superconductor Science and Technology*, 28(2):025008.

De Silva KSB, Xu X, Gambhir S, Wang XL, Li WX, Wallace GG, Dou SX (2011) “Flux Pinning Mechanisms in Graphene Doped MgB_2 Superconductors”, *Scripta Materialia*, 65(7):634.

Dew-Hughes D (2001) “The Critical Current of Superconductors: An Historical Review”, *Low Temperature Physics*, 27(9):713.

Dhallé M, Toulemonde P, Beneduce C, Musolino N, Decroux M, Flükiger R (2001) “Transport and Inductive Critical Current Densities in Superconducting MgB_2 ”, *Physica C: Superconductivity*, 363(3):155.

Dou SX, Horvat J, Soltanian S, Wang XL, Qin MJ, Zhou SH, Liu HK, Munroe PG (2003a) “Transport Critical Current Density in Fe-sheathed Nano- SiC Doped MgB_2 Wires”, *IEEE Transactions on Applied Superconductivity*, 13(2):3199.

Dou SX, Shcherbakova O, Yeoh WK, Kim JH, Soltanian S, Wang XL, Senatore C, Flukiger R, Dhalle M, Husnjak O, Babic E (2007) “Mechanism of Enhancement in

Electromagnetic Properties of MgB₂ by Nano SiC Doping”, Physical Review Letters, 98(9):097002.

Dou SX, Soltanian S, Horvat J, Wang XL, Munroe P, Zhou SH, Lonescu M, Liu HK, Tomsic M (2002) “Enhancement of The Critical Current Density and Flux Pinning of MgB₂ Superconductor by Nanoparticle SiC Doping”, Applied Physics Letters, 81:3419.

Dou SX, Yeoh WK, Horvat J, Ionescu M (2003b) “Effect of Carbon Nanotube Doping on Critical Current Density of MgB₂ Superconductor”, Applied Physics Letters 83:24.

Dunanda DC (2001) “Synthesis of Superconducting Mg/MgB₂ Composites”, Applied Physics Letters, 79(25):4186.

Edelson E (1973) “How Scientists Are Detecting Cancer With Supermagnets”, Popular Science, 202 (3):99.

Egilmez M, Ozyuzer L, Tanoglu M, Okur S, Kamer O, Oner Y (2006) “Electrical and Mechanical Properties of Superconducting MgB₂/Mg Metal Matrix Composites”, Superconductor Science and Technology, 19(4):359.

Eisterer M, Glowacki BA, Weber HW, Greenwood LR, Majoros M (2002) “Enhanced Transport Currents in Cu Sheathed MgB₂ Wires”, Superconductor Science and Technology, 15(7):1088.

Eisterer M, Schoppl KR, Weber HW, Sumption MD, Bhatia M (2007) “Neutron Irradiation of SiC Doped and Magnesium Rich MgB₂ Wires”, IEEE Transactions on Applied Superconductivity, 17(2):2814.

Feng Y, Yan G, Zhao Y, Wu XJ, Pradhan AK, Zhang X, Liu CF, Liu XH, Zhou L (2003) “High Critical Current Density in MgB₂/Fe Wires”. Superconductor Science and Technology, 16(6):682.

Feng Y, Zhao Y, Pradhan AK, Cheng CH, Yau J, Zhou L, Koshinzuka N, Murakami M (2002), “Enhanced Flux Pinning in Zr Doped MgB₂ bulk Superconductors Prepared at Ambient Pressure”, Journal of Applied Physics, 92(5):2614.

Fischer C, Rodig C, Häbeler W, Perner O, Eckert J, Nenkov K, Fuchs G, Wendrock H, Holzapfel B, Schultz L (2003) “Preparation of MgB₂ Tapes Using a Nanocrystalline Partially Reacted Precursor”, Applied Physics Letters, 83:1803.

Flukiger R, Al Hossain MS, Senatore C, Buta F, Rindfleisch M (2011) “A New Generation of In-situ Wires With Improved and Values Obtained by Cold Densification (CHPD)”, IEEE Transactions on Applied Superconductivity, 21(3):2649.

Flukiger R, Hossain MSA, Senatore C (2009) “Strong Enhancement of J_c and B_{irr} in Binary In-situ MgB₂ Wires after Cold High Pressure Densification”, Superconductor Science and Technology, 22(8):085002.

Flukiger R, Lezza P, Beneduce C, Musolino N, Suo HL (2003) “Improved Transport Critical Current and Irreversibility Fields in Mono- and Multifilamentary Fe/MgB₂ Tapes and Wires Using Fine Powders”, *Superconductor Science and Technology*, 16:264.

Ford PJ, Saunders GA (2005) *The Rise of The Superconductors*, CRC Press, United States of America.

Fu BQ, Feng Y, Yan G, Liu CF, Zhou L, Cao LZ, Ruan KQ, Li XG (2003) “High Transport Critical Current in MgB₂/Fe Wire by In-situ Powder-in-tube Process”, *Physica C: Superconductivity*, 392:1035.

Fuchs G, Müller KH, Handstein A, Nenkov K, Narozhnyi VN, Eckert D, Wolf M, Schultz L (2001) “Upper Critical Field and Irreversibility Line in Superconducting MgB₂”, *Solid state communications*, 118(10):497.

Fujii H, Kumakura H, Togano K (2002) “Improved Critical Current in MgB₂ Tapes Sheathed With Carbon Steels”, *Journal of Materials Research*, 17(09):2339-2345.

Fujii H, Ozawa K, Kitaguchi H (2014) “The Effect of Refinement of Carbon-Substituted MgB₂ Filling Powder Using Various Starting Powders on The Microstructure and Critical Current Density of Ex-situ Processed Superconducting Tapes”, *Superconductor Science and Technology*, 27(3):035002.

Fujii H, Togano K, Kumakura H (2002) “Enhancement of Critical Current Densities of Powder-in-tube Processed MgB₂ Tapes by Using MgH₂ as a Precursor Powder”, *Superconductor Science and Technology*, 15:1571.

Gajda D, Morawski A, Zaleski A, Cetner T, Małeczka M, Presz A, Rindfleisch M, Tomsic M, Thong CJ, Surdacki P (2013) “Comparison of Critical Current Density in SiC-Doped In-situ MgB₂ Coils and Straight Wire Samples Processed by HIP”, *Superconductor Science and Technology*, 26(11):115002.

Gajda D, Morawski A, Zaleski A, Kurnatowska M, Cetner T, Gajda G, Presz A, Rindfleisch M, Tomsic M (2014) “The Influence of HIP on The Homogeneity, J_c , B_{irr} , T_c and F_p in MgB₂ Wires”, *Superconductor Science and Technology*, 28(1):015002.

Gao Z, Ma Y, Zhang X, Wang D, Yang H, Wen H, Watanabe K (2007a) “Influence of Sintering Temperature on The Superconducting Properties of Zn-Stearate-Doped MgB₂ Tapes”, *Superconductor Science and Technology*, 21(1):015016.

Gao Z, Ma Y, Zhang X, Wang D, Yu Z, Watanabe K, Yang H, Wen H (2007b) “Strongly Enhanced Critical Current Density in MgB₂/Fe Tapes by Stearic Acid and Stearate Doping”, *Superconductor Science and Technology*, 20(5):485.

Gao Z, Ma Y, Zhang X, Wang D, Yu Z, Yang H, Wen H, Mossang E (2007c) “Enhancement of The Critical Current Density and The Irreversibility Field in Maleic Anhydride Doped MgB₂ Based Tapes”, *Journal of Applied Physics*, 102(1):013914.

Geng HF, Liu FS (2013) “Microstructures of Ti–Ni–Fe Wire After Severe Cold-Drawing and Annealing”, *Rare Metals*, 32(6):550.

Giri R, Tiwari RS, Srivastava ON (2007) “Influence of Simultaneous Doping of Sb and Pb on Phase Formation, Superconducting and Microstructural Characteristics of $\text{HgBa}_2\text{Ca}_2\text{Cu}_3\text{O}_{8+\delta}$ ”, *Physica C: Superconductivity*, 451(1):1.

Giunchi G (2003a) “High density MgB_2 obtained by reactive liquid Mg infiltration”, *International Journal of Modern Physics B*, 17(04n06):453.

Giunchi G, Ceresara S, Ripamonti G, Di Zenobio A, Rossi S, Chiarelli S, Spadoni M, Wesche R, Bruzzone PL (2003b) “High Performance New MgB_2 Superconducting Hollow Wires”, *Superconductor Science and Technology*, 16(2):285.

Glowacki BA, Majoros M (2001a) *Studies of Superconductors (Advances in Research and Applications)*, MgB_2 , ed A Narlikar (Huntington, NY: Nova), 38:361.

Glowacki BA, Majoros M, Vickers M, Evetts JE, Shi Y, McDougall I (2001b) “Superconductivity of Powder-in-tube MgB_2 Wires”, *Superconductor Science and Technology*, 14(4):193.

Goldacker W, Schlachter SI, Zimmer S, Reiner H (2001) “High Transport Currents in Mechanically Reinforced MgB_2 Wires”, *Superconductor Science and Technology*, 14(9):787.

Goto D, Machi T, Zhao Y, Koshizuka N, Murakami M, Arai S (2003) “Improvement of Critical Current Density in MgB_2 by Ti, Zr and Hf Doping”, *Physica C: Superconductivity*, 392:272-275.

Grivel JC, Andersen NH, Pinholt R, Kovác P, Hušek I, Hässler W, Herrmann M, Perner O, Rodig C, Homeyer J (2006) “In-situ Studies of Fe_2B Phase Formation in MgB_2 Wires and Tapes by Means of High-Energy X-ray Diffraction”, *Journal of Physics: Conference Series*, 43:123–126.

Grivel JC, Namazkar S, Alexiou A, Holte OJ (2014) “Preparation and Characterisation of Os Doped MgB_2 ”. *Physica C: Superconductivity and Its Applications*, 507:70-74.

Grovenor CRM, Goodsir L, Salter CJ, Kovac P, Husek I (2004) “Interfacial Reactions and Oxygen Distribution in MgB_2 Wires in Fe, stainless steel and Nb sheaths”, *Superconductor Science and Technology* 17:479.

Gurevich A (2003) “Enhancement of The Upper Critical Field by Nonmagnetic Impurities in Dirty Two-Gap Superconductors”, *Physical Review B*, 67(18):184515.

Han G, Wang Y, Han H, Wang Z, Wang S, Yuan W, Huang Q, Liu Z, Chen J (1993) “Transport Critical Current and Voltage-Current Characteristics of Bi (2223) Silver-Clamped Thick Films”, *Applied Physics A*, 57(4):363.

Handstein A, Hinz D, Fuchs G, Müller KH, Nenkov K, Gutfleisch O, Narozhnyi VN, Schultz L (2001) “Fully Dense MgB₂ Superconductor Textured by Hot Deformation”, Journal of Alloys and Compounds, 329(1):285-289.

Hata S, Yoshidome T, Sosiati H, Tomokiyo Y, Kuwano N, Matsumoto A, Kitaguchi H, Kumakura H (2006) “Microstructures of MgB₂/Fe Tapes Fabricated by an In-situ Powder-in-tube Method Using MgH₂ as a Precursor Powder”, Superconductor Science and Technology, 19(2):161.

Hinks DG, Claus H, Jorgensen JD (2001) “The Reduced Total Isotope Effect and Its Implications on The Nature of Superconductivity in MgB₂”, Nature, 411:457.

Hossain MSA, Motaman A, Çiçek Ö, Ağıl H, Ertekin E, Gencer A, Wang XL, Dou SX (2012) “The Effects of Annealing Temperature on The in-Field J_c and Surface Pinning in Silicone Oil Doped MgB₂ Bulks and Wires”, Cryogenics, 52(12):755.

Hossain MSA, Senatore C, Rindfleisch MA, Tomsic MJ, Kim JH, Dou SX (2009) “The Enhanced J_c and B_{irr} of In-situ MgB₂ Wires and Tapes Alloyed With C₄H₆O₅ (Malic Acid) After Cold High Pressure Densification”, Superconductor Science and Technology, 22(9):095004.

Hwang SM, Sung K, Choi JH, Kim W, Joo J, Lim JH, Kim CJ, Park YS, Kim DH, (2010) “O-Free Polyacrylonitrile Doping to Improve the $J_c(B)$ and H_{c2} of MgB₂ Wires”, Physica C: Superconductivity, 470(20): 1430.

Hull JR (2003) “Applications of High-Temperature Superconductors in Power Technology”, Reports on Progress in Physics, 66(11):1865.

Hur JM, Togano K, Matsumoto A, Kumakura H, Wada H, Kimura K (2008) “Fabrication of High-Performance MgB₂ Wires by an Internal Mg Diffusion Process”, Superconductor Science and Technology, 21(3):032001.

HyperTech Research, Incorporation (2008) Superconductors for Medical and Energy Products, www.hypertechresearch.com/page4.html, USA, (01, 09, 2016).

Jin S, Mavoori H, Bower C, Van Dover RB (2001) “High Critical Currents in Iron-Clad Superconducting MgB₂ Wires”, Nature, 411(6837):563.

Jiang CH, Kumakura H (2007) “Stoichiometry Dependence of The Critical Current Density in Pure and Nano-SiC Doped MgB₂/Fe Tapes”, Physica C: Superconductivity, 451(1):71-76.

Jiang CH, Nakane T, Kumakura H (2005) “Enhanced J_c - B Performance in MgB₂/Fe Tapes with Nanometre Si₃N₄ Addition”, Superconductor Science and Technology, 18(6):902.

Jiang J, Senkowicz BJ, Larbalestier DC, Hellstrom EE (2006) “Influence of Boron Powder Purification on The Connectivity of Bulk MgB₂”, Superconductor Science and Technology, 19(8):L33.

Jones ME, Marsh RE (1954) “The Preparation and Structure of Magnesium Boride, MgB₂”, *Journal of the American Chemical Society*, 76(5):1434.

Jun BH, Kim JH, Kim CJ, Choo KN (2015) “Improved Transport Critical Current Properties in Glycerin-Doped MgB₂ Wire Using Milled Boron Powder and a Solid-State Reaction of 600 °C”, *Journal of Alloys and Compounds*, 650:794.

Jung MH, Jaime M, Lacerda AH, Boebinger GS, Kang WN, Kim HJ, Choi EM, Lee SI (2001) “Anisotropic Superconductivity in Epitaxial MgB₂ Films”, *Chemical Physics Letters*, 343(5):447-451.

Kambara M, Babu NH, Sadki ES, Cooper JR, Minami H, Cardwell DA, Campbell AM, Inoue IH (2001) “High Intergranular Critical Currents in Metallic MgB₂ Superconductor”, *Superconductor Science and Technology*, 14(4):L5.

Kario A, Morawski A, Häbler W, Nenkov K, Schubert M, Herrmann M, Ringsdorf B, Schlachter SI, Goldacker W, Holzapfel B, Schultz L (2010) “Ex-situ MgB₂ Barrier Behavior of Monofilament In-situ MgB₂ Wires with Glidcop® Sheath Material”, *Superconductor Science and Technology*, 23(11):115007.

Kim KH, Kang WN, Kim MS, Jung CU, Kim HJ, Choi EM, Park MS, Lee SI (2001) “Origin of the High DC Transport Critical Current Density for the MgB₂ Superconductor”, 0103176.

Kim JH, Zhou S, Hossain MS, Pan AV, Dou SX (2006) “Carbohydrate Doping to Enhance Electromagnetic Properties of MgB₂ Superconductors”, *Applied Physics Letters*, 89(14):142505.

Kortus J (2007) “Current Progress in the Theoretical Understanding of MgB₂”, *Physica C: Superconductivity*, 456(1):54.

Kortus J, Mazin II, Belashchenko KD, Antropov VP, Boyer LL (2001) “Superconductivity of Metallic Boron in MgB₂”, *Physical Review Letters*, 86(20):4656.

Kováč P, Hušek I, Melišek T, Martínez E, Dhalle M (2006) “Properties of Doped Ex- and In-situ MgB₂ Multifilament Superconductors”, *Superconductor Science and Technology*, 19(10):1076.

Kovac P, Husek I, Melisek T, Strbik V (2005) “Basic Properties of Rectangular MgB₂/FeNiCo and MgB₂/Fe Wires Made In-situ”, *Superconductor Science and Technology*, 18:856.

Kováč P, Hušek I, Pachla W, Kulczyk M, Melišek T, Dvorak T (2011) “As-Deformed Filament's Density and Transport Currents of MgB₂/Ti/Glidcop Wire”, *Journal of Alloys and Compounds*, 509(35):8783.

Kováč J, Šouc J, Kováč P, Hušek I (2014) “Magnetization AC Losses in MgB₂ Wires Made by IMD Process”, *Superconductor Science and Technology*, 28(1):015013.

Kumakura H, Hur J, Togano K, Matsumoto A, Wada H, Kimura K (2011) "Superconducting Properties of Diffusion-Processed Multifilamentary Wires", IEEE Transactions on Applied Superconductivity, 21(3):2643.

Kumakura H, Matsumoto A, Fujii H, Togano K (2001) "High Transport Critical Current Density Obtained for powder-in-tube Processed MgB₂ Tapes and Wires Using Stainless Steel and Cu-Ni Tubes", Applied Physics Letter, 79:2435.

Kumakura H, Kitaguchi H, Matsumoto A, Yamada H (2005) "Upper Critical Field, Irreversibility Field, and Critical Current Density of Powder-in-tube Processed MgB₂/Fe Tapes", Superconductor Science and Technology, 18(8):1042.

Kumakura H, Matsumoto A, Nakane T, Kitaguchi H (2007) "Fabrication and Properties of Powder-in-tube Processed MgB₂ Tape Conductors", Physica C: Superconductivity, 456(1):196.

Kumar RA, Vinod K, Varghese N, Syamaprasad U, Roy SB (2007) "Reactivity of Sheath Materials with Mg/B in MgB₂ Conductor Fabrication", Superconductor Science and Technology, 20(3):222.

Kuroda T, Nakane T, Kumakura H (2009) "Effects of Doping With Nanoscale Co₃O₄ Particles on The Superconducting Properties of Powder-in-tube Processed MgB₂ Tapes", Physica C: Superconductivity, 469(1):9.

Larbalestier DC, Cooley LD, Rikel MO, Polyanskii AA, Jiang J, Patnaik S, Cai XY, Feldman DM, Gurevich A, Squitieri AA, Naus MT, Eom CB, Hellstrom EE, Cava RJ, Regan KA, Rogado N, Hayward MA, He T, Slusky JS, Khalifah P, Inumaru K, Haas M (2001) "Strongly Linked Current Flow in Polycrystalline Forms of The Superconductor MgB₂", Nature, 410(6825):186.

Lee CM, Lee SM, Park GC, Joo J, Lim JH, Kang WN, Yi JH, Jun BH, Kim CJ (2010) "Investigation of Lauric Acid Dopant as a Novel Carbon Source in MgB₂ Wire", Physica C: Superconductivity, 470(20):1438.

Li XH, Du XJ, Qiu M, Ma YW, Xiao LY (2007) "Design and Experimental demonstration of an MgB₂ based 1.5 T MRI Test Magnet "Physica C, 463:1338.

Li WX, Zeng R, Wang JL, Li Y, Dou SX (2012) "Dependence of Magnetoelectric Properties on Sintering Temperature for Nano-SiC-Doped MgB₂/Fe Wires Made by Combined In-situ/Ex-situ Process", Journal of Applied Physics, 111(7):07E135.

Lorenz B, Meng RL, Chu CW (2001) "High Pressure Study on MgB₂". Physical Review B, 64(1):012507.

Ma Y, Kumakura H, Matsumoto A, Hatakeyama H, Togano K (2003) "Improvement of Critical Current Density in Fe-Sheathed MgB₂ Tapes by ZrSi₂, ZrB₂ and WSi₂ Doping", Superconductor Science and Technology, 16(8):852.

Ma Y, Kumakura H, Matsumoto A, Takeya H, Togano K (2004) “Superconducting Properties of Powder-in-tube MgB₂ Tapes Without and With WSi₂ Addition”, *Physica C: Superconductivity*, 408:138.

Ma Z, Liu Y, Gao Z (2010) “The Synthesis and Grain Connectivity of Lamellar MgB₂ Grains by Cu-Activated Sintering at Low Temperature”, *Scripta Materialia*, 63(4):399.

Ma Z, Liu Y, Hu W, Gao Z, Yu L, Dong Z (2009) “The Enhancement of J_c in Nano SiC-Doped MgB₂ Superconductors Rapidly Synthesized by Activated Sintering at Low Temperature”, *Scripta Materialia*, 61(8):836.

Malagoli A, Braccini V, Bernini C, Romano G, Vignolo M, Putti M, Ferdeghini C (2010) “Study of The MgB₂ Grain Size Role in Ex-situ Multifilamentary Wires With Thin Filaments”, *Superconductor Science and Technology*, 23(2):025032.

Malagoli A, Braccini V, Scati N, Roncallo S, Siri AS, Grasso G (2002) “Fabrication and Superconducting Properties of Powder-in-tube Processed MgB₂ Tapes”, *Physica C: Superconductivity*, 372:1245.

Malagoli A, Braccini V, Tropeano M, Vignolo M, Bernini C, Fanciulli C, Romano G, Putti M, Ferdeghini C, Mossang E, Polyanskii A, Larbalestier DC (2008) “Effect of Grain Refinement on Enhancing Critical Current Density and Upper Critical Field in Undoped MgB₂ Ex-situ Tapes”, *Journal of Applied Physics*, 104(10):103908.

Massachusetts Institute of Technology (MIT) (2003) *Superconducting Magnets*, US. Matsumoto A, Kumakura H, Kitaguchi H, Fujii H, Togano K (2002) “The Annealing Effects of MgB₂ Superconducting Tapes”, *Physica C: Superconductivity*, 382(2):207.

Matsumoto A, Kumakura H, Kitaguchi H, Hatakeyama H (2003) “Effect of SiO₂ and SiC Doping on The Powder-in-tube Processed MgB₂ Tapes”, *Superconductor Science and Technology*, 16(8):926.

Matsumoto A, Kumakura H, Kitaguchi H, Senkowicz BJ, Jewell MC, Hellstrom EE, Zhu Y, Voyles PM, Larbalestier DC (2006) “Evaluation of Connectivity, Flux Pinning, and Upper Critical Field Contributions to The Critical Current Density of Bulk Pure and SiC-alloyed MgB₂”, *Applied Physics Letters*, 89(13):132508.

Mickelson W, Cumings J, Han WQ, Zettl A (2002) “Effects of Carbon Doping on Superconductivity in Magnesium Diboride”, *Physical Review B*, 65(5):052505.

Monteverde M, Nunez-Regueiro M, Rogado N, Regan KA, Hayward MA, He T, Loureiro SM, Cava RJ (2001) “Pressure Dependence of The Superconducting Transition Temperature of Magnesium Diboride”, *Science*, 292(5514):75.

Mourachkine A (2004) “Room Temperature Superconductivity”, Cambridge Int Science Publishing, UK.

Mustapić M, Horvat J, Hossain MS, Skoko Ž, Dou SX (2013) “Enhancing Superconducting Properties of MgB₂ Pellets by Addition of Amorphous Magnetic Ni–Co–B Nanoparticles”, *Superconductor Science and Technology*, 26(7):075013.

Nakane T, Kumakura H (2009) “Evaluation of the Effect of Area Factors on the Grain Connectivity of Ex-Situ Cores”, *IEEE Transactions on Applied Superconductivity*, 19(3):2793.

Nakane T, Kitaguchi H, Kumakura H (2006) “Ex-situ Fabrication of MgB₂/Al Tapes With High Critical Current Density”, *Superconductor Science and Technology*, 19(6):528.

Nagamatsu J, Nakagawa N, Muranaka T, Zenitani Y, Akimitsu J (2001) “Superconductivity at 39 K in Magnesium Diboride”, *Nature*, 410(6824):63-64.

Nakane T, Takahashi K, Kuroda T, Kumakura H (2008) “Pressurizing Effect for The Precursor Mixtures of Starting MgB₂ Powder on The J_c - B Performance of Product Ex-situ Tape”, *Physica C: Superconductivity*, 468(15):1805.

Nardelli D, Matera D, Vignolo M, Bovone G, Palenzona A, Siri AS, Grasso G (2013) “Large Critical Current Density in MgB₂ Wire Using MgB₄ as Precursor”, *Superconductor Science and Technology*, 26(7):075010.

Novosel N, Galić S, Pajić D, Skoko Ž, Lončarek I, Mustapić M, Zadro K, Babić E (2012) “Enhancement of The Critical Current Density in MgB₂ Wires Doped With Ni Nanoparticles”, *Superconductor Science and Technology*, 25(9):095018.

Novosel N, Galić S, Pajić D, Zadro K, Babić E (2015) “Enhancing Superconducting Properties of MgB₂ by Addition of Magnetic Particles”, *Journal of Superconductivity and Novel Magnetism*, 28(2):425.

Qin F, Cai Q, Chen H (2015) “Partial Dissolution of MgO and the Effect on Critical Current Density in Urea-Doped MgB₂ Bulks”, *Journal of Alloys and Compounds*, 633:201.

Onnes HK (1911) “The Superconductivity of Mercury”, *Communications Laboratory of Physics at University of Leiden*, 122:124.

Pachla W, Kováč P, Hušek I, Melišek T, Müller M, Štrbík V, Mazur A, Presz A (2005) “The Effect of Hydrostatic Extrusion on The $J_c(B)$ Characteristic of Ex-situ MgB₂ Wires”, *Superconductor Science and Technology*, 18(4):552.

Pan XF, Matsumoto A, Kumakura H, Cheng CH, Zhao Y (2011) “Cooperative Doping Effects of Ti and Nano-SiC on Transport Critical Current Density and Grain Connectivity of In-situ MgB₂ Tapes”, *Physica C: Superconductivity*, 471(21):1128.

Pan XF, Zhao Y, Feng Y, Yang Y, Cheng CH (2008) “Effects of Graphite Doping on Critical Current Density and Microstructure of MgB₂ Bulks by an Improved Mg-Diffusion Method”, *Physica C: Superconductivity*, 468(15):1169.

Pan AV, Zhou S, Liu H, Dou S (2003) “Properties of Superconducting MgB₂ Wires: In-situ Versus Ex-situ Reaction Technique”, *Superconductor Science and Technology*, 16(5):639.

Panek JS, Tuttle JG, Marrero V, Mustafi S, Edmonds R, Gray A, Riall S (2004) “Astro-E2 Magnesium Diboride High Current Leads”, *Advances in Cryogenic Engineering, Transactions of the Cryogenic Engineering Conference-CEC*, 710(1):952.

Parisiades P, Liarokapis E, Zhigadlo ND, Katrych S, Karpinski J (2009) “Raman Investigations of C-, Li- and Mn-Doped MgB₂”. *Journal of Superconductivity and Novel Magnetism*, 22(2):169.

Patnaik S, Cooley LD, Gurevich A, Polyanskii AA, Jiang J, Cai XY, Squitieri AA, Naus MT, Lee MK, Choi JH, Belenky L, Bu SD, Letteri J, Song X, Schlom DG, Babcock SE, Eom CB, Hellstrom EE, Larbalestier DC (2001) “Electronic Anisotropy, Magnetic Field-Temperature Phase Diagram and Their Dependence on Resistivity in c-axis Oriented MgB₂ Thin Films”, *Superconductor Science and Technology*, 14(6):315.

Pradhan AK, Shi ZX, Tokunaga M, Tamegai T, Takano Y, Togano K, Kito H, Ihara H (2001) “Electrical Transport and Anisotropic Superconducting Properties in Single Crystalline and Dense Polycrystalline MgB₂”, *Physical Review B*, 64(21):212509.

Romano G, Vignolo M, Braccini V, Malagoli A, Bernini C, Tropeano M, Fanciulli C, Putti M, Ferdeghini C (2009) “High-Energy Ball Milling and Synthesis Temperature Study to Improve Superconducting Properties of Ex-situ Tapes and Wires”, *IEEE Transactions on Applied Superconductivity*, 19(3):2706.

Rose-Innes AC, Rhoerick EH (1978) “Introduction to Superconductivity”, Revised Second Edition, Pergamon Press Ltd., U.K.

Rosová A, Kováč P, Hušek I, Brunner B, Dobročka E (2015) “Microstructure of MgB₂ Superconducting Wire Prepared by Internal Magnesium Diffusion and In-situ Powder-in-tube Processes—Secondary Phase Intergrain Nanolayers as an Oxygen Content Indicator”, *Physica C: Superconductivity and Its Applications*, 516:1.

Salama K, Zhou YX, Hanna M, Alessandrini M, Putman PT, Fang H (2005) “Electromechanical Properties of Superconducting MgB₂ Wire”, *Superconductor Science and Technology*, 18(12):S369.

Sandu V, Aldica G, Popa S, Badica P, Cimpoiasu E, Dumitrache F, Sandu E (2011) “Transport Properties of Superconducting MgB₂ Composites With Carbon-Encapsulated Fe Nanospheres”, *Journal of Applied Physics*, 110(12):123921.

Sangwal K, Borc J, Kavetsky T (2011) “Study of Microindentation Cracks in Bismuth-Doped Arsenic Selenide Glasses”, *Journal of Non-Crystalline Solids*, 357(16):3117.

Scheuerlein C, Boutboul T, Leroy D, Oberli L, Rehmer B (2007) “Hardness and Tensile Strength of Multifilamentary Metal–Matrix Composite Superconductors for The Large Hadron Collider (LHC)”, *Journal of Materials Science*, 42(12):4298.

Schlachter SI, Goldacker W, Frank A, Ringsdorf B, Orschulko H (2006) “Properties of MgB₂ Superconductors With Regard to Space Applications”, *Cryogenics*, 46(2):201.

Serquis A, Civale L, Hammon DL, Liao XZ, Coulter JY, Zhu YT, Jaime M, Peterson DE, Mueller FM, Nesterenko VF, Gu Y (2003) “Hot Isostatic Pressing of Powder-in-tube MgB₂ Wires”, *Applied Physics Letters*, 82:2847.

Serquis A, Serrano G, Moreno SM, Civale L, Maiorov B, Balakirev F, Jaime M (2007) “Correlated Enhancement of H_{c2} and J_c in Carbon Nanotube Doped MgB₂”, *Superconductor Science and Technology*, 20(4):L12.

Shah MS, Shahabuddin M, Alzayed NS, Parakkandy JM (2014) “Flux Pinning Mechanism and H_{c2} Anisotropy in Melanin Doped Bulk MgB₂”, *Physica C: Superconductivity*, 501:19.

Shahabuddin M, Alzayed NS, Jafar MP, Asif M (2011) “Effect of Ball Milling Time on The Substitution of Carbon in Glucose Doped MgB₂ Superconductors: Dispersion Behavior of Glucose”, *Physica C: Superconductivity*, 471(23):1635.

Shcherbakova OV, Pan AV, Wang JL, Shcherbakov AV, Dou SX, Wexler D, Babic H, Jercinovic M, Husnjak O (2007) “Sugar as an Optimal Carbon Source for The Enhanced Performance of MgB₂ Superconductors at High Magnetic Fields”, *Superconductor Science and Technology*, 21(1):015005.

Sheahen TP (2002) “Introduction to High Temperature Superconductivity”, Kluwer Academic Publishers, United States of America.

Shimada Y, Kubota Y, Hata S, Ikeda K, Nakashima H, Matsumoto A, Togana K, Kumakura H (2011) “Electron Microscopy Observations of MgB₂ Wire Prepared by an Internal Mg Diffusion Method”, *Physica C: Superconductivity*, 471(21):1137-1141.

Shinde SR, Ogale SB, Biswas A, Greene RL, Venkatesan T (2001) “Observation of Large Anisotropy in c-axis Oriented Thin Films of MgB₂ Prepared by an In-situ Pulsed Laser Deposition Process”, 0110541.

Slusky JS, Rogado N, Regan KA, Hayward MA, Khalifah P, He T, Inumaru K, Loureiro SM, Haas MK, Zandbergen HW, Cava RJ (2001) “Loss of Superconductivity With The Addition of Al to MgB₂ and a Structural Transition in Mg_{1-x}Al_xB₂”, *Nature*, 410(6826):343.

Sobrero CE, Malachevsky MT, Serquis A (2015) “Core Microstructure and Strain State Analysis in MgB₂ Wires with Different Metal Sheaths”, *Advances in Condensed Matter Physics*, 297363.

Soltanian S, Horvat J, Wang XL, Munroe P, Dou SX (2003) “Effect of Nano-carbon Particle Doping on The Flux Pinning Properties of MgB₂ Superconductor”, *Physica C: Superconductivity*, 390(3):185.

Soltanian S, Wang XL, Horvat J, Dou SX, Sumption MD, Bhatia M, Collings EW, Munroe P, Tomsic M (2005) “High Transport Critical Current Density and Large H_{c2} and H_{irr} in Nanoscale SiC Doped MgB₂ Wires Sintered at Low Temperature”, *Superconductor Science and Technology*, 18(5):658.

Soltanian S, Wang XL, Horvat J, Li AH, Liu HK, Dou SX (2002) “Improvement of Critical Current Density in the Cu/MgB₂ and Ag/MgB₂ Superconducting Wires Using the Fast Formation Method”, *Physica C: Superconductivity*, 382(2):187.

Sumption MD, Bhatia M, Buta F, Bohnenstiehl S, Tomsic M, Rindfleisch M, Yue J, Phillips J, Kawabata S, Collings EW (2006) “Solenoid and Racetrack Coils Wound from MgB₂ Strand”. *Advances in Cryogenic Engineering*, 824(1):455.

Suo H, Beneduce C, Dhallé M, Musolino N, Genoud JY, Flukiger R (2001) “Large Transport Critical Currents in Dense Fe-and Ni-clad MgB₂ Superconducting Tapes”, *Applied Physics Letters*, 79:3116.

Suo HL, Ma L, Jiang JM, Li YM, Zhang ZL, Liu M, Zhao Y, He DY, Zhou ML (2007a) “High Critical Current Densities in SiC Doped In-Situ MgB₂ Wires Prepared by Continuous Tube Forming and Filling Technique”, *IEEE Transactions on Applied Superconductivity*, 17(2):2822.

Suo H, Wang Y, Ma H, Ma L, Liu M, Zhao Y, Zhou M (2007b) “Study on The Annealing Process of In-situ MgB₂/Fe Tapes by Advanced Spark Plasma Sintering (SPS) Technique”, *Physica C: Superconductivity and Its Applications*, 460:620.

Susner MA, Sumption MD, Bhatia M, Peng X, Tomsic MJ, Rindfleisch MA, Collings EW (2007) “Influence of Mg/B Ratio and SiC Doping on Microstructure and High Field Transport J_c in MgB₂ Strands”, *Physica C: Superconductivity*, 456(1):180.

Takahashi M, Okada M, Nakane T, Kumakura H (2009) “The Influence of Magnesium Grain Size and Ball Milling Time on the Phase Formation of MgB₂ Tapes”, *Superconductor Science and Technology*, 22(12):125017.

Takano Y, Takeya H, Fujii H, Kumakura H, Hatano T, Togano K, Kito H, Ihara H (2001) “Superconducting Properties of MgB₂ Bulk Materials Prepared by High Pressure Sintering”, *Applied Physics Letters*, 78:2914.

Tanaka K, Okada M, Kumakura H, Kitaguchi H, Togano K (2002) “Fabrication and Transport Properties of MgB₂ Wire and Coil”, *Physica C: Superconductivity*, 382(2):203.

Tang S, Wang D, Zhang X, Zhang Q, Li C, Ma Y, Oguro H, Awaji S, Watanabe K (2014) “Improved Transport J_c in MgB₂ Tapes by Graphene Doping”, *Journal of Superconductivity and Novel Magnetism*, 27:2699.

Thomas S, Varghese N, Rahul S, Devadas KM, Vinod K, Syamaprasad U (2012) "Enhancement of Bending Strain Tolerance and Current Carrying Property of MgB₂ Based Multifilamentary Wires", *Cryogenics*, 52(12):767.

Thompson JR, Paranthaman M, Christen DK, Sorge KD, Kim HJ, Ossandon JG (2001) "High Temporal Stability of Supercurrents in MgB₂ Materials", *Superconductor Science and Technology*, 14(5):L17.

Togano K, Fujii H, Takeuchi T, Kumakura H (2007) "An Internal Mg - Li Alloy Composite Process for The Fabrication of MgB₂ Wire", *Superconductor Science and Technology*, 20(7):629.

Tomsic M, Rindfleisch M, Yue J, McFadden K, Doll D, Phillips J, Sumption MD, Bhatia M, Bohnenstiehl S, Collings EW (2007) "Development of Magnesium Diboride (MgB₂) Wires and Magnets Using In-situ Strand Fabrication Method", *Physica C: Superconductivity*, 456(1):203.

Varghese N, Vinod K, Rahul S, Devadas KM, Thomas S, Pradhan S, Syamaprasad U (2011) "Influence of Nano-Cu Additive on MgB₂ Phase Formation, Processing Temperature and Transport Properties", *Journal of Applied Physics*, 109(3):3902.

Viljamaa J, Kulich M, Kovac P, Melisek T, Reissner M (2011) "Comparison on Effects of, and SiC Doping on Performance of Conductors", *IEEE Transactions on Applied Superconductivity*, 21(3):2659.

Vinod K, Kumar RA, Syamaprasad U (2006) "Prospects for MgB₂ Superconductors for Magnet Application", *Superconductor Science and Technology*, 20(1):R1.

Vinod K, Upendran S (2010) "Studies on Development of MgB₂ Superconductor With Improved in-Field Critical Current Density", *In Advanced Materials Research*, 117:63.

Wang D, Gao Z, Zhang X, Yao C, Wang C, Zhang S, Ma Y, Awaji S, Watanabe K (2011) "Enhanced J_c - B Properties of MgB₂ Tapes by Yttrium Acetate Doping", *Superconductor Science and Technology*, 24(7):075002.

Wang D, Wang C, Zhang X, Gao Z, Yao C, Ma Y, Kanazawa M, Yamada Y, Oguro H, Awaji S, Watanabe K (2012) "Enhancement of J_c - B Properties for Binary and Carbon-Doped MgB₂ Tapes by Hot Pressing", *Superconductor Science and Technology*, 25(6):065013.

Wang D, Zhang X, Tang S, Xu D, Yao C, Dong C, Xu Z, Ma Y, Oguro H, Awaji S, Watanabe K (2015a) "Influence of Crystalline Boron Powders on Superconducting Properties of C-Doped Internal Mg Diffusion Processed MgB₂ Wires", *Superconductor Science and Technology*, 28(10):105013.

Wang D, Zhang H, Zhang X, Tang S, Ma Y, Oguro H, Awaji S, Watanabe K (2015b) "Effects of Three Different Homemade Nanocarbons Doping on The Superconducting Properties of MgB₂ Tapes". *Physica C: Superconductivity and Its Applications*, 508:49.

Wang DL, Ma YW, Gao ZS, Yao C, Wang L, Zhang XP, Nishijima G, Awaji S, Watanabe K (2010) “Influence of Acetone Doping on The J_c Anisotropy of MgB₂/Fe Tapes”, *Physica C: Superconductivity*, 470(20):1435.

Wang J, Bugoslavsky Y, Berenov A, Cowey L, Caplin AD, Cohen LF, MacManus Driscoll JL, Cooley LD, Song X, Larbalestier DC (2002) “High Critical Current Density and Improved Irreversibility Field in Bulk MgB₂ Made by a Scaleable, Nanoparticle Addition Route”, *Applied Physics Letters*, 81:2026.

Wang X, Cheng Z, Dou SX (2007) “Silicon oil: A Cheap Liquid Additive for Enhancing in-Field Critical Current Density in MgB₂”, *Applied Physics Letters*, 90:042501.

Wang XL, Soltanian S, Horvat J, Liu AH, Qin MJ, Liu HK, Dou SX (2001) “Very Fast Formation of Superconducting MgB₂/Fe Wires With High J_c ”, *Physica C: Superconductivity*, 361(3):149.

Wen C, Hu M, Yu H, Hong T, Chen H, Qu R, Fang H (2015) “Design of a MgB₂ Superconducting Synchronous Generator”, *IEEE Transactions on Applied Superconductivity*, 25(3):1.

Wu F (2014) “The Improved Superconducting Properties in the Ex-situ Sintered MgB₂ Bulks with Mg Addition”, *Journal of Low Temperature Physics*, 177(3-4):157.

Xi XX (2008) “Two-band Superconductor Magnesium Diboride”, *Reports on Progress in Physics*, 71(11):116501.

Xiang JY, Zheng DN, Li JQ, Li SL, Wen HH, Zhao ZX (2003) “Effects of Al Doping on The Superconducting and Structural Properties of MgB₂”, *Physica C: Superconductivity*, 386:611.

Xu D, Wang D, Li C, Yuan P, Zhang X, Yao C, Dong C, Huang H, Ma Y, Oguro H, Awaji S, Watanabe K (2016) “Microstructure and Superconducting Properties of Nanocarbon-Doped Internal Mg Diffusion-Processed MgB₂ Wires Fabricated Using Different Boron Powders”, *Superconductor Science and Technology*, 29(4):045009.

Xu M, Kitazawa H, Takano Y, Ye J, Nishida K, Abe H, Matsushita A, Kido G (2001a) “Single Crystal MgB₂ With Anisotropic Superconducting Properties”, *Applied Physics Letters*, 79:2779.

Xu M, Kitazawa H, Takano Y, Ye J, Nishida K, Abe H, Matsushita A, Tsujii N, Kido G (2001b) “Anisotropy of Superconductivity From MgB₂ Single Crystals”, *Applied Physics Letters*, 79(17):2779.

Yamada H, Hirakawa M, Kumakura H, Matsumoto A, Kitaguchi H (2004) “Critical Current Densities of Powder-in-tube MgB₂ Tapes Fabricated With Nanometer-size Mg Powder”, *Applied Physics Letter*, 84:1728.

Yamada H, Igarashi M, Kitaguchi H, Matsumoto A, Kumakura H (2009) “Influence of Heat Treatment on In-situ Powder-in-tube Processed MgB₂ Tapes With Added

Ethyltoluene and SiC Powder”, *Superconductor Science and Technology*, 22(7):075005.

Yamamoto A, Shimoyama JI, Ueda S, Horii S, Kishio K (2006) “Doping Effects of TiC and Mo₂C on Critical Current Properties of MgB₂ Tapes”, *IEEE Transactions on Applied Superconductivity*, 16:1411.

Yamamoto A, Shimoyama JI, Ueda S, Iwayama I, Horii S, Kishio K (2005) “Effects of B₄C Doping on Critical Current Properties of MgB₂ Superconductor”, *Superconductor Science and Technology*, 18(10):1323.

Yamamoto A, Shimoyama JI, Ueda S, Katsura Y, Horii S, Kishio K (2004) “Improved Critical Current Properties Observed in MgB₂ Bulks Synthesized by Low-Temperature Solid-State Reaction”, *Superconductor Science and Technology*, 18(1):116.

Yang F, Li SQ, Yan G, Feng JQ, Xiong XM, Zhang SN, Wang QY, Pang YC, Zou HF, Li CS, Feng Y (2015) “Improved Superconducting Properties in Ti-Doped MgB₂ Prepared by Two-Step Reaction Method and High-Energy Ball Milling”, *Journal of Alloys and Compounds*, 622:714.

Yao C, Zhang X, Wang D, Gao Z, Wang L, Qi Y, Wang C, Ma Y, Awaji S, Watanabe K (2011) “Doping Effects of Nd₂O₃ on The Superconducting Properties of Powder-in-tube MgB₂ Tapes”, *Superconductor Science and Technology*, 24(5):055016.

Ye S, Matsumoto A, Togano K, Zhang Y, Ohmura T, Kumakura H (2014) “Fabrication of MgB₂ Superconducting Wires With a Hybrid Method Combining Internal-Mg-Diffusion and Powder-in-tube Processes”, *Superconductor Science and Technology*, 27(5):055017.

Ye SJ, Song M, Matsumoto A, Togano K, Zhang Y, Kumakura H, Takeguchi M, Teranishi R, Kiyoshi T (2012) “Enhancing The Critical Current Properties of Internal Mg Diffusion-Processed MgB₂ Wires by Mg Addition”, *Superconductor Science and Technology*, 25(12):125014.

Yeoh WK, Horvat J, Kim JH, Xu X, Dou SX (2007) “Effect of Processing Temperature on High Field Critical Current Density and Upper Critical Field of Nanocarbon Doped MgB₂”, *Applied Physics Letters*, 90:122502.

Yeoh WK, Kim JH, Horvat J, Xu X, Qin MJ, Dou SX, Jiang CH, Nakane T, Kumakura H, Munroe P (2006) “Control of Nano-carbon Substitution for Enhancing The Critical Current Density in MgB₂”, *Superconductor Science and Technology*, 19(6):596.

Yilmazlar M, Terzioglu C, Dogruer M, Karaboga F, Soylu N, Zalaoglu Y, Yildirim G, Ozturk O (2014) “Evaluation of Microstructural and Mechanical Properties of Ag-Diffused Bulk MgB₂ Superconductors. *Journal of Superconductivity and Novel Magnetism*, 27(1):77.

Zhang X, Ma Y, Gao Z, Wang D, Wang L, Liu W, Wang C (2008a) “Strongly Enhanced Current-Carrying Performance in MgB₂ Tape Conductors by Novel C⁶⁰ Doping”, *Journal of Applied Physics*, 103:103915.

Zhang X, Ma Y, Gao Z, Wang D, Yu Z, Wang L (2007) “Systematic Study of The Microstructures and Electrical and Superconducting Properties of Nanocarbon Doped MgB₂ Tapes”, *Superconductor Science and Technology*, 20(12):1198.

Zhang X, Ma Y, Gao Z, Yu Z, Nishijima G, Watanabe K (2006) “Enhancement of J_c - B Properties in MoSi₂-Doped MgB₂ Tapes”, *Superconductor Science and Technology*, 19(8):699.

Zhang X, Wang D, Gao Z, Wang L, Ma Y, Qi Z, Watanabe K (2008b) “The Doping Effect of Activated Carbon on The Superconducting Properties of MgB₂ Tapes”, *Superconductor Science and Technology*, 21(7):075008.

Zhang Y, Xu X, Zhao Y, Kim JH, Lu C, Zhou SH, Dou SX (2008c) “Significant Improvement of J_c in MgB₂ Bulk Superconductor Using Ball-Milled High-Purity Crystalline Boron”, *Superconductor Science and Technology*, 21(11):115004.

Zhang YB, Shan XJ, Bai XW, Liu TY, Zhu HM, Cai CB (2012) “In-situ Synthesis and Current-Carrying Characteristics of Superconducting MgB₂-B₄C Composites With MgB₂ Fractions Ranging from 18% to 85%”, *Superconductor Science and Technology*, 25(9):095003.

Zhao Y, Huang DX, Feng Y, Cheng CH, Machi T, Koshizuka N, Murakami M (2002) “Nanoparticle Structure of MgB₂ With Ultrathin TiB₂ Grain Boundaries”, *Applied Physics Letters*, 80(9):1640.

Zhao Y, Rui XF, Cheng CH, Zhang H, Munroe P, Zeng HM, Koshizuka N, Murakami M (2003) “Improved Irreversibility Behaviour and Critical Current Density in MgB₂-Diamond Nanocomposites”, *Applied Physics Letters* 83:2916.

Zhou S, Liu H, Horvat J, Dou S (2003) “Effect of Ti Doping on The Superconductivities of MgB₂/Fe Wires”, *Journal of Low Temperature Physics*, 131(3-4):687.

Zhou S, Pan AV, Dou SX (2009a) “An Attempt to Improve The Superconducting Properties of MgB₂ by Doping With Zn-Containing Organic Compound”, *Journal of Alloys and Compounds*, 487(1):42.

Zhou S, Pan AV, Liu H, Dou S (2002) “Single- and Multifilamentary Fe-Sheathed MgB₂ Wires”, *Physica C: Superconductivity*, 382(4):349.

Zhou S, Zhang Y, Pan AV, Dou SX, Chung KC, Kim Y, Yoo JM (2009b) “Effects of Sintering Atmosphere on The Superconductivity of MgB₂”, *Superconductor Science and Technology*, 22(4):045018.

CURRICULUM VITAE

Name SURNAME : Fırat KARABOĞA

Place and Date of Birth : İZMİR- 26.01.1986

Universities

- Bachelor's Degree : Abant İzzet Baysal

MSc Degree : Abant İzzet Baysal

e-mail : karabogafirat@gmail.com

Address : AİBÜ lojmanları Meşe A2B D:10

List of International Publications

- Koca, M., **Karaboga, F.**, Yıldırım, G., Kirilmis, C., 2012. *The Arabian Journal for Science and Engineering*, Density functional theory study on the identification of Pd (Me–Xanthate) 2., 37 (5): 1283-1291.
- Dogruer, M., **Karaboga, F.**, Yildirim, G., Terzioglu, C., Ozturk, O., 2013. *Journal of Materials Science: Materials in Electronics*, A comprehensive study on mechanical properties of $\text{Bi}_{1.8}\text{Pb}_{0.4}\text{Sr}_2\text{Mn}_x\text{Ca}_{2.2}\text{Cu}_{3.0}\text{O}_y$ superconductors., 24 (8): 2659-2666.
- Dogruer M., **Karaboga, F.**, Yildirim, G., and Terzioglu, C., 2013. *Journal of Materials Science: Materials in Electronics*, Comparative study on indentation size effect, indentation cracks and superconducting properties of undoped and MgB2 doped Bi-2223 ceramics., 24 (7): 2327-2338.
- **Karaboga, F.**, Soykan, U., Dogruer, M., Ozturk, B., Yildirim, G., Cetin, S., Terzioglu, C., 2013. *Spectrochimica Acta Part A: Molecular and Biomolecular Spectroscopy*, Experimental and theoretical approaches for identification of p-benzophenoneoxycarbonylphenyl acrylate., 113: 80-91.

- **Karaboga F.**, Soykan, U., Çetin S., Ozturk B., Dogruer, M., Yildirim G., Terzioglu C., 2013. *Journal of Molecular Structure*. Synthesis and Characterization of p-benzophenoneoxycarbonylphenyl Acrylate By Means of Experimental Measurements and Theoretical Approaches, and Bulk Melt Polymerization., 1049: 479-487.
- Dogruer M., Gorur O., **Karaboga F.**, Yildirim G., Terzioglu C., 2013. *Powder Technology*. Zr diffusion coefficient and activation energy calculations based on EDXRF measurement and evaluation of mechanical characteristics of $\text{YBa}_2\text{Cu}_3\text{O}_{7-x}$ bulk superconducting ceramics diffused with Zr nanoparticles., 246: 553-560.
- Yildirim G., Dogruer M., **Karaboga F.**, Terzioglu C., 2014. *Journal of Alloys and Compounds (JALCOM)*. Formation of nucleation centers for vortices in Bi-2223 superconducting core by dispersed Sn nanoparticles., 584: 344-351.
- Yilmazlar M., Terzioglu C., Dogruer M., **Karaboga F.**, Soylu N., Zalaoglu Y., Yildirim G., Ozturk O., 2014. *Journal of Superconducting Novel Magnetism*. Evaluation of Microstructural and Mechanical Properties of Ag-Diffused Bulk MgB_2 Superconductors., 27 (1): 77-82.
- Cakir, I., Soykan, U., Cetin, S., **Karaboga F.**, Zalaoglu, Y., Dogruer, M., Terzioglu, C., Yildirim, G., 2014. *Spectrochimica Acta Part A: Molecular and Biomolecular Spectroscopy*, Electrochemical and spectroscopic characteristics of p-acryloyloxybenzoyl chloride and p-acryloyloxybenzoic acid and antimicrobial activity of organic compounds 132: 502-513.
- Akdogan, M., Yetis, H., Gajda, D., **Karaboga, F.**, Ulgen, A.T., Demirturk, E., and Belenli I., 2015. *Journal of Alloys and Compounds (JALCOM)*. Effect of the initial filling density on the critical current of in-situ Fe/ MgB_2 wires., 649: 1007-1010.
- **Karaboga, F.**, Yetis, H., Oz, M., and Belenli I., 2016. *Journal of Materials Science: Materials in Electronics*, Effect of different-sized h-BN nanoparticles on some properties of MgB_2 superconductors., 27 (7): 1-6.
- **Karaboga, F.**, Senol, M.A., 2016. *Journal of Superconductivity and Novel Magnetism (JOOSC)*, Microstructure and transport properties of compaction modified in-situ Fe/ MgB_2 wires., 29 (7): 1-7.

- Gajda, D., Morawski, A., Zaleski, A.J., Akdoğan, M., Yetiş, H., **Karaboğa, F.**, Cetner, T., Belenli, İ., 2016. *Journal of Alloys and Compounds (JALCOM)*. The influence of HIP process on critical parameters of MgB₂/Fe wires with big boron grains and without barriers., 687: 616-622.

List of National Publications

- Zalaoglu, Y., **Karaboga, F.**, Yildirim, G., Terzioglu, C., Erturk, A. S., Ulgen, A. T., 2011. *Balkan Physics Letters*, Ab Initio Hartree-Fock and Density Functional Theory Study on Characterization of 2-Nitro-n-(4-Nitrophenyl) Benzamide.
- **Karaboga, F.**, Yildirim, G., Terzioglu, C., Koca, M., Dogruer M., 2012. *Dumlupinar Universitesi Fen Bilimleri Dergisi* (2012 agustos sayisi), Theoretical Study on The Characterization of 1,3-Dibenzoylimidazolidine-2-Thione by Quantum Mechanical Methods.

Awards

:

- Award for the accepted A or A1 article by Izzet Baysal foundation in 2013.
- Award for the accepted A or A1 article by Izzet Baysal foundation in 2014.
- Award for the accepted A or A1 article by Izzet Baysal foundation in 2015.
- Award for the accepted A or A1 article by Izzet Baysal foundation in 2016.